RESEARCH TRIANGLE INSTITUTE

HETEROEPITAXIAL DIAMOND GROWTH

Annual Report

April 16, 1992 - December 31, 1992

RTI Project No. 83U-5294

Prepared for: Office of Naval Research
800 N. Quincy Street
Arlington, VA 22217-5000

Prepared by: Ronald A. Rudder
Research Triangle Institute
Center for Semiconductor Research
P.O. Box 12194
Research Triangle Park, NC 27709

REPORT DOCUMENT PAGE

Form Approved
OMB No 0704-0188

1. AGENCY USE ONLY *(Leave blank)*	2. REPORT DATE	3. REPORT TYPE AND DATES COVERED
	12 January 1993	Annual Report April 16, 1992 -- December 31, 1992

4. TITLE AND SUBTITLE

Heteroepitaxial Diamond Growth

5. FUNDING NUMBERS

N00014-92-C-0081

6. AUTHOR(S)

R.J. Markunas, R.A. Rudder, J.B. Posthill, R.E. Thomas, G. C. Hudson, and D.P. Malta

7. PERFORMING ORGANIZATION NAME(S) AND ADDRESS(ES)

Research Triangle Institute
P. O. Box 12194
Research Triangle Park, NC 27709

8. PERFORMING ORGANIZATION REPORT NUMBER

83U-5294

9. SPONSORING/MONITORING AGENCY NAME(S) AND ADDRESSES(ES)

Office of Naval Research
800 N. Quincy Street
Arlington, VA 22217-5000

10. SPONSORING/MONITORING AGENCY REPORT NUMBER

11. SUPPLEMENTARY NOTES

12a. DISTRIBUTION/AVAILABILITY STATEMENT

Approved for public release; unlimited distribution

12b. DISTRIBUTION CODE

13. ABSTRACT

Progress continued in 1992 in the two major thrust areas of the diamond program; diamond consolidation, and heteroepitaxial nucleation. We have been developing a consolidation technology as one approach to large area diamond single crystals. During this phase of the program, techniques were developed for a) bonding of natural diamond seed crystals to non-diamond substrates, b) overgrowth for consolidation, c) ion-implantation for lift-off of thin diamond platelets. Experimental and theoretical progress was also made on heteroepitaxial growth of diamond. Theoretical modeling indicated a possible role of subsurface carbon in Ni(111) in preventing diamond nucleation. Experimental studies have provided evidence for several roles for oxygen on diamond surfaces during diamond growth. Progress was also made in developing techniques for microstructural characterization of CVD diamond. TEM sample preparation methods were developed for cross-sectional and plan-view analysis of diamond films and substrates. A simple method for rapidly assessing defect densities in CVD and natural diamond was also developed.

14. SUBJECT TERMS

15. NUMBER OF PAGES

16. PRICE CODE

17. SECURITY CLASSIFICATION OF REPORT	18. SECURITY CLASSIFICATION OF THIS PAGE	19. SECURITY CLASSIFICATION OF ABSTRACT	20. LIMITATION OF ABSTRACT
UNCLASSIFIED	UNCLASSIFIED	UNCLASSIFIED	

Table of Contents

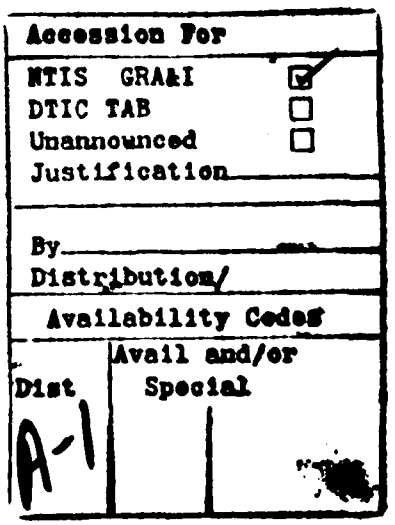

1.0 Annual Summary

This report is the 1992 annual report for the "Semiconducting Diamond Program" contract #N00014-92-C-0081 covering the period from April 1, 1992, to December 31, 1992. Work at Research Triangle Institute during that time period has concentrated on the development of CVD techniques for large-area single crystal diamond growth. The program has addressed this development by exploring two avenues toward this end. The *first* avenue has been continued work at diamond heteroepitaxy. This part of the program has sought specifically theoretical modeling to give new insight and direction to the scientific heteroepitaxial experiments. Given our investment in Ni technologies and given encouraging results in the community of oriented crystallites on Ni epitaxial layers, Theoretical work has concentrated on Ni surfaces attempting to understand how those surfaces change as foreign C, H, etc., atoms alter the near surface. The *second* avenue has been the development of epitaxial consolidation technologies to derive a large-area single crystal from relatively small diamond seed crystals. A major output of this part of the program has been the development of ion implantation/anneal processes for single crystal diamond platelet formation.

Along with the central program at RTI, the program has included subcontract tasks to

- Dr. Robert Nemanich NCSU
- Dr. Jerry Whitten NCSU
- Dr. Max Swanson UNC

This report includes sections from those investigators detailing their respective progress.

The program has addressed technologies for large-area single-crystal diamond production by:

1. RTI continued development of techniques for enhancing diamond nucleation on non-diamond substrates. This work has involved theoretical modeling by Dr. Jerry Whitten and Dr. Hong Yang (NCSU) of the Ni system. This work explored the effects of subsurface impurities in the Ni lattice on bond strength and bond order of adsorbed hydrocarbons.
2. RTI continued fundamental surface science studies of the diamond (100) surface with a particular emphasis on the role of oxygen on the stabilization of the (100) surface. That work lead by Dr. Raymond Thomas (RTI) has expounded the role of oxygen in low temperature diamond deposition. This work has enjoyed a very fruitful collaboration with Dr. Michael Frenklach (Penn State) whose theoretical work has helped elucidate the O-sites on the (100) surface and the creation of radical sites on the (100) surface following CO desorption.
3. RTI through subcontractual work with Dr. Max Swanson and Dr. Nalin Parikh (UNC) a codeveloped a C^+ and O^+ implantation/annealing process for the fabrication of thin single crystal diamond platelets (~ 2 μm thick).
4. In conjunction with (3), RTI has undertaken a critical analysis of various homoepitaxial growth processes (H_2/CH_4, H_2/CO, H_2/CH_4-CO, H_2O/CH_4O). This work has identified H_2O as critical to the perpetuation of topographically smooth homoepitaxy. The refinements determined here will allow consolidation of individual single crystals into large-area single crystals.
5. Development of any single crystal technology cannot be refined and developed unless microstructural techniques are available and routine. Besides adopting standard TEM sample preparation technique to diamond sample preparation, Dr. John Posthill and Dave Malta (RTI) developed a defect delineation technique involving preferential defect etching under an oxidizing chemical flame. This technique represents for diamond what standard etch pit delineation by wet chemicals has represented for the advancement of Si and GaAs technologies.

6. The microstructural techniques aforementioned are to be complemented by atomic resolution imaging of diamond surfaces performed at NCSU under the subcontract to Dr. Robert Nemanich. Atomic resolution of the regions where the CVD process consolidates the diamond platelets (3) and (4) will be critical in the development of diamond overgrowth and platelet bonding techniques for defect minimization.

2.0 Theoretical Modeling of the Ni (111) surface for Diamond Heteronucleation (Dr. J. Whitten, Dr. H. Yang, NCSU)

The three areas of major activity during the past year are:

- mechanistic studies of CH_4 and CH_3F on Si(111); H and F transfer to the surface
- mechanistic studies of H_2 desorption from the monohydride Si(100) surface
- effect of Na, C and H implants on the bonding of C to Ni(111)

Ab initio self-consistent-field (SCF) and configuration interaction (CI) theory is applied to embedded cluster models of the silicon and nickel surfaces. By formulating the problem so that a surface portion of the substrate is treated very accurately by CI while coupling this embedded cluster to the remainder of the lattice, we are able to achieve a reliable level of description of the reaction energetics. In the present studies, activation energies and overall heats of reaction between adsorbates and the surface are calculated and reaction mechanisms are discussed.

Our studies of the reaction of CH_4 and CH_3F with Si(111) were motivated by supersonic beam experiments by Wilson Ho and coworkers. Calculated heats of reaction and activation energies are as follows:

		ΔH	E_{act}
$CH_4 + Si(111)$	$= CH_3 + H\text{-}Si(111)$	13	24
$CH_3F + Si(111)$	$= CH_3 + F\text{-}Si(111)$	-24	19
$CH_3F + Si(111)$	$= CH_2F + H\text{-}Si(111)$	12	20

These results and similar results for gas phase reactions involving CH_xF_{4-x} species with SiH_3 suggest a modified interpretation of beam experiments. It is not the total translational energy of the impacting molecule that is directly relevant to the H and F transfer reactions. Instead, only the translational (and vibrational) energy of the two atoms directly involved in the transfer reaction, viz., the CF or CH portion of CH_3F and the CH portion of the CH_4, is available (to a first approximation) to surmount the

activation barrier. This means that increasing the kinetic energy by increasing the total mass of the beam molecule is less effective than one might at first suppose.

Mechanistic studies of H_2 desorption from Si(100)2x1H reveal that a symmetric desorption pathway gives the lowest desorption energy barrier; however, the barrier is 1.0 eV higher than experiment. A multi-step desorption mechanism which involves a delocalized process for forming a dihydride, SiH_2, is proposed to explain the experimental observations.

During this period, studies were also begun on the deposition of carbon on Ni(111), a surface nearly commensurate with that of diamond. Interstitial Na, C and H atoms are found to influence the reactivity of the Ni(111) surface and the structure of carbon species adsorbed on the surface. Subsurface Na and H stabilize tetrahedrally bonded carbon whereas subsurface C facilitates the formation of planar configurations of CH_3 and C_6H_6 adsorbed on nickel.

Calculated chemisorption energies of pyramidal CH_3 on Ni(111) are 38 for the clean surface and 50, 47, and 17 kcal/mol for the Na, H, and C implants, respectively. The energies required to distort tetrahedral CH_3 into a planar structure are 22 kcal/mol on clean Ni(111), 30 kcal/mol with the Na implant, 24 kcal/mol with the H implant, and 12 kcal/mol with the C implant, respectively.

In an extension of this work, the benzene molecule, C_6H_6, in planar and nonplanar geometries, is used to probe bonding at the surface. Adsorption energies of planar C_6H_6 at the most stable, 3fold, adsorption site are 0.83 eV for the Ni(111) surface, and 0.44, 0.83, and 1.89 eV in the presence of the Na, H, and C interstitials, respectively. The energies required for the planar to puckered distortion are 4.3 eV on Ni(111), 3.0 eV with the Na interstitial, 3.6 eV with H, and 5.8 eV with C compared to 8.6 eV for distortion of C_6H_6 in the gas phase. The possible relevance of these results to the growth of diamond on nickel lies in the fact that subsurface Na and H stabilize

tetrahedrally bonded carbon subunits of the diamond structure while subsurface C may make it easier for the overlayer to revert to a planar graphite structure.

3.0 Diamond Surface Science: The Role of Oxygen on the C (100) Surface

In response to the success of the water/alcohol process in growing diamond, we have pursued a series of studies to examine the role of oxygen in the diamond growth process. These studies not only provide insight into the diamond growth process but also yield valuable information on the nature of the chemical sites needed to promote diamond growth. By tailoring non-native surfaces to approximate the sites found on the diamond surface, we more closely approach conditions needed to generate true heteroepitaxy. We have taken the approach of studying the interactions of individual gasses under well controlled conditions, i.e. using ultra-high vacuum and single crystal diamond surfaces. The studies have relied on thermal desorption spectroscopy (TDS), low energy electron diffraction (LEED), Auger electron spectroscopy (AES), ands, more recently, electron energy loss spectroscopy (EELS). The studies have been very profitable and have illuminated several roles that oxygen may play in the growth process. The details of the studies are more fully covered in the attached papers but summaries of the main roles identified are as follows:

1) Opening of sites for carbon addition to the diamond lattice by desorption of CO. Thermal desorption studies have shown that desorption of CO from the (100) surface can occur at temperatures as low as 200°C. In conjunction with Michael Frenklach we will be studying adsorption of acetylene onto the sites opened by CO desorption. The sites opened by the acetylene desorption may be particularly amenable to adsorption of acetylene.

2) Maintaining and/or recovering the sp^3 hybridization on the diamond surface. LEED studies have shown that atomic oxygen will easily convert the 2x1 configuration on the diamond surface to a 1x1 structure. Earlier studies, both here and elsewhere,

have shown that the 2x1 configuration is not the preferred structure for diamond growth. In addition, annealing studies of oxygen terminated (100) surfaces show that surfaces that are only partially covered with oxygen are able to maintain the 1x1 configuration. This result is very different from the action of hydrogen where conversion to the 2x1 configuration is observed as soon as hydrogen begins to leave the surface. We have begun experiments with Dr. Nemanich and Dr. Humphreys of NCSU to use STM and AFM to study the nature of the sites created during the partial desorption of oxygen from the diamond surface.

3) Removal of hydrogen from the surface. Dosing studies have shown that oxygen readily removes hydrogen from the surface. This allows processes described in 1) and 2) to operate. However, the reverse reaction, hydrogen removing oxygen from the surface does not appear to be nearly as efficient.

4) We believe that oxygen will also prove to be quite efficient at removing non-diamond carbon from the surface. Experiments by other groups have indicated that oxygen will preferentially etch graphite over diamond. Reactions of atomic oxygen with diamond and graphite will be among the first experiments performed with the modulated beam apparatus when it comes on line later in 1993.

All of the above growth mechanisms discussed for oxygen are believed to operate for atomic hydrogen. However, they appear to be more efficient or to operate at lower temperatures with atomic oxygen. The desorption of CO at 200°C may help explain the success of the water/alcohol process in growing diamond at much lower temperatures. We are continuing informal collaborations with Michael Frenklach of Penn State to study the surface processes of oxygen on diamond (100). We expect to derive dynamic calculations of desorption processes and static calculations of oxygen binding on the (100) surface.

After discussions with Dr. Pehr Pehrsson and Dr. John Russell at NRL, we have recently added the capability of performing electron energy loss spectroscopy. The electron loss mechanism acts as a sensitive probe of the surface electronic states. Figures 3.1 and 3.2 show results from early experiments on the diamond (100) surface. In Figure 3.1 we can easily distinguish features associated with the conversion of the surface from the 1x1 configuration to the 2x1 configuration by annealing. A new peak appears on the spectra approximately 5 eV from the elastic peak. If either atomic oxygen or atomic hydrogen is added to the surface, this 5 eV peak disappears (Figure 3.2). In the case of oxygen, the LEED shows that the surface has converted back to the 1x1 configuration. However for hydrogen we still observe the 2x1 configuration. Further experiments are underway with this new tool, and we expect that EELS will provide a powerful method for understanding the surface structure of adsorbed gasses.

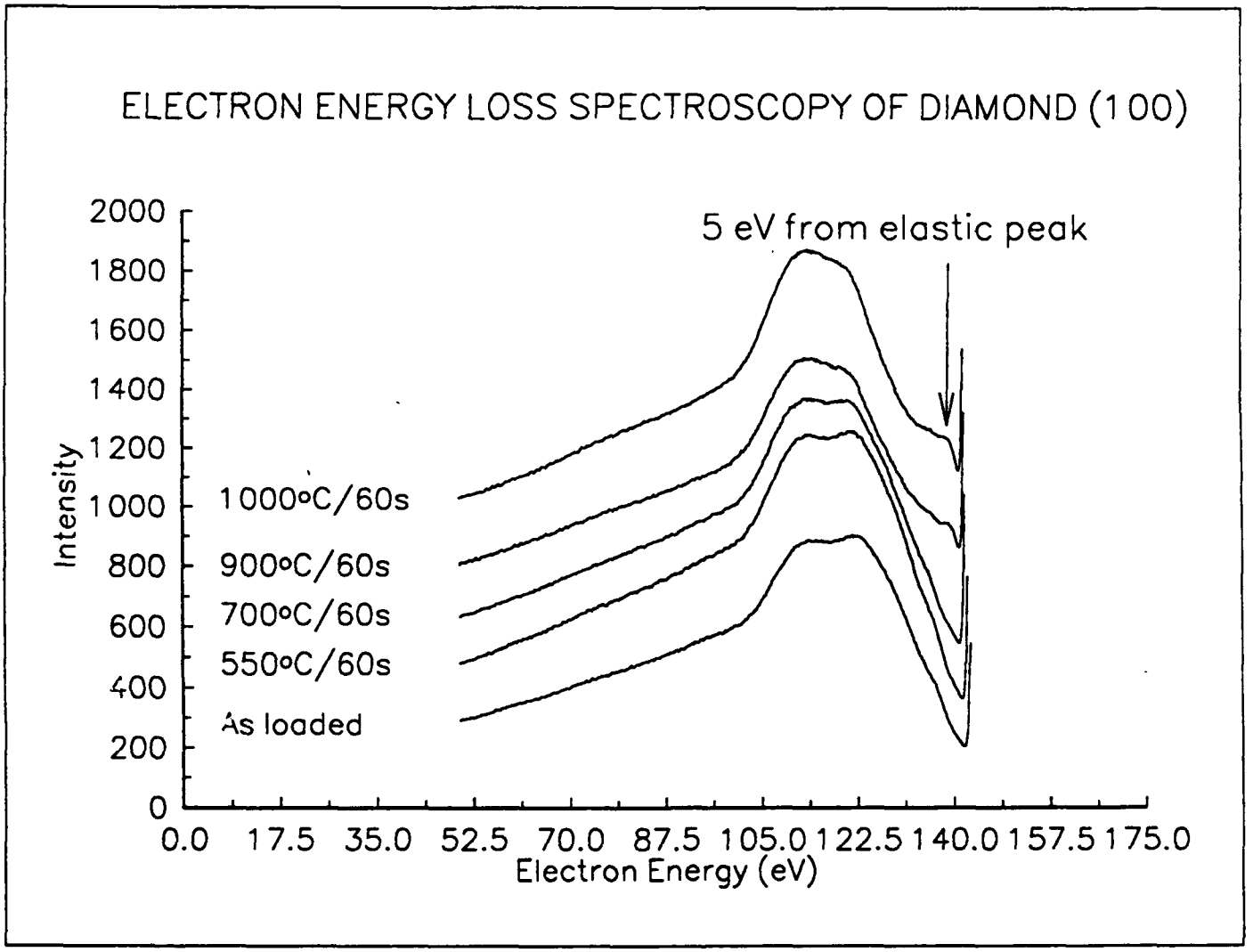
ELECTRON ENERGY LOSS SPECTROSCOPY OF DIAMOND (100)
5 eV from elastic peak
Intensity
2000
1800
1600
1400
1200
1000
800
600
400
200
0
1000°C/60s
900°C/60s
700°C/60s
550°C/60s
As loaded
0.0 17.5 35.0 52.5 70.0 87.5 105.0 122.5 140.0 157.5 175.0
Electron Energy (eV)

Figure 3.1

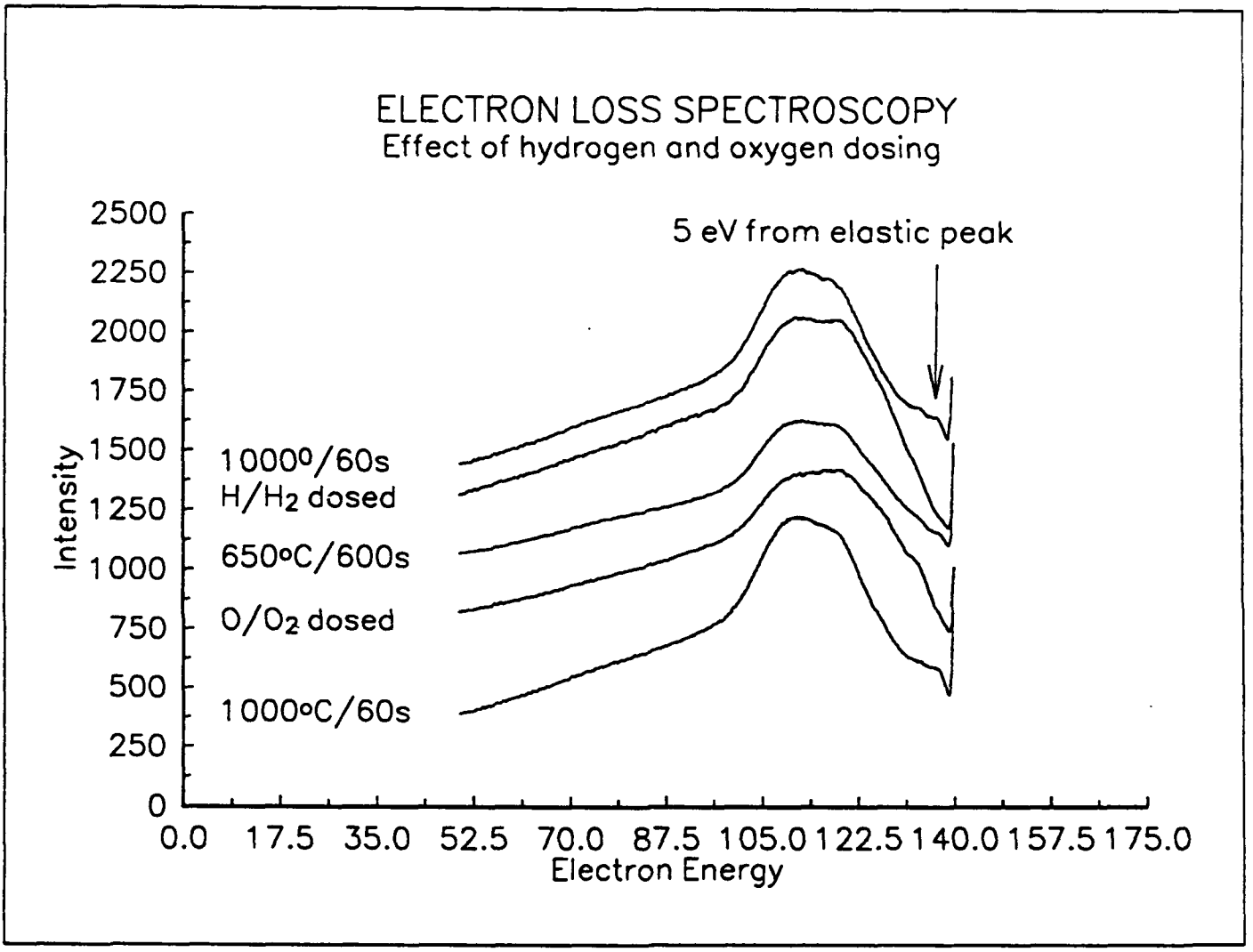
ELECTRON LOSS SPECTROSCOPY
Effect of hydrogen and oxygen dosing
5 eV from elastic peak
Intensity
2500
2250
2000
1750
1500
1250
1000
750
500
250
0
1000°/60s
H/H2 dosed
650°C/600s
O/O2 dosed
1000°C/60s
0.0 17.5 35.0 52.5 70.0 87.5 105.0 122.5 140.0 157.5 175.0
Electron Energy

Figure 3.2

4.0 Diamond Single Crystal Platelet Technology
(Dr. N. Parikh, Dr. M. Swanson, UNC)

As mentioned in previous reports, one strategy for obtaining a large-area diamond single crystal is to create a large-area template and then replicate it in some fashion. One scenario previously proposed by RTI is shown in Figures 4.1 and 4.2. UNC Chapel Hill has been an important link between this program and the high energy ion implantation facility at Oak Ridge National Laboratory (contact: C.W. White). A report detailing studies by UNC and a jointly authored manuscript describing the details and utility of this concept are attached.

MASTER TEMPLATE PRODUCTION

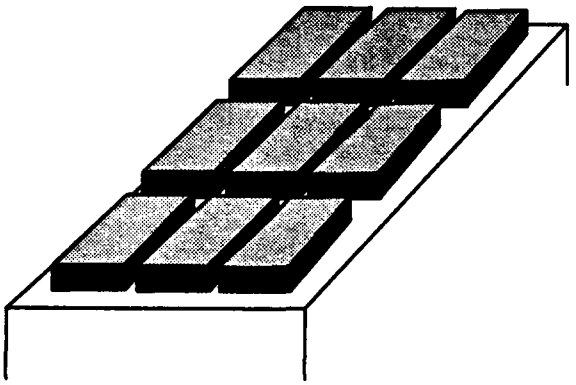

Step 1. Epitaxial bonding of diamond single crystals to host single crystal.

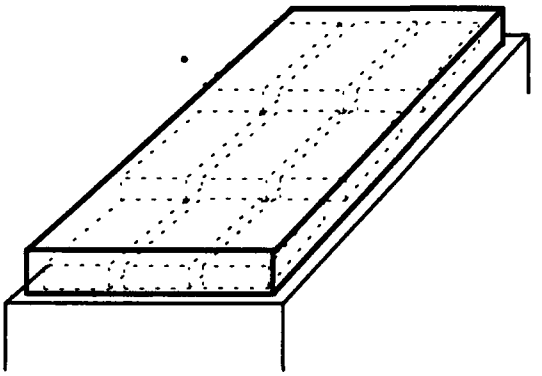

Step 2. Homoepitaxial growth to overgrow individual diamonds and create one large area diamond single crystal template.

Figure 4.1

LARGE-AREA REPLICATION FROM MASTER TEMPLATE

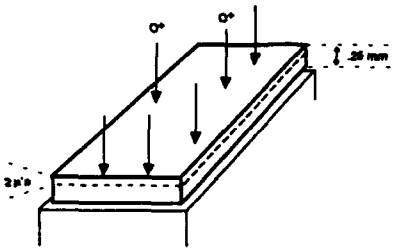

Step I. O^+ implantation to create single crystal diamond seed layer.

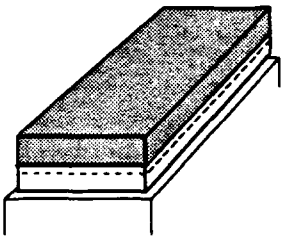

Step II. Bonding of seed layer to support.

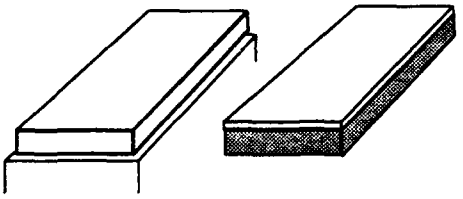

Step III. Vacuum anneal to release diamond seed layer.

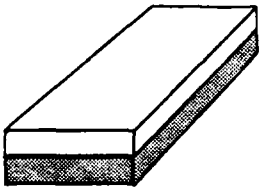

Step IV. Homoepitaxial growth on diamond seed layer to desired thickness.

Figure 4.2

Ion Implantation for Lift-off of Diamonds

Abstract

We have developed a method for removing thin, large area sheets of diamond from bulk or homoepitaxial diamond crystals. This method consists of an ion implantation step, followed by a selective etching procedure. High energy (4 to 5 MeV) carbon and oxygen ions of a suitable dose (10^{17}-10^{18} cm^{-2}), were implanted to create a well-defined layer of damaged diamond that is buried at ~2 μm below the surface. The preferential etching of the buried layer (graphitic) is achieved by annealing in flowing oxygen. The lifted plates have been analyzed by Rutherford backscattering/ channeling and Raman spectroscopy techniques to check the quality. This lift-off method, combined with well-established homoepitaxial growth processes, has considerable potential for the fabrication of large area single crystalline diamond sheets.

Background, Motivation and Objective

An essential hurdle yet to be cleared, before one can fabricate diamond electronic devices, is the creation of large area, flat, single crystalline diamond layers. A very promising beginning has been made by Pryor et al.[1], who have shown that homoepitaxial diamond layers can be grown by chemical vapor deposition onto a matrix of oriented diamond microcrystallites, which are imbedded in an array of etch pits on a Si substrate. However, this method is both costly and time-consuming, and the crystallites are only poorly oriented, thus causing low angle grain boundaries We propose to combine homoepitaxial growth with lift-off technology to permit large area diamond sheets to be economically fabricated from a master template. For example, such diamond films could be fabricated by placing together several small diamond crystals on which one then deposits a single crystalline layer; and then removing thin sheets of single crystalline diamond from the surface using a lift-off process. In this way, a large diamond template could be fabricated, from which large diamond sheets could be removed ad infinitum.

Results and Discussion

In our lift-off method, we have used ion implantation to create a buried damaged layer in a polished bulk diamond crystal, and then removed that damaged layer by selective etching, thus lifting a thin sheet of diamond from the surface[2]. The fundamental concepts of the method are the following. (a.) Most of the damage caused by ion implantation occurs at the end of the ion range, and thus is confined to a buried layer of material at a controllable depth. (b.) The damaged layer can be graphitized by annealing, and the graphitized layer has sharp boundaries because of the well-defined critical damage density necessary for conversion of diamond to graphite [3,4]. (c.) The graphitic layer can be preferentially etched at a much more rapid rate than that of the adjacent diamond.

The depth profile of ion beam damage can be calculated using Monte Carlo computer programs, such as TRIM[5]. Because high energy ions lose most of their energy via electronic collisions, there is relatively little damage near the surface of an ion-implanted sample. The damage is confined to a relatively narrow buried region near the end of the ion range, where the ions lose most of their energy via nuclear collisions. Thus, by varying the initial ion energy, the depth of the buried damaged layer can be controlled. The thickness of the buried damaged layer is almost independent of the ion energy. Consequently, a buried thin layer of graphite can be created in diamond by ion implantation followed by low temperature annealing.

Natural diamond type Ia and IIa crystals, in the form of polished thin plates 2x2 or 3x3 or 4x4 mm areal dimensions and 0.25 mm thick (from Dubbeldee Harris Diamond Corp.), were implanted with C+ or O^+ ions to doses of 10^{17}-10^{18} cm^{-2} at energies of 4 and 5 MeV respectively. The range of these MeV C+ and O^+ are 2.0 μm and 1.86 μm, respectively and the straggling is about ~0.05 μm. The highest dose was chosen for oxygen to give a peak concentration equal to the concentration of host C atoms in the graphitic layer. The implanted samples were annealed in flowing oxygen to lift-off the top plate. The samples were examined by both optical and scanning electron microscopy to monitor the etching. Rutherford backscattering/channeling and Raman spectroscopy techniques were employed to characterize the lifted piece.

One set of samples was implanted with 4 MeV C^+ ions to a fluence of $6 \cdot 10^{16}$ cm^{-2}, with the substrate at a temperature of approximately 80K. These samples were annealed in a vacuum of approximately 10^{-6} Torr for 30 min at 950°C to graphitize the buried damaged layers, and then annealed at successively higher temperatures in air to selectively etch the graphitized layers. A sample that was annealed for 2 h in air at 550°C showed undercutting of the diamond surface layer by about 9-13 mm from the edges, as demonstrated by interference fringes caused by an air gap between the partially under-cut surface layer and the substrate. The etching rate at 550°C was ~ 5-10 μm/h for the first 4 h. After ~ 20 μm had been undercut, the rate decreased markedly with time. Presumably the etch rate was limited by the penetration of the O_2 in from the edge, and/or by removal of the reaction products CO_x out of the constricted layer. The etching rate at 600°C was higher than at 550°C, but the diamond overlayer was also slowly etched at that temperature.

A second set of samples was implanted with 4 MeV C^+ ions to a fluence of $1 \cdot 10^{18}$ cm^{-2}, also with the substrate at 80 K. These samples were annealed in flowing oxygen at 550°C for 1 h. This annealing produced a partially under-cut surface layer, again shown by interference fringes. This sample was then annealed at 550°C for 4 more hours in flowing oxygen. The diamond overlayer had separated when the sample was removed from the furnace, demonstrating

that complete lift off required less than five hours at 550°C in flowing oxygen. Both the lifted-off plate and the diamond substrate are shown in Fig. 3. The lifted plate (on the bottom) is darker than the diamond substrate (on the top). Since darker coloring indicates more irradiation defects, this effect demonstrates that the maximum depth of ion implantation has a sharp cut-off; hence the diamond crystal template has less damage. The line near the edge of both the lifted-off layer and the substrate corresponds to the etching depth after the first hour (about 120μm). The black areas on both the lifted plate and the substrate are unetched graphite.The etching rate at 550°C was determined to be between 120 μm and 140 μm/h, which is much greater than that for the lower dose C-implanted sample described previously.

Fig. 3 Optical Micrograph of a lifted-off diamond layer. The lift-off was achieved by implantation with 5 MeV O^+ ions to a fluencies of $3 \cdot 10^{17}$ cm^{-2}, followed by annealing in flowing oxygen at 550 °C for 1 hr.

Several samples were implanted at ~80K with 5 MeV ^{16}O ions to fluences of 10^{17} to 10^{18} cm^{-2}. The highest dose was chosen to give a peak oxygen concentration equal to the concentration of host C atoms in the graphitic layer. One of the 10^{18} cm^{-2} samples was annealed at 950°C for 1 h in vacuum. Most of the diamond overlayer flaked off the surface (Fig.4), presumably because of the high pressure from the reaction products CO and CO_2 at high temperature . A unique mesa structure resulted, as shown in Fig 4a, where well-defined cleavage plane traces are visible. A scanning electron micrograph of one of the remaining pieces on the surface is shown in Fig. 4b. Here residual graphitic layers are visible both on the sample surface

and on the underside of the undercut diamond layer. One method by which this unwanted graphite can be removed is by annealing in flowing oxygen.

A second 4x4 mm diamond sample that had been implanted to 10^{18} O cm^{-2} was etched in flowing oxygen at 550°C for 1 h. Most of the 4x4 mm layer of diamond was removed in one piece, but it broke into 3 pieces while being handled. One of the pieces (4x1.5 mm) was then annealed in vacuum (10^{-5} Torr) at 950°C for 1 h to remove the residual damage. This annealing increased the transparency of the lifted diamond, leaving it curled with a translucent brownish hue, as shown in the SEM micrograph (Fig. 5).

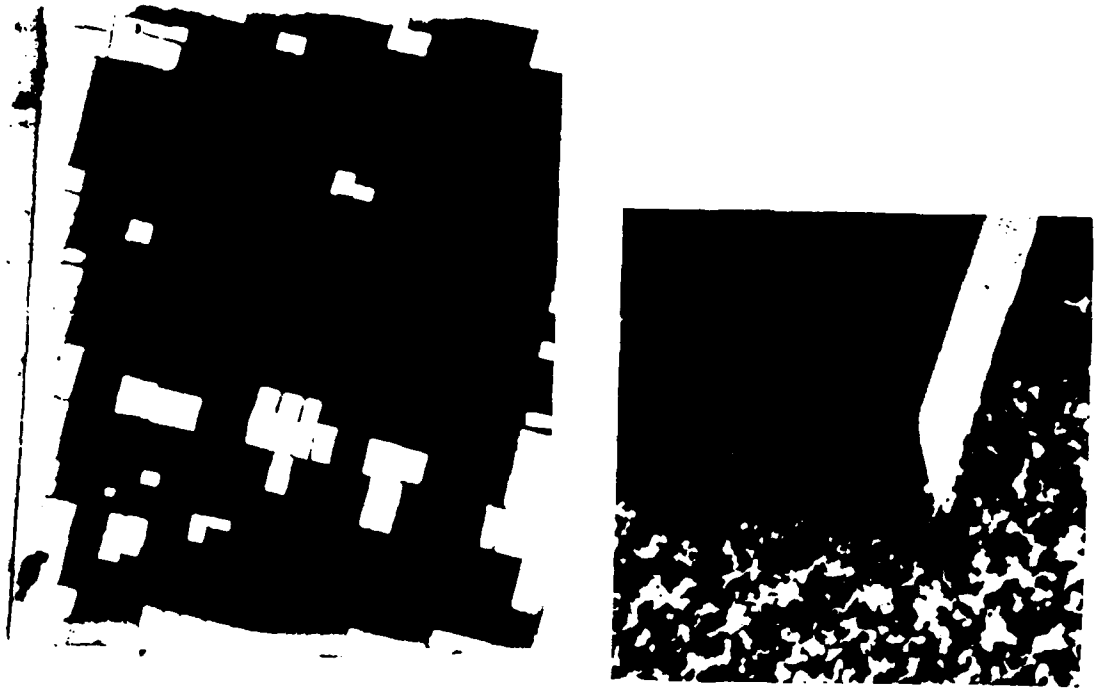

Fig. 4 (a.) Optical micrograph of a diamond crystal after implantation with 5 MeV O ions to a fluence of 10^{18} cm^{-2}, followed by annealing at 950°C for 1 h in vacuum. Most of the overlayer was lost, but a few rectangular-shaped pieces of the overlayer remained, and are seen as bright areas in the photograph. (b.) Scanning electron micrograph of one edge of a piece of diamond overlayer from the sample of Fig. 2(a.). The thickness of the layer was 2 mm.

To determine the minimum dose of oxygen needed to lift off a diamond layer, single crystals were implanted with 5 MeV $^{16}O^{+}$ to fluences of $1 \cdot 10^{17}$, $3 \cdot 10^{17}$, and $7 \cdot 10^{17}$ cm^{-2} at 80 K. A dose of $1 \cdot 10^{17}$ cm^{-2} was not sufficient to amorphize the diamond or to cause lift-off. However, successful lift-off was achieved for a dose of 3.10^{17} cm^{-2}. The sample was annealed

in flowing oxygen for 4 h at 550o C. The top layer, which lifted off in one piece, was darker than the diamond substrate, as in Fig. 3. Once again, the central part of the lifted layer appeared black, because of unburnt residual graphite. The $3 \cdot 10^{17}$ cm^{-2} fluence should produce a Frenkel defect concentration of ~10 % in the near-surface layer[5], which is close to the damage concentration that is completely recoverable, according to our earlier annealing results[4]. To avoid the curling of the lifted diamond layer, it would be necessary to deposit a thick (~10 μm) homoepitaxial layer before the lift-off in order to endow the top layer with greater mechanical strength.

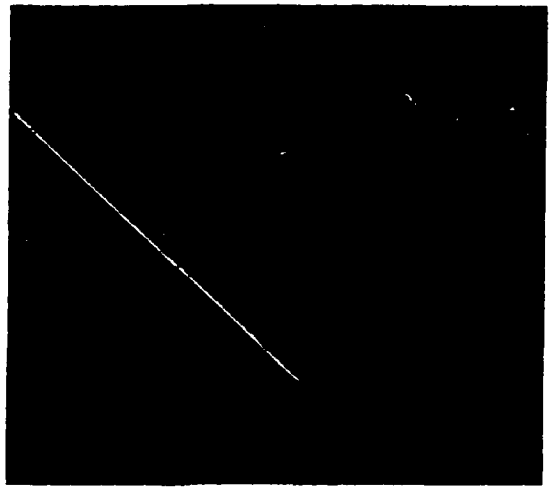

0.5 mm

Fig. 5 Scanning Electron Micrograph of a lifted-off diamond layer. The lift-off was achieved by implantation with 5 MeV O ions to a fluence of 10^{18} cm^{-2}, followed by annealing in flowing oxygen at 550°C for 1 h The sample was then vacuum annealed at 950°C for 1 h to remove radiation damage

The implanted pieces were analyzed to measure near surface damage by Rutherford backscattering/channeling and Raman spectroscopy. RBS/channeling analysis, using 1.5 MeV H^+,was performed on an as implanted diamond (10^{17}.cm^{-2} O^+ at 80 K) and annealed after rapid thermal annealing to 1000 °C for 90 sec. Fig 6 shows the channeled spectra of the virgin, as implanted and annealed diamond crystal in relation to a random, non-channeled, yield. It can be seen that the channeling yield after annealing drops at the surface indicating damage recovery is occuring, however it does not go back to the virgin level. High dechanneling present in the as implanted and annealed diamond is probably mostly due to distortion of the lattice because of high dose implant and not due to extended defects which are created during implantation at higher temperature. The peak near 900 keV is due to buried oxygen (1.85 μm deep).

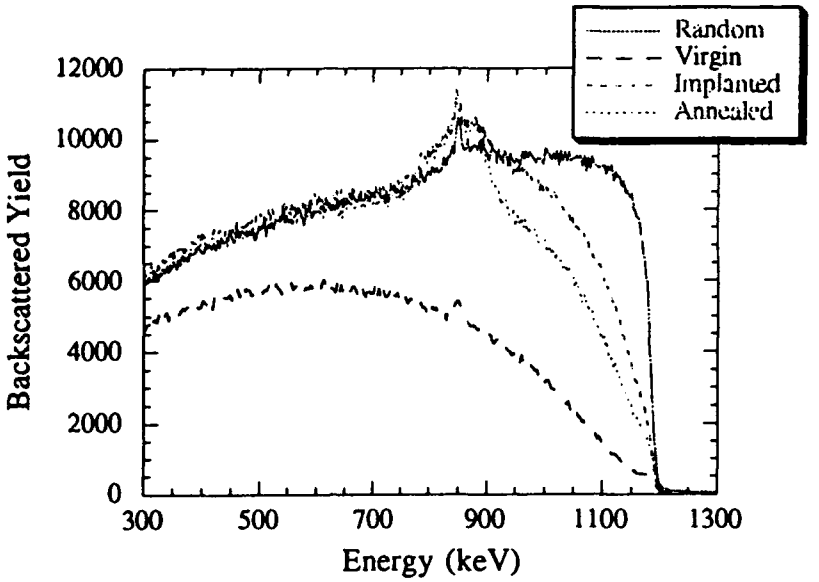

Fig. 6: RBS/Channeling spectra of random, virgin, as implanted and RTA annealed diamond crystal.

Raman spectrum for a sample implanted with $1 \cdot 10^{17}$ O/cm^2 at 5 MeV is shown in Fig. 7. The diamond line at 1332 cm^{-1} is still evident but the intensity has dropped, indicating the influence of the damaged layer.

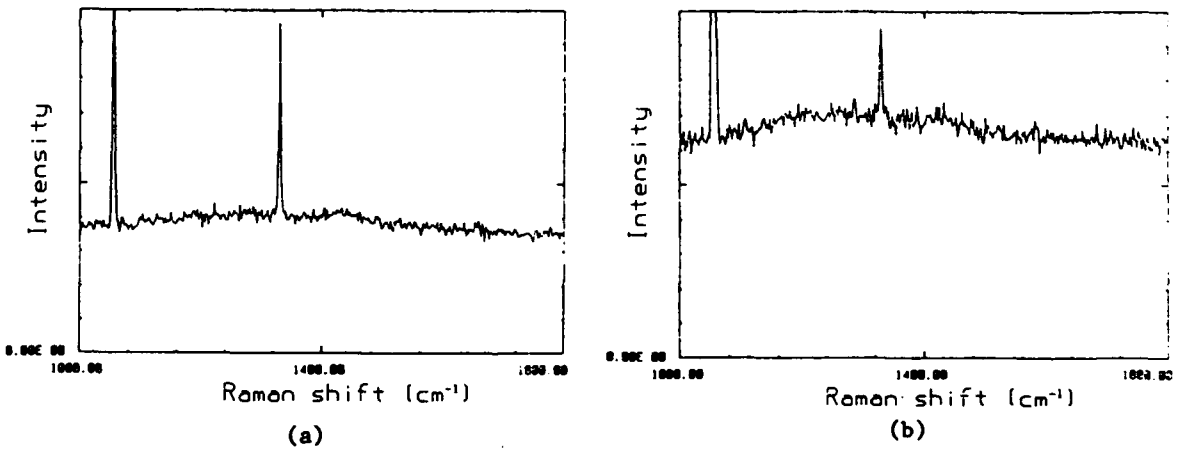

Fig. 7 Micro Raman of 5 MeV O(1.10^{17} cm^{-2}) implanted diamond (a) Back side (b) implanted side

Summary

We have demonstrated that square millimeter-sized areas of diamond can be lifted off intact from natural diamond crystals through a technique combining implantation and selective etching. Both 4 MeV C implantation, followed by selective etching in oxygen or in chromic acid, and 5 MeV O implantation, followed by vacuum annealing and/or annealing in O_2, were used. Sheets up to 4x4 mm in size were lifted off by the implantation method.

Acknowledgements

The authors acknowledge the technical assistance of Dale Hensley, and support from SDIO funds administered by ONR (contract No. N00014-92-C-0081). Research at the Oak Ridge National Laboratory was sponsored by the Division of Materials Science, U.S. Dept. of Energy, under contract DE-AC05-840R21400 with Martin Marietta Energy Systems, Inc. Partial support was received from SURA/ ORAU/ ORNL 1992 Cooperative program.

Conference Presentations

(1) Nalin Parikh, John Hunn, Elliot McGucken, Max Swanson, Woody White, Ron Rudder, Dave Malta, John Posthill, Robert Marcunas, "Ion Beam Applications for Diamond Growth and Lift-Off", Ion Beam Modification of Materials 1992, Heidelberg, Germany, Sept.5-12, 1992.

(2) Nalin Parikh "Ion Beam and Laser Assisted Processing of Diamond Single Crystals and Thin Films", Twelfth International Conference on the Application of Accelerators in Research and Industry, November 2-5, 1992, Denton, Texas. (Invited presentation)

Publications

(1) N.R. Parikh, J.D. Hunn, E. McGucken, M.L. Swanson, C.W. White, R.A. Rudder, D.P. Malta, J.B. Posthill, R.J. Marcunas, "Single Crystal Diamond Plate Lift-Off Achieved by Ion Implantation and Subsequent Annealing", Accepted for publication in Applied Physics Letters.

[1] R.W. Pryor, M.W. Geis, and H.R. Clark, Mat. Res. Soc. Symp. Proc. **242** (1992): to be published (Symp. G, Boston, 1991).

[2] J.D. Hunn and N.R. Parikh, unpublished research (patent disclosure, 1992).

[3] G. Braunstein, A. Talmi, R. Kalish, T. Bernstein and R. Beserman, Radiat. Eff. **48**, 138 (1980).

[4] J.D. Hunn, M.L. Swanson, E.A. Hill, N.R. Parikh and G. Hudson, in "New Diamond Science and Technology", eds. R. Messier et al. (MRS, Pittsburgh, 1991) p. 929.

[5] J.F. Ziegler, "Transport of Ions in Matter" (TRIM), IBM Corp. software (1991).

gle-crystal diamond plate liftoff achieved by ion implantation l subsequent annealing

N. R. Parikh, J. D. Hunn, E. McGucken, and M. L. Swanson
University of North Carolina, Chapel Hill, North Carolina 27599-3255

C. W. White
Oak Ridge National Laboratory, Oak Ridge, Tennessee 37831-6048

R. A. Rudder, D. P. Malta, J. B. Posthill, and R. J. Markunas
Research Triangle Institute, Research Triangle Park, North Carolina 27709-2194

(Received 7 August 1992; accepted for publication 18 October 1992)

We describe a new method for removing thin, large area sheets of diamond from bulk or homoepitaxial diamond crystals. This method consists of an ion implantation step, followed by a selective etching procedure. High energy (4–5 MeV) implantation of carbon or oxygen ions creates a well-defined layer of damaged diamond that is buried at a controlled depth below the surface. For C implantations, this layer is graphitized by annealing in vacuum, and then etched in either an acid solution, or by heating at 550–600 °C in oxygen. This process successfully lifts off the diamond plate above the graphite layer. For O implantations of a suitable dose (3×10^{17} cm^{-2} or greater), the liftoff is achieved by annealing in vacuum or flowing oxygen. In this case, the O required for etching of the graphitic layer is also supplied internally by the implantation. This liftoff method, combined with well-established homoepitaxial growth processes, has considerable potential for the fabrication of large area single crystalline diamond sheets.

.n essential hurdle yet to be cleared, before one can ate diamond electronic devices, is the creation of area, flat, single crystalline diamond layers. A very ising beginning has been made by Pryor *et al.*,[1] who shown that homoepitaxial diamond layers can be ı by chemical vapor deposition onto a matrix of ori- diamond microcrystallites, which are imbedded in an of etch pits on a Si substrate. However, this method h costly and time-consuming, and the crystallites are ɔoorly oriented, thus causing low angle grain bound- We propose to combine homoepitaxial growth with technology to permit large area diamond sheets to be mically fabricated from a master template. For ex-, such diamond films could be fabricated by tiling ıer several small diamond crystals on which one then its a single crystalline layer; and then removing thin of single crystalline diamond from the surface using ɔff process. In this way, a large diamond template be fabricated, from which large diamond sheets be removed ad infinitum. In this letter, we shall de- the use of ion implantation to lift thin sheets of ɔnd from a single-crystal substrate.

ı our liftoff method, we have used ion implantation to a buried damaged layer in a polished bulk diamond ıl, and then removed that damaged layer by selective ıg, thus lifting a thin sheet of diamond from the sur- The fundamental concepts of the method are the fol- g. (a) Most of the damage caused by ion implanta- ccurs at the end of the ion range, and thus is confined ɔuried layer of material at a controllable depth. (b) lamaged layer can be graphitized by annealing, and raphitized layer has sharp boundaries because of the lefined critical damage density necessary for conver- ıf diamond to graphite.[2,3] (c) The graphitic layer can be preferentially etched at a much more rapid rate than that of the adjacent diamond.

It is known[2,3] that ion beam damage caused by carbon implantation at low temperatures in diamond can be divided into four general regimes.

(i) At low doses ($<1.5\times10^{15}$ C^+ ions/cm^2 at 100 keV, corresponding to a Frenkel defect concentration of ~7%), the damage is almost completely recoverable by thermal annealing at about 900 °C in vacuum.

(ii) At doses between 1.5×10^{15} and 1×10^{16} C^+ ions/cm^2 at 100 keV, a stable damaged diamond structure (green diamond[3]) may be formed by annealing at 950 °C.

(iii) At doses greater than about 10^{16} C^+ ions/cm^2 at 100 keV, the damaged diamond is graphitized by thermal annealing at moderate temperatures (about 600 °C).

(iv) At very high doses, diamond is spontaneously graphitized. It should be noted, however, that diamond is much more resistant to such graphitization when the damaged layer is buried, perhaps because of the constraint on expansion due to the relatively undamaged overlying diamond.[4]

The depth profile of ion beam damage can be calculated using Monte Carlo computer programs, such as TRIM.[5] Because high energy ions lose most of their energy via electronic collisions, there is relatively little damage near the surface of an ion-implanted sample. The damage is confined to a relatively narrow buried region near the end of the ion range, where the ions lose most of their energy via nuclear collisions. Thus, by varying the initial ion energy, the depth of the buried damaged layer can be controlled. The thickness of the buried damaged layer is almost independent of the ion energy. Consequently, a buried thin layer of graphite can be created in diamond by ion implantation followed by low-temperature annealing.

 0003-6951/92/513124-03$06.00

Selective etching of the graphitic layer can be achieved by several methods.

(1) Since a hot chromic-sulfuric acid solution etches graphite much more rapidly than diamond, it is apparent that liftoff could be achieved by the graphitizing of a buried layer followed by an acid etch. However, the penetration of the acid into the narrow graphitic layer may be slow.

(2) The graphitic layer can be etched by annealing in an oxygen atmosphere,[6] i.e., burning the graphite to form CO or CO_2.

(3) In method (2), the oxygen must be supplied via diffusion from the edge of the sample. However, if the implanted species is oxygen, the implantation serves the dual role of creating the damaged layer and providing the required oxygen for etching.

Natural diamond types Ia and IIa crystals, in the form of polished thin plates 2×2 or 3×3 or 4×4 mm areal dimensions and 0.25 mm thick (from Dubbeldee Harris Diamond Corp.), were implanted with C^+ or O^+ ions to doses of 6×10^{16} cm^{-2}–10^{18} cm^{-2} at energies of 4–5 MeV. The ranges for 4 MeV C^+ and 5 MeV O^+ are 1.95 and 1.86 μm, and the straggling 0.07 and 0.05 μm, respectively. The C implanted samples were annealed in vacuum to graphitize the damaged layers, and then annealed in air or flowing oxygen. Some samples were etched in a chromic-sulphuric acid solution. The O implanted samples were annealed in vacuum at 500–900 °C to form CO_x in the damaged layer, and in some cases a further anneal in O_2 was used to complete the liftoff process. The samples were examined by both optical and scanning electron microscopy to monitor the etching.

One set of samples was implanted with 4 MeV C^+ ions to a fluence of 6×10^{16} cm^{-2}, with the substrate at a temperature of approximately 80 K. These samples were annealed in a vacuum of approximately 10^{-6} Torr for 30 min at 950 °C to graphitize the buried damaged layers, and then annealed at successively higher temperatures in air to selectively etch the graphitized layers. A sample that was annealed for 2 h in air at 550 °C showed undercutting of the diamond surface layer by about 9–13 μm from the edges, as demonstrated by interference fringes caused by an air gap between the partially undercut surface layer and the substrate. The etching rate at 550 °C was ~5–10 μm/h for the first 4 h. After ~20 μm had been undercut, the rate decreased markedly with time. Presumably the etch rate was limited by the penetration of the O in from the edge, and/or by removal of the reaction products CO_x out of the constricted layer. The etching rate at 600 °C was higher than at 550 °C but the diamond overlayer was also slowly etched at that temperature.

After the 950 °C vacuum anneal, one of these samples was etched in hot chromic-sulphuric acid, which also caused undercutting by removal of the graphitic layer. A 5 min etch gave an undercut depth of 0.35 μm, and the overlying natural diamond layer was 2 μm thick.

A second set of samples was implanted with 4 MeV C^+ ions to a fluence of 1×10^{18} cm^{-2}, also with the substrate at 80 K. These samples were annealed in flowing oxygen at 550 °C for 1 h. This annealing produced a partially undercut surface layer, again shown by interference fringes. This sample was then annealed at 550 °C for 4 more hours in flowing oxygen. The diamond overlayer had separated when the sample was removed from the furnace, demonstrating that complete liftoff required less than 5 h at 550 °C in flowing oxygen. Both the lifted-off plate and the diamond substrate are shown in Fig. 1. The lifted plate (on the right) is darker than the diamond substrate (on the left). Since darker coloring indicates more irradiation defects, this effect demonstrates that the maximum depth of ion implantation has a sharp cutoff; hence the diamond crystal template has less damage. The line near the edge of both the lifted-off layer and the substrate corresponds to the etching depth after the first hour (about 120 μm). The black areas on both the lifted plate and the substrate are unetched graphite. The etching rate at 550 °C was determined to be between 120 and 140 μm/h, which is much greater than that for the lower dose C implanted sample described previously.

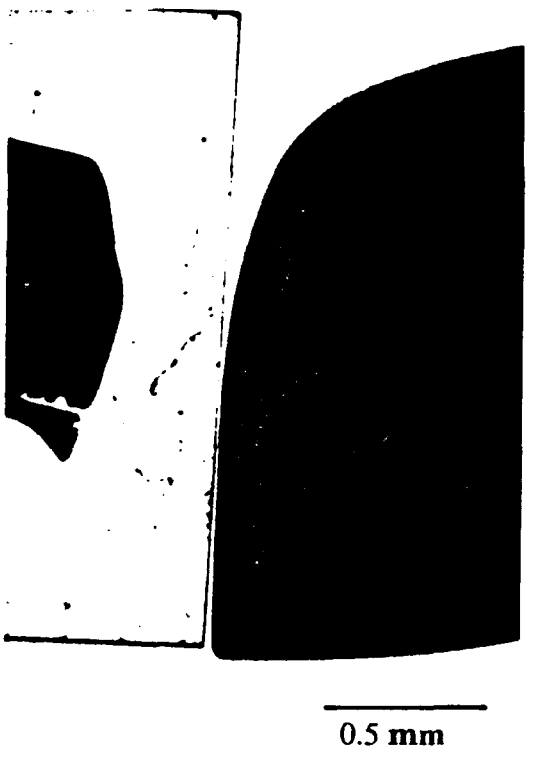

FIG. 1. Optical micrograph of lifted-off diamond layer (on the right) beside the original diamond crystal template (on the left). This liftoff was achieved by an implantation of 4 MeV C ions to a fluence of 1×10^{18} cm^{-2}, followed by an anneal at 550 °C for 5 h in flowing oxygen.

Several samples were implanted at ~80 K with 5 MeV ^{16}O ions to fluences of 10^{17}–10^{18} cm^{-2}. The highest dose was chosen to give a peak oxygen concentration equal to the concentration of host C atoms in the graphitic layer. One of the 10^{18} cm^{-2} samples was annealed at 950 °C for 1 h in vacuum. Most of the diamond overlayer flaked off the surface (Fig. 2), presumably because of the high pressure from the reaction products CO and CO_2 at high temperature. A unique mesa structure resulted, as shown in Fig. 2(a), where a well-defined cleavage plane traces are visible.

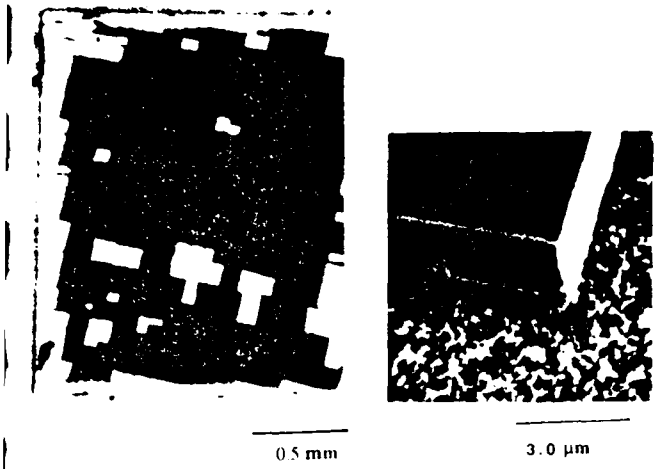

FIG. 2. (a) Optical micrograph of a diamond crystal after implantation with 5 MeV O ions to a fluence of 10^{18} cm^{-2}, followed by annealing at 950 °C for 1 h in vacuum. Most of the overlayer was lost, but a few rectangular-shaped pieces of the overlayer remained, and are seen as bright areas in the photograph. (b) Scanning electron micrograph of one edge of a piece of diamond overlayer from the sample of Fig. 3(a). The thickness of the layer was 2 μm.

A scanning electron micrograph of one of the remaining pieces on the surface is shown in Fig. 2(b). Here residual graphitic layers are visible both on the sample surface and on the underside of the undercut diamond layer. One method by which this unwanted graphite can be removed is by annealing in flowing oxygen.

A second 4×4 mm diamond sample that had been implanted to 10^{18} O ions/cm^2 was etched in flowing oxygen at 550 °C for 1 h. Most of the 4×4 mm layer of diamond was removed in one piece, but it broke into 3 pieces while being handled. One of the pieces (4×1.5 mm) was then annealed in vacuum (10^{-5} Torr) at 950 °C for 1 h to remove the residual damage. This annealing increased the transparency of the lifted diamond, leaving it curled with a translucent brownish hue, as shown in the SEM micrograph (Fig. 3).

To determine the minimum dose of oxygen needed to lift off a diamond layer, single crystals were implanted with 5 MeV $^{16}O^+$ to fluences of 1×10^{17}, 3×10^{17}, and 7×10^{17} cm^{-2} at 80 K. A dose of 1×10^{17} cm^{-2} was not sufficient to amorphize the diamond or to cause liftoff. However, successful liftoff was achieved for a dose of 3×10^{17} cm^{-2}. The sample was annealed in flowing oxygen for 4 h at 550 °C. The top layer, which lifted off in one piece, was darker than the diamond substrate, as in Fig. 1. The 3×10^{17} cm^{-2} fluence should produce a Frenkel defect concentration of ~10% in the near-surface layer,[5] which is close to the damage concentration that is completely recoverable, according to our earlier annealing results.[3] To avoid the curling of the lifted diamond layer, it would be necessary to deposit a thick (~10 μm) homoepitaxial layer before the liftoff in order to endow the top layer with greater mechanical strength.

FIG. 3. Scanning electron micrograph of a lifted-off diamond layer. The liftoff was achieved by implantation with 5 MeV O ions to a fluence of 10^{18} cm^{-2}, followed by annealing in flowing oxygen at 550 °C for 1 h. The sample was then vacuum annealed at 950 °C for 1 h to remove radiation damage.

We have demonstrated that square millimeter-sized areas of diamond can be lifted off intact from natural diamond crystals through a technique combining implantation and selective etching. Both 4 MeV C implantation, followed by selective etching in oxygen or in chromic acid, and 5 MeV O implantation, followed by vacuum annealing and/or annealing in O_2, were used. Sheets up to 4×4 mm in size were lifted off by the O implantation method.

The authors acknowledge the technical assistance of Dale Hensley, and support from SDIO funds administered by ONR (Contract No. N00014-92-C-0081). Research at the Oak Ridge National Laboratory was sponsored by the Division of Materials Science, U. S. Dept. of Energy, under contract DE-AC05-840R21400 with Martin Marietta Energy Systems, Inc. Partial support from SURA/DRAU/ORNL 1992 Summer Cooperative Program.

[1] R. W. Pryor, M. W. Geis, and H. R. Clark, Mater. Res. Soc. Symp. Proc. **242** (1992).
[2] G. Braunstein, A. Talmi, R. Kalish, T. Bernstein, and R. Beserman, Radiat. Eff. **48**, 138 (1980).
[3] J. D. Hunn, M. L. Swanson, E. A. Hill, N. R. Parikh, and G. Hudson, in *New Diamond Science and Technology*, edited by R. Messier (MRS, Pittsburgh, 1991), p. 929.
[4] G. S. Sandhu, B. Liu, N. R. Parikh, J. D. Hunn, M. L. Swanson, Th. Wichert, M. Deicher, H. Skudlik, W. N. Lennard, and I. V. Mitchell, Mater. Res. Soc. Symp. Proc. **162**, 189 (1990).
[5] J. F. Ziegler, Transport of Ions in Matter (TRIM), IBM Corp. software (1991).

5.0 Diamond Bonding and Consolidation

The need for a large-area diamond single crystal template has driven further progress in this area. We ordered and received (in the last quarter of this phase) several 3x3 mm diamond single crystals which have edges and faces oriented and polished on (100) planes (± 2°) and have begun to use these to fabricate initial tiled arrays. Critical to the success of this part of the program is the ability to meet several technological criteria simultaneously. Some of these criteria are:

1. The diamonds must be held closely together to minimize the amount of overgrowth necessary for consolidation.

2. The face of the diamond tiled array must be relatively flat so as to minimize the amount of diamond growth required for planarization.

3. The bonding scheme must be compatible with the chosen diamond growth process (growth temperature, cool-down, etc.)

4. The bonding scheme must preserve (or at least enable recovery of) the diamond single crystal surfaces such that good quality homoepitaxial diamond can nucleate and grow.

5. Finally, the bonding scheme must give consideration to the crystallographic alignment between diamond tiles to minimize dislocation densities at the "seams". Methods of checking the crystallographic alignment (non-destructively) and assessing the dislocation densities at seams must be used to establish the viability of any tiling technique.

5.1 Initial Experiments on Ni(100)

As Ni has been demonstrated to grow epitaxially on diamond and to be quite adherent, it was believed that it could be used as a single-crystal bonding layer to another crystal, which itself could be Ni. To begin to show viability of this concept, heteroepitaxial Ni was MBE grown on a C(100) crystal to a thickness of ~ 130 nm (Figure 5.1). SEM and RBS/channeling showed the Ni epilayer to be smooth and the Ni layer to be single crystal and of reasonable crystallographic quality ($X_{min} = 3\%$).

Next, to show the possibility of bonding Ni-coated diamonds, ~ 3.5 μm of heteroepitaxial Ni was grown on 2 C(100) crystals simultaneously. An "annealing press" was constructed of materials of different coefficient of thermal expansion such that when heated, a compressive load was placed any sample located in it. The 2 Ni epi coated C(100) crystals were placed in this annealing press with Ni-coated sides facing each other. By heating this assembled annealing press it was anticipated that the simultaneous application of a compressive load and elevated temperature would enable the 2 Ni-coated diamonds to diffusion bond together. Indeed, after subjecting it to 900°C for 30 minutes in an inert atmosphere, the 2 diamonds were bonded very strongly together, (Figure 5.2). Even after post-bonding cleaving to obtain SEM cross-section micrographs, the C/Ni-Ni/C bond did not fail. However, the diamonds themselves did show damage immediately after removal from the annealing press, and different materials were chosen for the annealing press to reduce the total compressive strain experienced by the sample upon excursion to 900°C.

Bonding was next attempted to a Ni(100) single crystal. 100 nm of heteroepitaxial Ni was grown on 2 edge-oriented and polished C(100) crystals (all faces and sides oriented to (100)-type planes). These crystals were then placed on a specially prepared Ni(100) crystal, which had the [010] direction scribed onto it using back reflection lane x-ray diffraction to locate the crystallographic direction. The [010] edges

Ni Heteroepitaxy on Diamond (100)

Sequence:
1. Load type Ia C(100) into MBE
2. Desorption/anneal at 900°C, 20 min.
3. Lower temperature for growth to 430°C
4. Deposit Ni at 1 Å - sec^{-1}

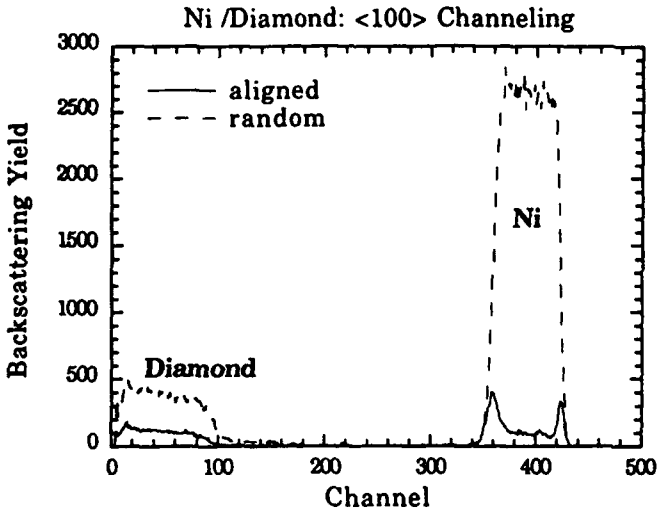

Good Ni Crystallinity
$\chi_{min} = 3\%$; $\chi_{int} = 15\%$
thickness = 1280 Å

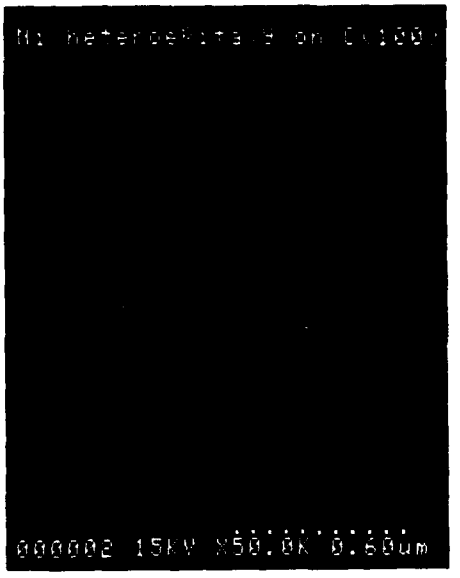

Excellent Topography

Figure 5.1

Diamond/Diamond Bonding Using Nickel

Sequence:
1. Ni MBE on each diamond face
2. Load into annealing press
3. Subject to 900°C, 30 min. in compression.

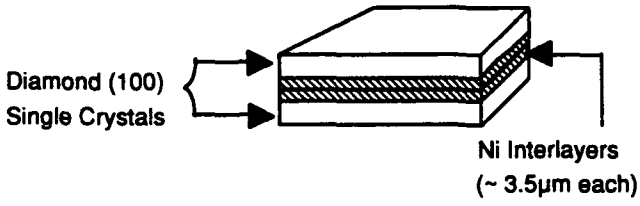

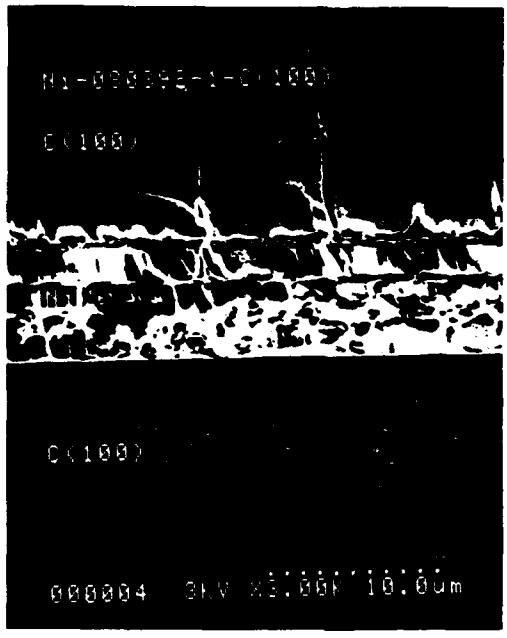

Cleaved Cross-Section Showing Diamond/ Diamond Bond Which Did Not Fail

Figure 5.2

of the Ni-coated diamond (100) crystals were aligned with the [010] scribe on the Ni(100) surface, while the diamonds were placed in dose proximity to each other. This assemblage (shown schematically in Figure 5.3) was placed in the annealing press and subjected to 900°C for 30 minutes.

The Ni-coated diamonds bonded to the Ni(100) crystal, as shown in Figures 5.3, 5.4, and 5.5. A slight off-set of the 2 crystals is evident due to the difficulty of placing the crystals in alignment by hand; no locating fixture was used for this experiment. We are impressed by the fact that, even with this crude placement technique, that the crystals were separated by only ~ 10 μm (Figure 5.5). The bonding was, again, found to be quite robust as these crystals stayed together after substantial shock to the assemblage and after surface polishing.

An attempt to overgrowth/join these crystals by growth of diamond was not successful. One crystal broke loose from the Ni substrate shortly after removal from the diamond reactor even though this time the sample was handled with greater care. Hence, several successes and deficiencies were identified from these initial experiments. In the next set of bonding experiments, issues of using a locating fixture and a substrate with a closer coefficient of thermal expansion (CTE) match to diamond were examined.

5.2 Bonding and Consolidation on Si(100)

It was also decided to separate the magnitude of the compressive load applied to the diamonds from the temperature chosen for bonding. A new annealing furnace was also constructed which enabled real time viewing of the arrayed diamonds. While Ni-coating of diamonds was continued to the initial success with that form of interlayer, the single crystal substrate was changed to Si(100). This made the substrate more easily available and cheaper, as well as enabling a closer CTE match with diamond. What is

Oriented Diamond (100) Bonding to Ni(100)

Sequence:
1. MBE heteroepitaxial Ni on C(100) Diamonds with polished {010} edge orientations
2. Place on Ni(100) surface ensuring that $[010]_C$ // $[010]_{Ni}$ and diamond edges are in contact
3. Load into annealing press
4. Subject to 900°C, 30 min. in compression

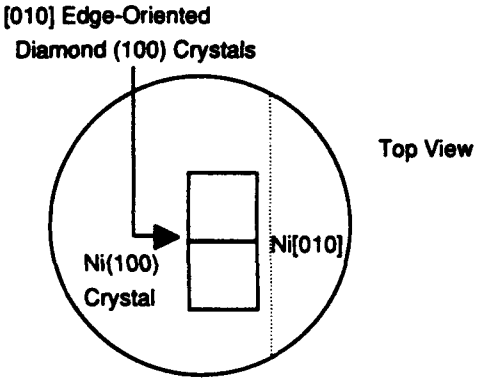

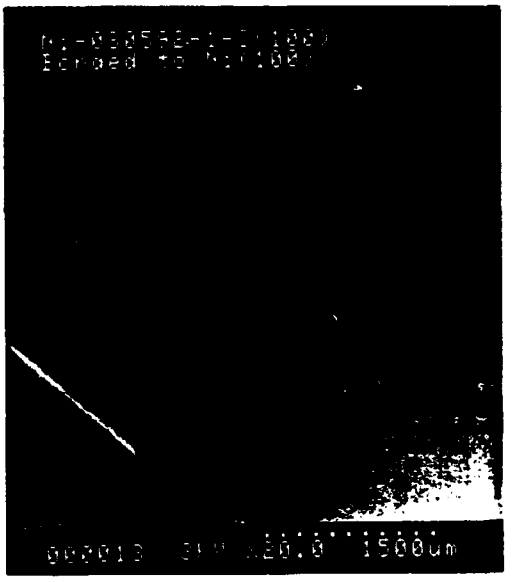

Entire Structure

Figure 5.3

Oriented Diamond (100) Bonding to Ni(100)

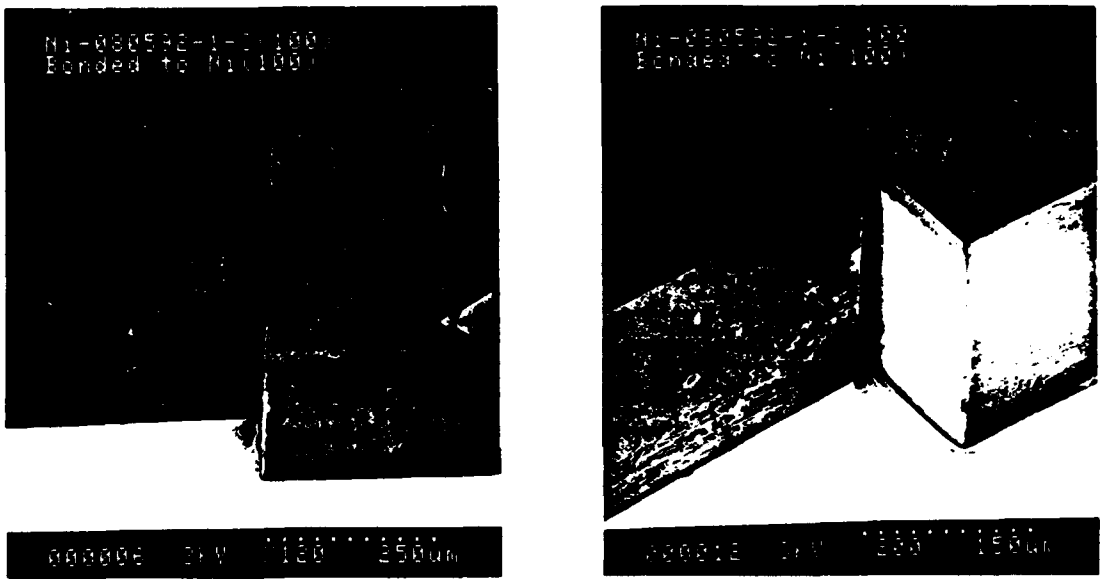

Showing:
1. Good registry
2. Deformation of Ni to accommodate different diamond crystal thickness
3. Excellent adherence. Micrographs taken after mishandling (shock) and surface polishing (shear)

Figure 5.4

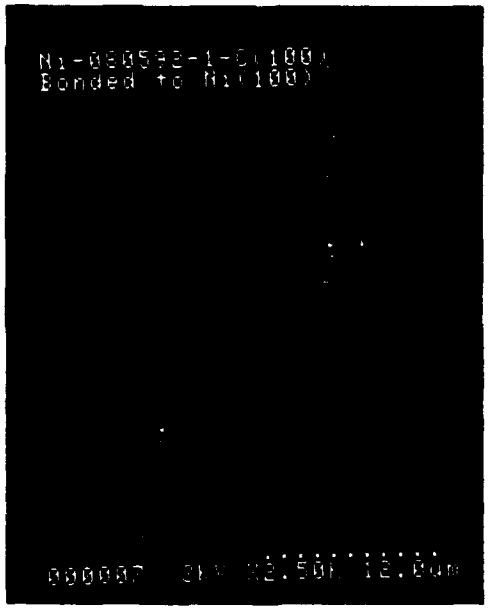

Showing 10 μm Diamond Separation

Figure 5.5

sacrificed is the lattice matching that Ni(100) provided. A number of attempts were made to grow a Ni heteroepitaxial film on Si (using a $NiSi_2$ epitaxial interlayer) to be used in these bonding experiments, but attacking this goal has been elusive due in part to Si substrate heating/cleaning problems in the MBE. This deficiency is currently being rectified by fabrication of a new MBE heater stage which should be on-line by 31 January 1993.

Therefore, initial attempts of Ni-coated diamond bonding to Si(100) were not done with epitaxial registry as the primary purpose. Issues of geometric alignment and materials bonding were emphasized. Several experiments were done to create a 2-dimensional array of edge-oriented diamonds. Culminating the work in this phase was the 2x2 array of 3x3 mm edge-oriented diamonds shown in Figure 5.6. For this array, the Ni-coated diamonds were bonded to a $Au/W/SiO_2/Si(100)$ structure. The separation varied between the diamonds, but was as low as 1.5 μm. Work in the follow-on phase will emphasize maintaining this spacing on all seams and simplifying the materials sequence necessary to achieve diamond bonding to silicon.

5.3 Diamond Crystal Orientation

Use of electron channeling patterns (ECP) in the SEM can enable determination of crystallographic directions of bulk single crystals. Furthermore, this can be done on relatively small areas (~ 100 μm^2). Obtaining ECPs from a semiconducting type IIb (100) diamond is straightforward due their adequate conduction and lack of charging in the SEM (high voltage ≥ 15 keV is required for this technique) as shown in Figure 5.7. However, we are mainly using insulating type IIa and Ia diamonds which cannot be imaged at high voltages without charging. However, evaporation of a small amount of amorphous carbon (~ 20 nm) permits charge bleed-off while preserving the details of the

Diamond Tiled Array Using 4 Diamonds

Heteroepitaxial Ni on (100) Diamond Bonded to Au/W/SiO_2-Coated Si(100) Wafer

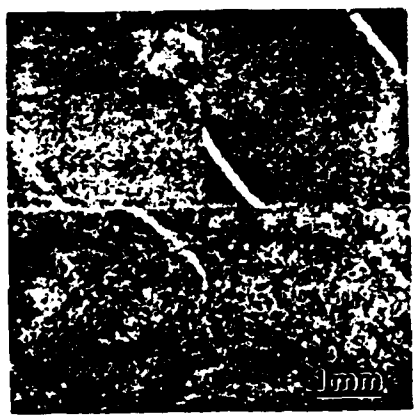

Low Magnification Showing Entire Array (Background Contrast is Due to Ni and Au at Bonded Interface)

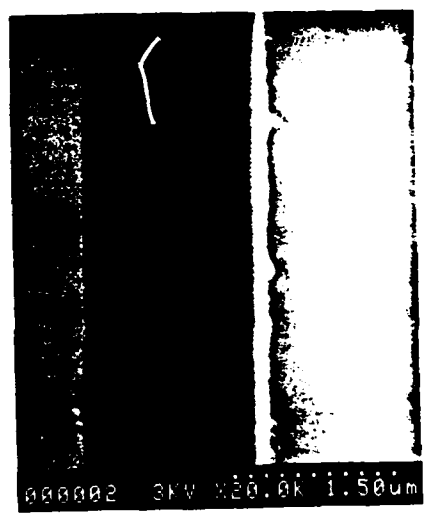

High Magnification of (011) Oriented and Polished Edges of Two of the Diamonds (Separation ≈ 1.5 μm)

Figure 5.6

Examples of Electron Channeling Patterns

C(100) IIb

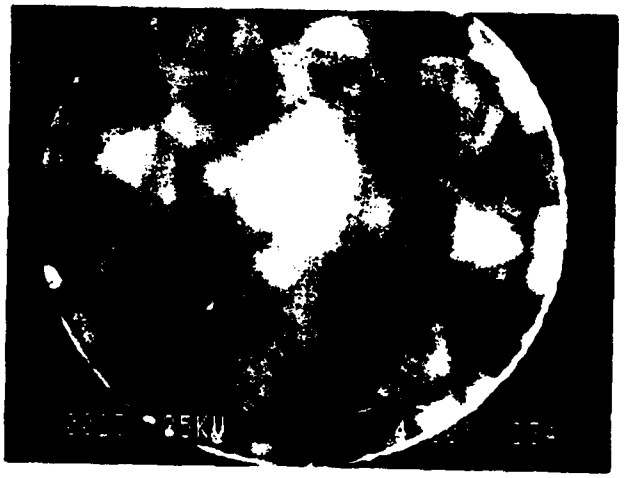

Ni on C(100) Ia

Figure 5.7

ECP (Figure 5.7). We intend to use this method to directly compare the crystallographic orientation of diamonds in an array in the next phase of this program.

6.0 Homoepitaxial Growth Studies

Key to the consolidation of individual crystals into a large single crystal will be the homoepitaxial process. We at Research Triangle Institute have been focusing on refinement of the CVD process to enable extended homoepitaxial growth. This capability will be critical not only just for the consolidation but also for the generation of additional single crystals through cloning of the proprietor consolidated single crystal. The homoepitaxial technology at RTI has been published on quite widely, but all those reports were for fairly thin (< 2 μm) epitaxial layers. The results reported there for homoepitaxy on the diamond (100) surface were quite encouraging. Even polishing lines on the (100) surface were quickly planarized by the CVD process.

First attempts at extended homoepitaxy using CH_4 in H_2 gas mixtures resulted in extremely roughened surface topographies. Figure 6.1 shows the deposition conditions for a 6 hour growth (~ 3 μm) using 0.33% CH_4 in H_2. The surface topography has been accentuated, not planarized by this process. These results were unexpected. To observe the transition from the polished as-received surfaces to this rough "shingled" morphology, an epitaxial growth was performed for a slightly longer duration, but by interrupting the deposition at 1 hour, 3 hours, and 6.5 hours. Figures 6.2 and 6.3 show SEM micrographs from these epitaxial layers. The topography after the 6.5 hour interrupted growth was distinctly smoother than the "shingled" topography observed previously for the uninterrupted 6.0 hour growth.

The interruption and exposure to room ambient proved beneficial. We suspected that the graphite susceptor above transfer into the room ambient absorbed considerable water vapor. Upon reintroduction into the vacuum environment of the deposition system and upon heating, the susceptor would desorb the water into the system. Water vapor released from the heated susceptor would be adsorbed onto the nearby water-cooled

Mixture: 0.33% CH_4/H_2

T ≡ 900°C; P = 5 Torr

rf Power ≡ 1800W

t = 6 hrs.

Rough, "Shingled" Morphology

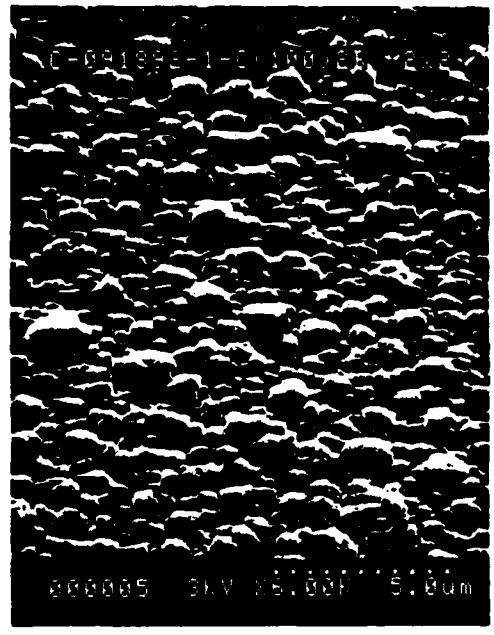

Figure 6.1

Mixture: 0.33% CH_4/H_2

T ≅ 900°C; P = 5 Torr

rf Power ≅ 1800W

t = 1, (1+2), (1+2+3.5) hrs.

= 6.5 hrs. total

Smooth Morphology Observed After Each Relatively Short Run. Water "Contamination" Introduced at Start of Each Run Thought to be Beneficial.

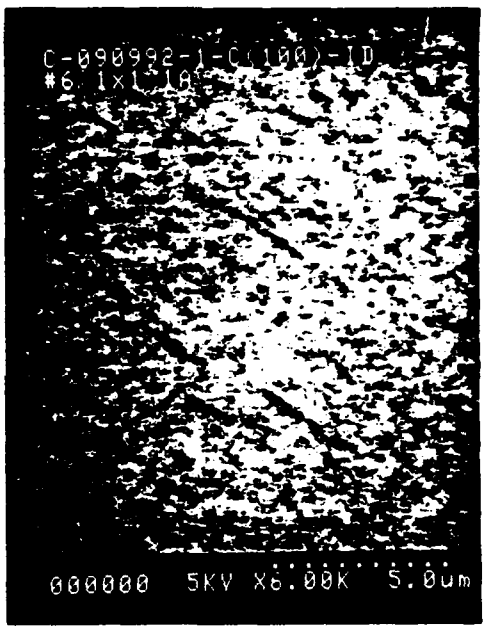

After 1 hour

Figure 6.2

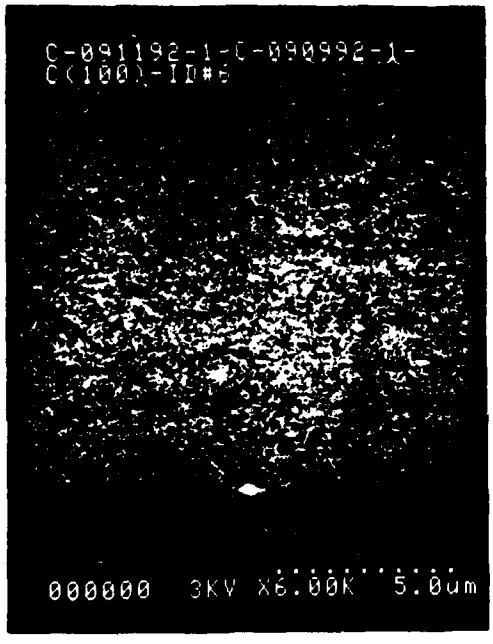

After 1 + 2 hours

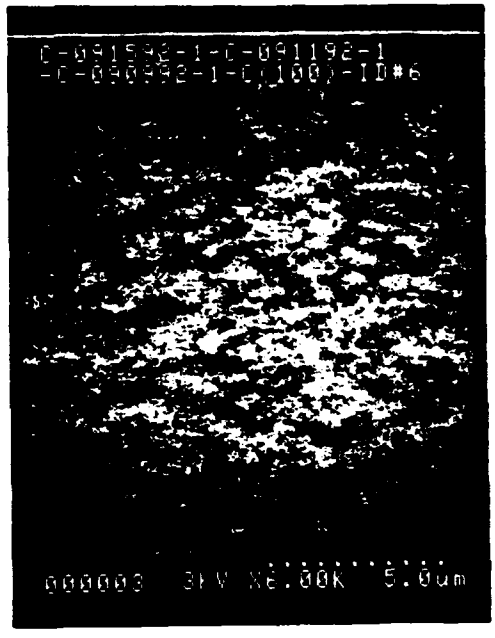

After 1 + 2 + 3.5 hrs.

Figure 6.3

quartz walls. Water vapor would be slowly released from the quartz walls resulting in the system having a prolonged memory for water.

To corroborate this hypothesis, feedstock gases containing oxygen were deliberately introduced for extended homoepitaxial growths. Figure 6.4 shows a SEM micrograph from a diamond deposition using 1.14% CO, 0.43% CH_4, and H_2, uninterrupted for 6.5 hours. The surface topography appears nearly identical to the SEM micrograph from the 6.5 hour interrupted growth using 0.33% CH_4 in H_2. Oxygen addition (as H_2O, CO, etc.) appears essential to the growth of smooth (100) homoepitaxy. Elimination of the oxygen seriously degrades the morphology. RTI has extensive research on the role of oxygen on the (100) surface (see Section 3.0).

Oxygen on the diamond (100) surface is seen to:

1) stabilize the 1 x 1 structure;
2) upon desorption, create reactive sites for radical insertion; and
3) extract H from the surface.

Work is planned in the near future to evaluate extended homoepitaxial growths using water vapor as the intentional oxygen source. We have already observed that water addition to a 1% CH_4 in H_2 process dramatically reduces the secondary nucleation during polycrystalline growth.

Mixture: 1.14% CO/0.43% CH_4/H_2

T ≅ 900°C; P = 5 Torr

rf Power ≅ 1800W

t = 6.5 hrs.

Smooth Surface Morphology

Figure 6.4

7.0 Microstructural Analysis

Considerable progress has been made in this phase on our ability to critically assess grown diamond crystals from a microstructural suitability point of view. First, an ion mill was purchased using RTI capital equipment funds to facilitate diamond TEM sample preparation. This unit is installed and operational. Second, we have benefited from fruitful collaborations with other laboratories on the analysis of our diamond thin films. These collaborations include: Dr. T. George, et.al. (see manuscript below) at Jet Propulsion Laboratory, Dr. Roger Graham (spatially resolved CL: TEM-based) at Arizona State University, and Dr. Gene Fitzgerald (spatially resolved CL: SEM-based) at AT&T Bell Laboratory. Thirdly, we have developed a means to rapidly assess defect densities in diamond single crystals using an open flame (see Section 7.2). This technique appears extendible to polycrystalline diamond as well.

7.1 Collaboration with JPL on TEM Studies of Diamond

Attached below is a jointly authored manuscript that describes a method to more quickly prepare plan-views TEM sample from bulk diamond. It is intended that this technique be used in the next phase of the program to critically examine diamond homoepitaxial films - overgrown (tiled) and otherwise.

Below band-gap laser ablation of diamond for transmission electron microscopy

T. George, M. C. Foote, R. P. Vasquez and E. P. Fortier

Center for Space Microelectronics Technology

Jet Propulsion Laboratory, California Institute of Technology

Pasadena, California 91109

J. B. Posthill

Research Triangle Institute

Research Triangle Park, North Carolina 27709-2194

ABSTRACT

A 248nm excimer laser was used to thin naturally occurring type 1a diamond substrates at normal and glancing (22°) incidence. Perforation of a 250μm thick substrate was achieved in about 15 minutes at normal incidence. Whilst the substrate thinned at glancing incidence was found to have large electron-transparent areas, that thinned at normal incidence required additional argon ion milling to achieve electron transparency. X-ray photoelectron spectroscopy of the back surface of the diamond failed to detect any graphite or glassy carbon, confirming that damage due to laser ablation occurs only at the incident surface. Samples prepared using this technique imaged in the transmission electron microscope were observed to have retained the nitrogen platelets characteristic of such type 1a diamonds.

Submitted to:
Applied Physics Letters
December 1992

Recently, interest in diamond as a bulk substrate and as a coating material has grown, for a variety of applications.[1] Transmission electron microscopy (TEM), both in the conventional and analytical modes, will continue to be an important technique for the characterization of diamond based materials. However, the main barrier to the widespread use of TEM as a characterization tool is the lack of a suitable technique to produce electron transparent thin foils in a controlled and timely manner. Natural diamond is the hardest substance known and consequently thinning of diamond has been a centuries-old problem, particularly among manufacturers of diamond jewelry. Traditionally the grinding and polishing of diamond is achieved with diamond-based abrasives and is a time consuming process. Alternatively, argon ion milling[2], oxidation[3] in a furnace, and laser ablation[4] have been used as means of obtaining electron-transparent specimens. The furnace oxidation approach suffers from a lack of controllability in the desired area for TEM examination and possible surface structural modification, making the technique unsuitable for producing TEM specimens from homoepitaxial samples. Argon ion milling is a time-consuming process with a very low sputter rate of approximately 1μm/hr[3]. Laser ablation has been attempted previously although only using radiation above the band gap (193nm)[4]. This letter describes the results of an in-depth study of the laser ablation approach using below band-gap laser radiation with a view towards its applicability in producing TEM specimens from homoepitaxial samples without significantly damaging the epitaxial layers. The use of below band-gap laser radiation confines most of the energy of the laser pulse in the surface carbon layer formed during ablation and minimizes the absorption and consequent structural damage in the bulk of the diamond.

In this work, 2mm x 2mm x 0.25mm, (100) oriented, type 1a natural diamond substrates were used. The substrates were mounted in a copper holder in the as-received condition without the use of optically absorbent coatings. Thinning was performed in air, using an excimer laser (Questek 2960) operated at 248 nm (KrF), at a pulse rate of 5Hz and with an output energy of 600mJ, at normal and glancing (22°) incidence. Although the

band-gap of natural diamond is around 5.48eV (226nm), a high concentration of nitrogen impurities in type 1a diamond lowers the uv absorption edge to 340nm.[5] The laser output was first reduced in size by passing the beam through a 3mm diameter aperture: the remaining 15mJ was focused on to the diamond substrate using a 30 cm focal-length fused-quartz lens. The substrate was placed near the focal point of the lens to produce an laser spot of approximately 300x500μm at normal incidence. The fluence at the center of this spot is estimated to be 20 J/cm^2.

Following laser thinning the resultant surface morphology was studied using scanning electron microscopy (SEM). TEM observations were conducted at 200kV. The diamond substrate thinned at glancing incidence could be imaged directly. However, the substrate thinned at normal incidence required the removal of the layer formed on the ablated surface of graphitic and amorphous carbon by argon ion milling at 5kV and 0.5mA for electron transparency. X-ray photoelectron spectroscopy (XPS) data were taken with a Surface Science Instruments SSX100-501 spectrometer using monochromatic Al K_α x-rays (1486.6 eV) with a beam of diameter 150μm or 300μm . Prior to XPS measurements, the diamond samples were degreased in hot trichloroethylene, acetone and methanol to minimize surface organic contaminants. The effects of sample charging during XPS data accumulation were minimized with the use of a low energy electron flood gun.

Low-magnification SEM micrographs of the the laser-thinned diamond substrates are shown in figure 1. The laser-exposed surfaces on both substrates are rough whereas the unexposed back surfaces retain their original surface polish. It was found that an absorbent coating was not necessary to initiate the laser-thinning process. A black surface layer, presumably a mixture of graphitic and amorphous carbon, forms very soon in the ablation process. This layer is consistent with the results from earlier furnace-oxidation studies of diamond which have shown the formation of a surface carbon (non-diamond) layer.[3] These studies determined that above 850°C a carbon (non-diamond) layer appeared on the (100) surface of the diamond. The formation of a surface carbon layer would reduce the

absorption depth of the laser radiation significantly and also have a lower thermal diffusivity than the underlying diamond, leading to localization of the laser pulse energy within the surface layer.[4,6] Rothschild *et. al.*[6] have proposed that thinning in such circumstances involves a sustained process of conversion of diamond to a graphite/amorphous carbon layer followed by evaporation or reaction of this layer with the ambient. However, unlike their etching method which used above band-gap 193nm laser radiation, this work uses a laser energy below the band gap of the diamond, with the bulk of the pulse energy being absorbed in the surface carbon layer thus minimizing absorption in the interior of the diamond. Although an optically absorbent coating was not used in the present study to initiate the thinning, such a coating could potentially be used with lasers having wavelengths in the optical trasmission regime for diamond but within the absorption range for graphite or glassy carbon. The only requirement would be that the lasers have sufficiently high energy densities for sustaining the ablation process.

For the laser-thinning technique to be utilized in future TEM studies of homoepitaxial diamond layers, it is necessary to demonstrate that there is negligible damage in the form of graphitization to the back surface of the substrate. The presence of a surface graphite/amorphous carbon layer can be detected using XPS. Although both diamond and graphite contain only carbon and have C 1s core level XPS peaks at the same binding energy of 284.3 eV, the C 1s signals for these materials are distinguishable by their lineshapes and characteristic energy losses. Diamond is an insulator with a C 1s signal which is symmetric, while graphite is a semimetal whose C 1s signal exhibits a pronounced asymmetry on the high binding energy side and a characteristic energy loss peak at 291 eV which is absent in the signal from diamond.[7,8] Glassy carbon also exhibits spectral characteristics similar to those of graphite.[7] The diamond substrate laser-thinned at a glancing angle was selected for the XPS study. The C 1s signals from the samples measured in this work, including a virgin diamond crystal, consist of a single main peak with shoulders at both low and high binding energy. The only significant contaminant is O,

which is present at a level of ~0.5 - 1 monolayer assuming surface localization. Surface C-O or C-OH bonding may account for the high binding energy shoulder on the main C 1s peak. Alternatively, the C 1s lineshape may indicate some differential charging of the sample surface. However, the 291 eV energy loss peak characteristic of graphite or glassy carbon was not observed, even near the spot where the laser had ablated completely through the sample. This result demonstrates that laser-induced heating does not damage the back surface of the diamond substrate in these experiments.

Figure 2 shows a TEM micrograph of a diamond substrate thinned at glancing incidence. This specimen contains large electron-transparent regions which exhibit thickness fringes. The substrate thinned at normal incidence however, required argon ion-milling at 12° for an hour following laser ablation to achieve electron transparency. Also, very small areas were available for observation as compared to the sample thinned at glancing angle, due the presence of steep sidewalls surrounding the perforated region. The presence of graphitic and amorphous carbon on the ablated surface of the diamond thinned at normal incidence was determined via electron diffraction. It was found that the graphitic and amorphous carbon layer could be removed by extended ion-milling. Figure 3 contains a diffraction pattern obtained from a <$\bar{1}2\bar{1}1$> oriented graphite particle found on the diamond substrate laser-thinned at normal incidence. Figure 4 contains a high magnification electron micrograph showing the presence of nitrogen platelets lying on {100} planes in the diamond thinned at normal incidence, which is characteristic of type 1a natural diamond. These results provide ample evidence for the viability of laser ablation as a TEM specimen preparation process.

In summary, a novel technique for the rapid thinning of diamond using below band-gap laser radiation is described. An optically absorbent surface carbon layer is formed during irradiation which then sustains the ablation process. XPS measurements were not able to detect damage in the form of graphitic/amorphous carbon formation on the unexposed side of the diamond substrate.

We would like to thank Dr. M. W. Geis and Dr. C. Deats for suggesting the laser ablation approach and Dr. W. T. Pike for helpful technical discussions. The authors gratefully acknowledge the support of this work by the Strategic Defence Initiative Organization/Innovative Science and Technology through the Office of Naval Research (Contract# N00014-92-C0081). This work was performed by the Center for Space Microelectronics Technology and the Space Materials Science and Technology Section, Jet Propulsion Laboratory, California Institute of Technology and was sponsored by the SDIO through an agreement with the National Aeronautics and Space Administration.

REFERENCES

1. For a recent review in this field see, "Status and applications of diamond and diamond-like materials: An emerging technology" Report of the committee on superhard materials, National Materials Advisory Board, NMAB-445, National Academy Press, 1990.
2. T. Myers and J. B. Posthill, unpublished research (1992).
3. T. Evans in "*Physical Properties of Diamond*", edited by R. Berman, pp.122-124 (1965).
4. M. W. Geis, M. Rothschild, R. R. Kunz, R. L. Aggarwal, K. F. Wall, C. D. Parker, K. A. McIntosh, N. N. Efremow, J. J. Zayhowski, D. J. Ehrlich, and J. E. Butler, Appl. Phys. Lett. **55**, 2295 (1989).
5. "Physics of Group IV Elements and III-V Compounds" Landolt-Bornstein New series, edited by O. Madelung, **17a** 36 (1982).
6. M. Rothschild, C. Armone and D. J. Ehrlich, J. Vac. Sci. Technol. **B4**, 310 (1986).
7. F. R. McFeely, S. P. Kowalczyk, L. Ley, R. G. Cavell, R. A. Pollak and D. A. Shirley, Phys. Rev. B **9**, 5268 (1974).
8. R. P. Vasquez, Surface Science Spectra (in press).

LIST OF FIGURES

1 mm

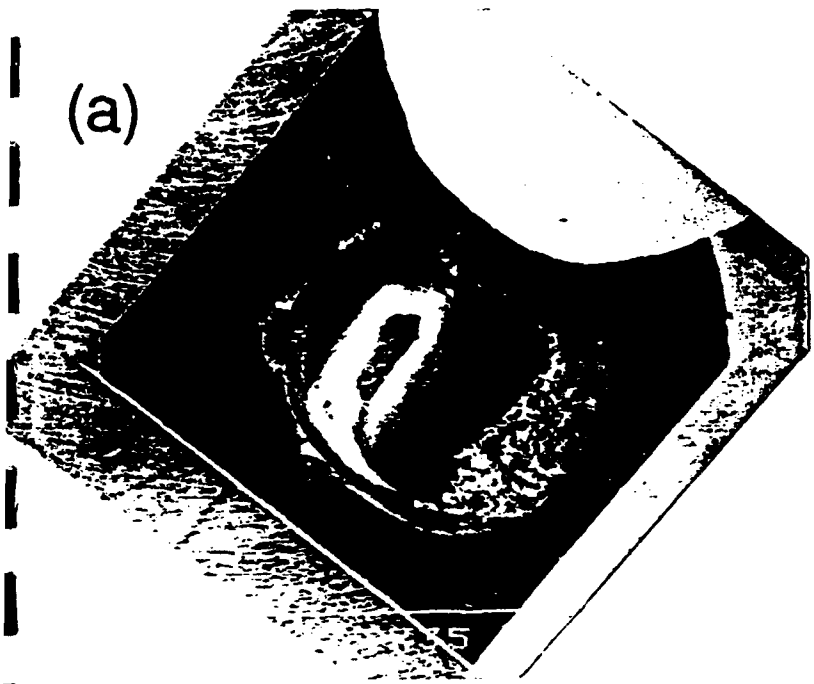

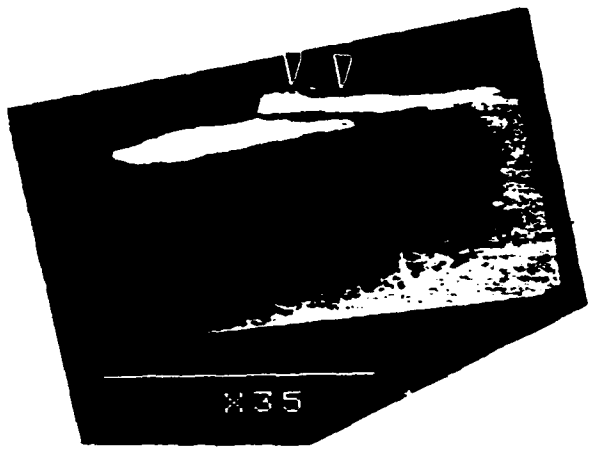

Fig. 1

Fig. 2

(a)

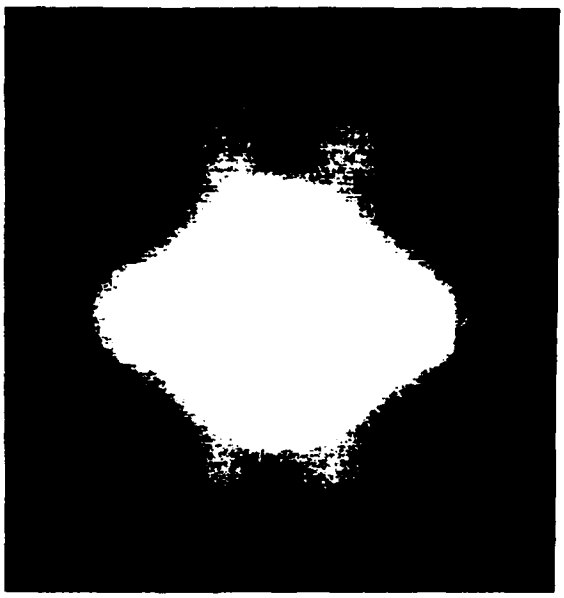

(b)

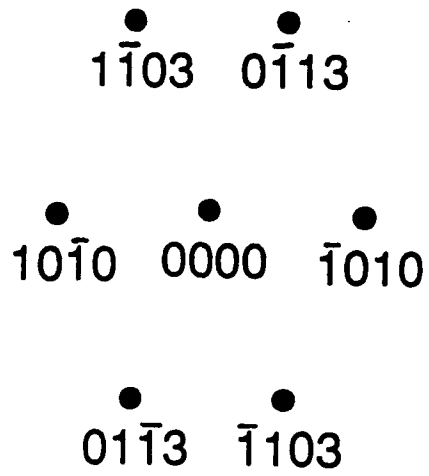

Fig. 3

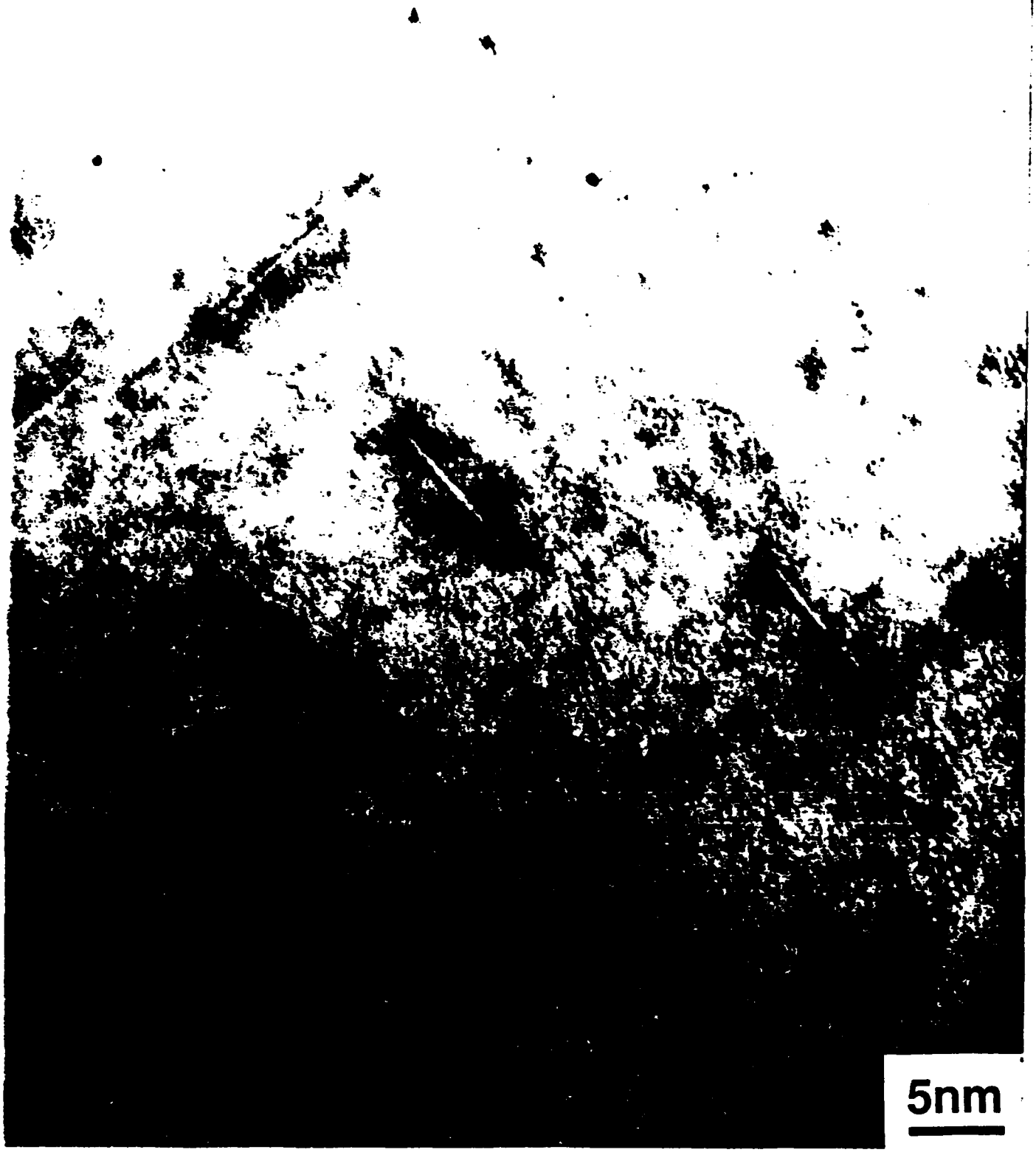

Fig. 4

7.2 Etch Delineation of Defects

Attached below is a manuscript describing the technique used to etch - delineate defects using an oxidizing flame. Corroboration with TEM is included. Again, we anticipate using these methods to critically assess defect densities in homoepitaxial diamond films in the next phase of the program.

ETCH-DELINEATION OF DEFECTS IN DIAMOND BY EXPOSURE TO AN OXIDIZING FLAME

D.P. Malta, J.B. Posthill, R.A. Rudder, G.C. Hudson and R.J. Markunas

Research Triangle Institute
Research Triangle Park, North Carolina 27709-2194

ABSTRACT

An experimental study of the the etching properties of defects in diamond using propane flame exposure in air is presented. Both natural diamond crystals and polycrystalline diamond films were exposed to a flame for an optimum time of 3-4 seconds. This process topographically delineates defects in diamond via an accelerated etch rate at defect sites. Using transmission electron microscopy (TEM) to determine the exact nature and density of defects present in the diamond, we have found a direct correlation between topographical delineation observed by scanning electron microscopy (SEM) and the defect structure observed by TEM.

Submitted to:
Journal of Materials Research
December 1992

Diamond has several properties which make it desirable for electronic applications[1]. Foremost is diamond's high thermal conductivity ($\sim$2000 W m^{-1}K^{-1}) and wide band gap (5.48eV). However, before the impressive attributes of diamond can be fully exploited for electronic device purposes, several manufacturing technologies must be developed. First among these is the growth of electronic-quality diamond thin films of high microstructural perfection. Considerable world-wide effort has gone into developing chemical vapor deposition (CVD) techniques for growing high quality diamond[e.g.,2,3] and considerable progress has been made. And, by analogy with the historical development of other semiconductor materials, techniques are evolving to accurately determine the crystalline quality of grown diamond. For example, Raman spectroscopy has been used extensively to ascertain the presence of unwanted sp^2 bonding in diamond films[e.g.4]. In other semiconductor material technologies, wet chemical etch delineation is used to ascertain defects at the per cm^{-2} level. But this technique is lacking in diamond technology, as diamond is virtually impervious to standard wet chemical etchants. This communication describes a defect delineation method for diamond, which involves anisotropic defect etching using a propane torch.

Previous etching studies on diamond have been undertaken to investigate feasibility of patterning[5], to determine etch removal rates[6–11] to identify the role of non-diamond phase removal during the growth process[5] and to assess crystalline quality through preferential etching of defects[8,12], to name a few. Several methods which have

proven successful in etching both diamond and non-diamond phases have employed both (a) an oxygen-containing gas and (b) an activation mechanism. Etching under these conditions is generally believed to occur via the oxidation and volatilization of the carbon phase(s). It has been suggested that etching of diamond proceeds through graphitization followed by oxidation of the graphitic phase[8]. Several observations regarding etch rates have been made: (1) non-diamond phases etch faster than diamond[5,7,9,11], (2) natural diamond etches faster than plasma-enhanced chemical vapor deposition (PECVD)-grown diamond[6,9,11] and (3) diamond etches faster at grain boundaries and other defects than non-defective regions[8,9,11,12]. Oxidation/etching experiments recently reported have employed either a temperature–activated[6,8–11] or plasma–activated[5,7,12] process using air or oxygen-containing gas mixtures. We have achieved temperature-activated etching of diamond using only a short exposure to an oxidizing flame. Our results indicate that accurate, reproducible etch-delineation of defects is possible with minimal investment. These results have been correlated with TEM analysis.

A continuous polycrystalline film was grown at 350 °C by low pressure rf-induction PECVD on Si(100) using an acetic acid/water/methanol mixture at 0.5 Torr and 350 °C, similar to results described elsewhere[3]. For comparison, a natural type IIb semiconducting diamond stone sectioned into thin (100μm) wafers with (100) orientation was obtained from a commercial vendor. Both sample types were examined by

TEM in order to assess crystalline quality. TEM samples were prepared by ion milling. Each sample type was immersed in a propane flame for various lengths of time and then topographically examined by field-emission scanning electron microscopy (FESEM).

Plan-view TEM of the polycrystalline diamond film revealed a high degree of microtwinning within the grains (Fig. 1a). After immersion of the sample in the flame for an optimum time of 3-4 seconds (Fig. 1b). the microtwin boundaries were clearly delineated as were grain boundaries which were attacked more vigorously (arrow).

TEM analysis of the type IIb natural diamond over relatively large areas found only line defects with an area density of $\sim 10^8 cm^{-2}$ (Fig. 2a). Immersion of the diamond in the flame for an optimum time of 3-4 seconds produced roughly square etch pits with an equivalent area density of $\sim 10^8 cm^{-2}$ (Fig. 2b). Note that after this exposure the remnants of the unidirectional scratches left over from the commercial polishing process are still evident. Shorter exposure times resulted in fewer, smaller pits; longer exposure resulted in larger (but few additional) pits and a roughened surface no longer showing scratches.

The results are consistent with those obtained by furnace annealing in an oxygen atmosphere at 700 °C-800 °C for several hours[8] and by air microwave plasma etching for 15-30 minutes[12]. In this work, the accelerated etch rate obtained through flame

exposure produced verified topographical defect delineation requiring only several seconds at negligible cost. The value of this method for routine and rapid evaluation of diamond is considerable. Future research will extend this technique to homoepitaxial diamond films grown by PECVD.

Acknowledgements: The authors gratefully acknowledge the support of this work by the Strategic Defense Initiative Organization/Innovative Science and Technology through the Office of Naval Research (Contract No. N00014-92-C-0081). We also thank Tami Myers for technical assistance.

References

1. *The Properties of Diamond*, Ed. J.E. Field (Academic Press, London 1979)
2. R.A. Rudder, G.C. Hudson, J.B. Posthill, R.E. Thomas, R.C. Hendry, D.P. Malta, R.J. Markunas, T.P. Humphreys, and R.J. Nemanich, Appl. Phys. Lett., 60, 329 (1992).
3. R.A. Rudder, J.B. Posthill, G.C. Hudson, D.P. Malta, R.E. Thomas, R.J. Markunas, T.P. Humphreys and R.J. Nemanich, Mater. Res. Soc. Symp. Proc., 23 (1992).
4. R.J. Nemanich, J.T. Glass, G. Luckovsky, and R.E. Shroder, J. Vac. Sci. Technol. A, 6, 1783 (1988).
5. R. Ramesham and B.H. Loo, J. Electrochem. Soc., 139 (7) 1988 (1992)
6. Q. Sun and M. Alam, Proceedings of the Second International Symposium on Diamond Materials, Washington, DC, The Electrochemical Society Proceedings Vol. 91-8, 463 (1991)
7. G.S. Sandhu and W.K. Chu, Appl. Phys. Lett. 55 (5) 437 (1989)
8. W. Zhu, X. Hong Wang, A. Badzian and R. Messier, New Diamond Science and Technology, Washington, DC, Materials Research Society Conference Proceedings. 812 (1990).

9. A. Joshi, R. Nimmagadda and J. Herrington, J. Vac. Sci. Technol.A 8 (3) 2137 (1990)

10. K. Tankala and T. DeBroy, New Diamond Science and Technology, Washington, DC, Materials Research Society Conference Proceedings, 827 (1990)

11. Linda S. Plano, S. Yokota and K.V. Ravi, Proceedings of the First International Symposium on Diamond Materials, Los Angelas, CA. The Electrochemical Society, Proceedings Vol. 89-12, 380 (1989)

12. Y. Sato, C. Hata, T. Ando and M. Kamo, New Diamond Science and Technology, Washington, DC, Materials Research Society Conference Proceedings, 537 (1990).

FIGURE 1: Microscopic images of PECVD-grown polycrystalline diamond; (a) plan-view TEM shows very high density of microtwins and, (b)FESEM image of sample after exposure to an oxidizing flame which shows delineated microtwin boundaries (parallel grooves) and grain boundary (arrow).

FIGURE 2: (a) Plan-view TEM of natural type IIb diamond shows dislocations. Examination of large areas found that dislocations tended to cluster and overall density was $\sim 10^8 cm^{-2}$. (b) etch pits in natural type IIb diamond formed at dislocation sites upon exposure to an oxidizing flame. Density measured over large areas was averaged to be $\sim 10^8 cm^{-2}$. Both results were obtained from the exact same crystal: the etching work was followed by ion milling the $100\mu m$ thick wafer from both sides to electron transparency.

Plan-View TEM and SEM of Diamond Grown on Silicon

2:2:1 Acetic Acid:Water:Methanol

P = 1 Torr; T ≅ 600 °C; Power (rf) ≅ 1 kW

Photo on right: **Oxidizing Flame Exposure for 3 sec.**

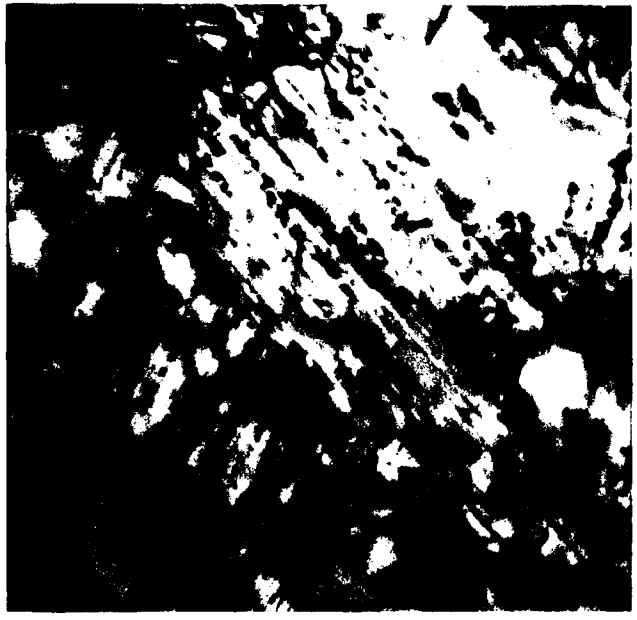

0.25 μm

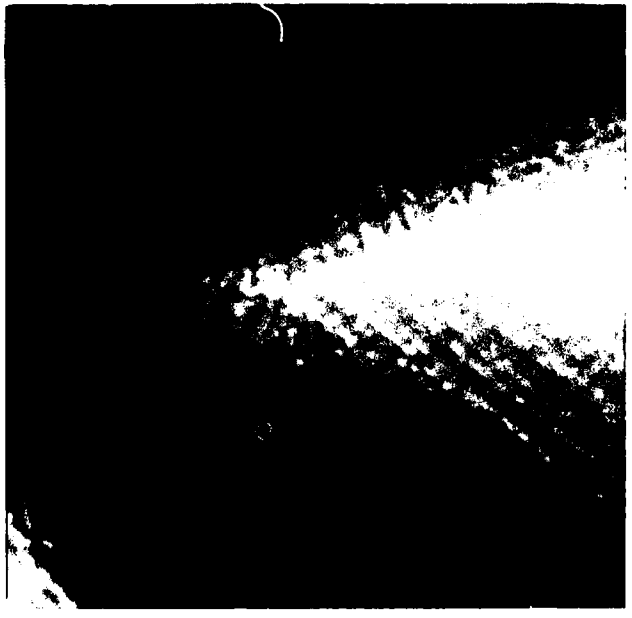

0.25 μm

RTI

Plan-View TEM and SEM of Type IIb Diamond

RTI

Density of dislocations ≈ density of etch pits ≈ 10^8 cm^{-2}

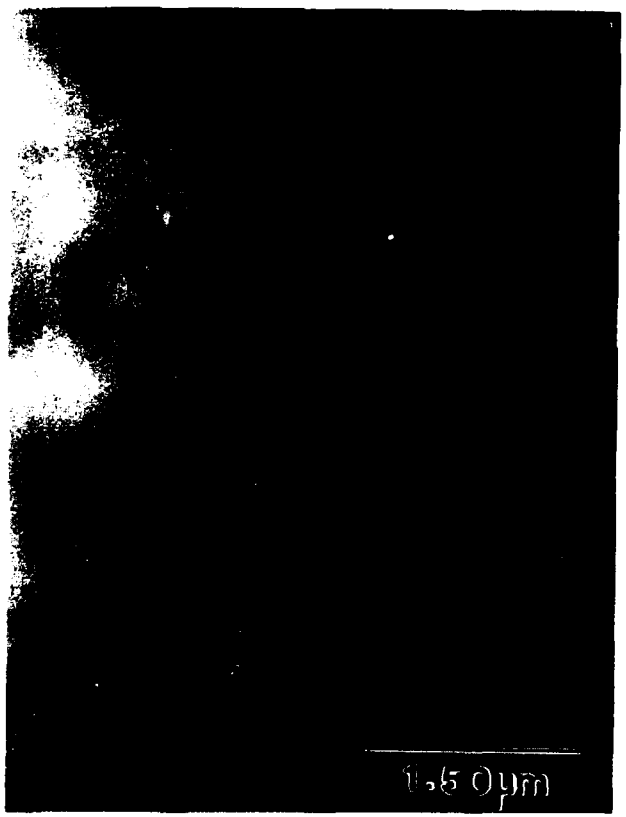

TEM

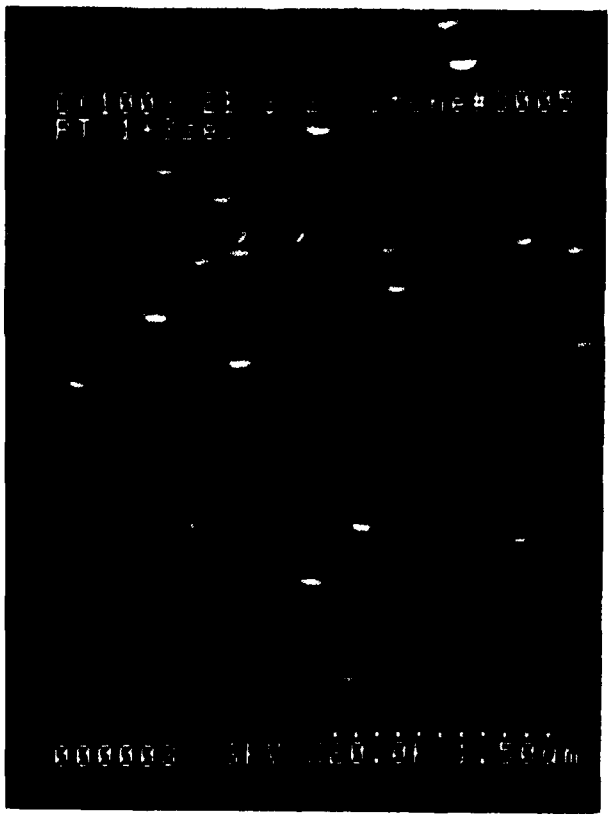

SEM after oxidizing
flame exposure for 3 sec.

8.0 Atomic Force Microscopy
(Dr. R.J. Nemanich, Dr. T.P. Humphreys, NCSU)

This section summarizes the current research achievements and the present collaborative experiments that have been performed during the past 6 months by Robert J. Nemanich and Trevor P. Humphreys of the Department of Physics at North Carolina State University. The main research topics include Raman Spectroscopy, silicide growth and surface structural analysis of chemically prepared diamond surfaces using STM and AFM.

8.1 Raman Spectroscopy (Phase identification and defect structure)

To date, Raman spectroscopy analysis has been routinely employed to examine numerous thin film diamond structures grown at RTI. In particular, these studies have included an investigation of various polycrystalline and homoepitaxial diamond films. In addition, diamond overgrowth studies pertaining to RTI's tiling process are currently under investigation. More specifically, we compare the crystalline quality and defect structure of the diamond overgrowth regions with those films deposited directly on the diamond platelets. The Raman analysis has recently been expanded to include more complete defect analysis, strain and epitaxial alignment.

8.2 Silicide Growth and Characterization

Several nickel silicide films have been grown at NCSU using electron beam evaporation and these samples have been used as substrate "templates" in an attempt to grow heteroepitaxial diamond films. We have previously explored the growth of epitaxial Ni-diamond structures. The Ni-silicide films may exhibit an improved chemical

stability for CVD diamond growth. Corresponding epitaxial silicide films have been also been fabricated in collaboration with Dr. John Posthill and David Malta at RTI. The crystallographic phase of these films have been characterized by Raman spectroscopy.

8.3 Surface Structural Analysis of Single Crystal C(001) Substrates and Films

Currently in progress is a study to explore the surface and electronic structures of single crystal diamond C(001) substrates and homoepitaxial films. This work is performed in collaboration with Dr. Ray Thomas and has been initiated in an attempt to obtain a fundamental understanding of the mechanism that promotes the 2x1 surface reconstruction following a high-temperature ultra-high vacuum anneal of the C(001) surface. To date, thermal annealing studies have been performed both at RTI and NCSU on various polished and chemically cleaned C(001) substrates. In particular, low energy electron diffraction (LEED), angle-resolved, ultra-violet photoelectron spectroscopy (ARUPS) and ex-situ scanning tunneling microscopy (STM) techniques are currently employed to characterize the diamond surface. Present annealing studies at 1100°C of the natural semiconducting (p-type) C(001) surfaces have failed to obtain the 2x1 hydrogen terminated surface structure. Indeed, it has been suggested that the bulk 1x1 LEED pattern which is observed as a consequence of oxygen termination of the C(001) surface results from wet chemical cleaning. Moreover, it has also been proposed that atomic imaging of the hydrogenated C(001) surface may also be possible using ex-situ STM. In an attempt to investigate this behavior, atomic hydrogen gas dosing experiments performed at RTI and corresponding STM measurements conducted at NCSU are currently in progress.

In November 1992 we received from Park Scientific Instruments an UHV-STM head. At present, we are modifying the existing chamber design of our vacuum chamber to accommodate the STM scanner. This new capability which we plan to have operational by March 1993 will enable in-situ atomic scale probing of the diamond surface. In addition, the corresponding scanning tunneling spectroscopy (STS) technique will enable a correlation with the local density of electronic states on the surface. Consequently, present experiments that are now performed under ambient conditions will be repeated in UHV.

8.4 Atomic Force Microscopy of Insulating Diamond Films

Recently acquired and operational is an ambient atomic force microscopy system (AFM) which will enable structural imaging of as-grown (undoped) diamond films and structures. Shown in Fig. 1 is an AFM image of the surface a single crystal C(001) diamond substrate. The fine unidirectional lines in this image are characteristic of scratches on the as-polished substrate. It is interesting to note that although the diamond crystal was semiconducting (type IIb) it was too resistive to be probed by STM. The current application of the AFM is to explore the nucleation and growth of diamond in the tiling process developed at RTI.

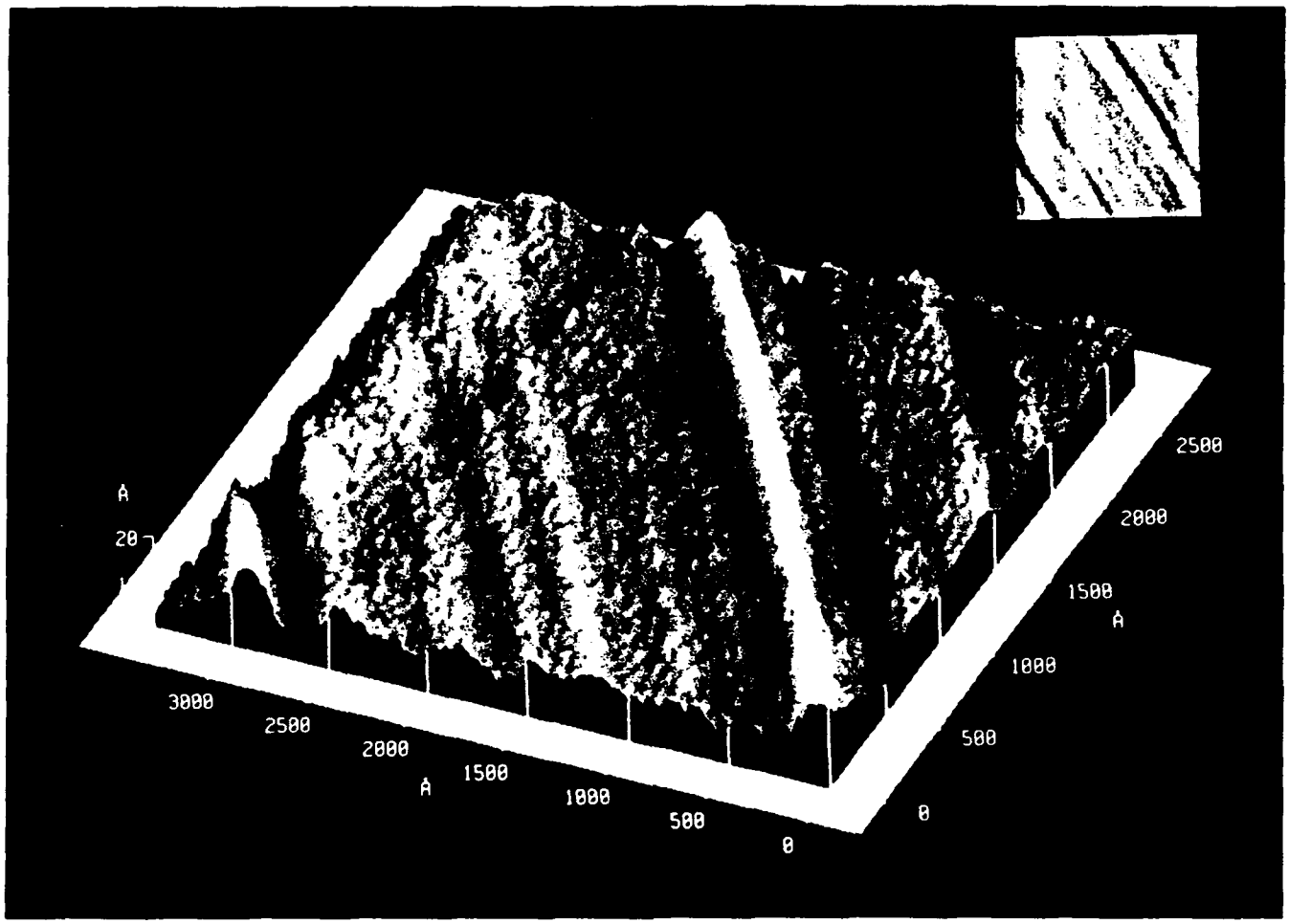

Fig. 8.1 AFM image of the surface of a C(001) diamond substrate. The unidirectional lines are indicative of scratches which have resulted from polishing damage (peak to peak depth is ~ 25).

8.5 Future Studies

Implement studies pertaining to AFM characterization of diamond substrates that are to be used as platelets in the RTI tiling process. Here, we anticipate that it will be possible to characterize a substantial number (if not all) of the initial diamond substrates. Subsequent investigation of diamond nucleation and growth on platelets and diamond overgrowth regions. Of particular interest will be the effect of surface morphology on the overgrowth process. Corresponding defect delineation and mapping using AFM of diamond single crystals following oxygen torch exposure will also be implemented. In-situ UHV STM and related STS atomic imaging of single crystal diamond substrates whose surfaces have been exposed to various processing gases. Integration of the UHV STM into the multi-chamber growth/characterization system at NCSU. This will allow structural and electronic analysis of plasma exposed diamond surfaces.

9.0 Publications/Presentations

1. H. Yang, J.L. Whitten, R.E. Thomas, R.A. Rudder, R.J. Markunas, *Effects of Subsurface Na, H and C on CH_3 Adsorption on Ni(111)*, Surface Science Letters, **277**, 1992, L95-L99.

2. N.R. Parikh, J.D. Hunn, E. McGucken, M.L. Swanson, C.W. White, R.Ad. Rudder, D.P. Malta, J.B. Posthill, and R.J. Markunas, *Single Crystal Diamond Plate Lift-Off Achieved by Ion Implantation and Subsequent Annealing*, Appl. Phys. Lett. **61**, 3124 (1992).

3. R. Rudder, G.C. Hudson, R.C. Hendry, R.E. Thomas, J.B. Posthill, R.J. Markunas, *Formation of Diamond Films from Low Pressure rf-Induction Discharges*, (presented at the International Conference on Metallurgical Coatings and Thin Films, San Diego, CA, April 1992,) Surface and Coatings Technology, **54/55**, 1992, 397-402.

4. R.E. Thomas, R.A. Rudder, R.J. Markunas, *Hydrogen-Halogen Exchange Reaction on Silicon(100)*, Materials Research Society Symp. Proc., Vol. **204**, April 1991, 327-332.

5. R.E. Thomas, R.A. Rudder, G.C. Hudson, R.J. Markunas, *Surface Processes During Diamond Growth from Water-alcohol Vapor rf-Plasma Discharges*, presented at Diamond 1992 Conference, Heidelberg, Germany, August 1 - September 4, 1992, published in Diamond 1992 Conference Abstracts, 12.3.[490]

6. R.A. Rudder, G.C. Hudson, J.B. Posthill, and R.J. Markunas, *The Effect of Local Carbon Sources on Diamond Nucleation*, submitted Int. Conf. on Metallurgical Coatings and Thin Films.

7. T.P. Humphreys, P.K. Baumann, K.F. Turner, R.J. Nemanich, K. Das, R.G. Alley, D.P. Malta, and J.B. Posthill, *Growth and Characterization of SiGe Contacts on Semiconducting Diamond Substrates*, submitted, Third Intl. Symp. and Diamond Materials (ECS, Hawaii, 1993).

8. D.P. Malta, J.B. Posthill, E.A. Fitzgerald, R.A. Rudder, G.C. Hudson, and R.J. Markunas, *A Correlative Investigation of Defects in Natural and PECVD-Grown Diamond*, submitted, Third Intl. Symp. and Diamond Materials (ECS, Hawaii, 1993).

9. J.B. Posthill, D.P. Malta, R.A. Rudder, G.C. Hudson, R.E. Thomas, R.J. Markunas, *Homoepitaxial Diamond Layers Grown with Different Gas Mixtures in a rf Plasma Reactor*, to be presented at the Third International Symposium on

Diamond Materials (as part of the 183rd Meeting of The Electrochemical Society), Honolulu, Hawaii, May 16-21, 1993.

10. R.E. Thomas, R.A. Rudder, and R.J. Markunas, *Diamond Surface Studies of Growth Mechanisms from Water-Alcohol Deposition Chemistries*, submitted, Third Intl. Symp. on Diamond Materials (ECS, Hawaii, 1993).

11. R.A. Rudder, R.E. Thomas, G.C. Hudson, J.B. Posthill, D.P. Malta, and R.J. Markunas, *Low Temperature Diamond Growth: Development of Water-Based Techniques for Diamond CVD*, submitted, Third Intl. Symp. on Diamond Materials (ECS, Hawaii, 1993).

12. J.B. Posthill, D.P. Malta, R.E. Thomas, G.C. Hudson, and R.J. Markunas, *Nucleation of Diamond Films on Non-Native Substrates*, invited talk, 1992 TMS Fall Meeting, Chicago, IL.

13. R.E. Thomas, R.A. Rudder, R.J. Markunas, O. Huang, M. Frenklach, *Atomic Hydrogen Adsorption on the Resconstructed Diamond (100) - (2×1) Surface*, Journal of Chemical Vapor Deposition, 1, 6, 1992.

14. R.A. Rudder, G.C. Hudson, J.B. Posthill, R.E. Thomas, R.C. Hendry, D.P. Malta, R.J. Markunas, *Chemical Vapor Deposition of Diamond Films from Water Vapor rf-Plasma Discharges*, Appl. Phys. Lett. **60** (3), January 1992, 329-331

15. R.A. Rudder, J.B. Posthill, G.C. Hudson, D.P. Malta, R.E. Thomas, R.J. Markunas, T.P. Humphreys, R.J. Nemanich, *Chemical Vapor Deposition of Diamond Films Using Water-Alcohol:Organic-Acid Solutions*, Mat. Res. Soc. Symp. Proc. Vol. **242**, 1992, 24-30.

16. R.A. Rudder, G.C. Hudson, J.B. Posthill, R.E. Thomas, R.C. Hendry, D.P. Malta, R.J. Markunas, *Chemical Vapor Deposition of Diamond Films from Water Vapor rf-Plasma Discharges*, Appl. Phys. Lett. **60** (3), January 1992, 329-331.

17. R.E. Thomas, R.A. Rudder, R.J. Markunas, *Thermal Desorption from Hydrogenated and Oxygenated Diamond (100) Surfaces*, J. Vac. Sci. Technol., A **10**(4), Jul/Aug 1992, 2451-2457.

18. R.E. Thomas, M.J. Mantini, R.A. Rudder, D.P. Malta, S.V. Hattangady, R.J. Markunas, *Carbon and Oxygen Removal from Silicon (100) Surfaces by Remote Plasma Cleaning Techniques*, J. Vac. Sci. Technol. A **10**(4), Jul/Aug 1992, 817-822.

19. V. Venkatesan, K. Das, G.G. Fountain, R.A. Rudder, J.B. Posthill, R.J. Markunas, *Effect of Thin Interfacial SiO_2 Films on Metal Contacts to B Doped Diamond Films*, J. Electrochem. Soc., Vol. **139**, No. 5, May 1992.

20. T.P. Humphreys, H. Jeon, R.J. Nemanich, J.B. Posthill, R.A. Rudder, D.P. Malta, G.C. Hudson, R.J. Markunas, J.D. Hunn, N.R. Parikh, *Growth and Characterization of Heteroepitaxial Nickel Films on Diamond Substrates*, Materials Research Society Symposium Proceedings, Vol. **202**, 1991, 463.

21. R.J. Graham, J.B. Posthill, R.A. Rudder, R.J. Markunas, *Cathodoluminesence from Diamond Films Grown by Plasma-Enhanced Chemical Vapor Deposition in Dilute Co/H_2. CF_4/H_2 and CH_4/H_2 Mixtures*, Applied Physics Letters, Vol. **59**, 1991, 2463.

Surface Science Letters 277 (1992) L95–L99
North-Holland

surface science letters

Surface Science Letters

Effects of subsurface Na, H and C on CH_3 adsorption on Ni(111)

Hong Yang, Jerry L. Whitten
Department of Chemistry, North Carolina State University, Raleigh, NC 27695-8204, USA

Raymond E. Thomas, Ronald A. Rudder and Robert J. Markunas
Research Triangle Institute, Research Triangle Park, NC 27709-2194, USA

Received 26 June 1992; accepted for publication 6 August 1992

Ab initio valence orbital configuration interaction calculations are used to study the energy effect of Na, H and C atom subsurface species on CH_3 chemisorption at a hollow 3-fold site on Ni(111). The lattice is modeled as an embedded three layer cluster of 41 atoms. Ni 3d orbitals are explicitly included on seven nickel atoms on the surface. The calculated chemisorption energies of pyramidal CH_3 on Ni(111) are 38 for the clean surface and 50, 47, and 17 kcal/mol for the Na, H, and C implants, respectively. The energies required to distort tetrahedral CH_3 into a planar structure are 22 kcal/mol on clean Ni(111), 30 kcal/mol with the Na implant, 24 kcal/mol with the H implant, and 12 kcal/mol with the C implant, respectively. Thus, Na below the surface may stabilize a carbon overlayer to a tetrahedral diamond structure. CH_3-surface distances, C–H stretching and surface–CH_3 vibrational frequencies are also reported.

1. Introduction

In the past decade, diamond film growth has received a great deal of attention not only due to the pure scientific interest in the low pressure formation of metastable diamond but also due to the many practical applications that exist for diamond films [1–9]. Despite the progress that has been made in developing a variety of techniques for diamond film formation, understanding the mechanisms for diamond formation is still a subject of current debate. Continued progress in diamond film technology will depend in particular on developing a better understanding of diamond heteronucleation and correspondingly heteroepitaxy. Heteroepitaxial growth of diamond on c-BN has been successful, but the availability of c-BN limits the utility of this technology. Epitaxial growth on other closely lattice matched materials such as Ni, Cu, or Co have had only limited success. The formation of aligned diamond crystals in a small local area has been reported for diamond growth on Ni [10]. One difficulty in diamond heteroepitaxy is the poor chemical bonding between adsorbate and substrate. During heteronucleation, adsorbate species such as methyls are receiving substantial fluxes of atomic H. Under this high flux, carbon adsorbates on the surface are gasified, defeating diamond nucleation. As a result, diamond nucleation and growth is sporadic and highly three-dimensional.

In the present studies, ab initio cluster model calculations are used to investigate the energy effect of subsurface interstitials such as Na, H, and C on the bonding of a CH_3 radical to a hollow 3-fold site on Ni(111). The calculated results show that the presence of electropositive subsurface species in Ni dramatically increase the bond strength between a CH_3 radical and the Ni surface. Correspondingly, electronegative subsurface species such as C dramatically weaken a CH_3–Ni surface bond. In addition, the energy required to planarize a tetrahedral CH_3 on Ni(111) increases when electropositive species reside interstitially below the Ni surface.

Calculations are performed in the context of a many-electron embedding theory that permits the accurate computation of molecule–solid surface interactions at an ab initio configuration interaction level. The CH_3 and local surface region are treated as embedded in a lattice electron distribution which is modeled as a 41-atom, three layer cluster.

The objective of the present paper is to calculate the adsorption energy of CH_3 on Ni(111) with subsurface Na, H, and C implants and then to calculate the energy required to distort the tetrahedral CH_3 into a planar structure on the surface.

2. The theory and calculations

The purpose of the embedding theory employed in this work is to treat adsorbed species and a surface region of the metal with sufficient accuracy to describe reaction energetics, while at the same time maintaining a proper coupling of the surface region to the bulk [11–13]. The present approach most closely resembles that in refs. [14,15], where the details of the method are discussed. Calculations are performed by first obtaining self-consistent-field (SCF) solutions for the nickel cluster plus adsorbed species. The occupied and virtual orbitals of the SCF solution are then transformed separately to obtain orbitals spatially located about all the atoms of the cluster except those in the seven-atom surface region shown in fig. 1. This unitary transformation of orbitals is based upon exchange maximization with the valence orbitals of atoms outside the surface region and is designed to enhance convergence of the configuration interaction (CI) expansion [11–13].

The CI calculations involve single and double excitations from multiple parent configurations within a 28 or 29-electron subspace to 28 possible localized virtual orbitals. All configurations arising from excitations with an interaction energy greater than 1×10^{-5} hartree with the parent SCF configuration are explicitly retained in the expansion; contributions of excluded configurations are estimated using second order perturbation theory. For all geometries calculated, the SCF solution is the dominant configuration. Configurations with coefficients > 0.05 are included as parent configurations. Details of the procedure are given in ref. [16]. Basis superposition contributions to the total energy were taken into account by calculating the energy of the Ni cluster with the adsorbed species' virtual basis present (but not the adsorbate nuclei).

The cluster geometry and local region of the nickel cluster used to model the (111) crystal face of nickel are shown in fig. 1. The three layer, 88-atom cluster, consists of a surface layer of 37

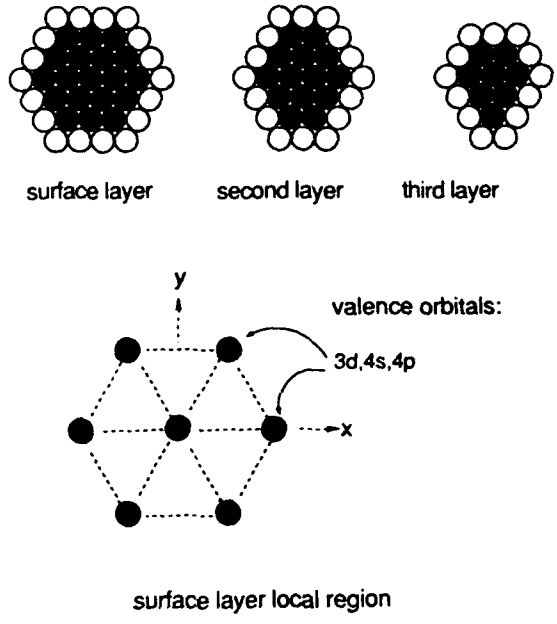

Fig. 1. Cluster geometry and local region of the nickel cluster used to model the (111) crystal face of nickel. The three layer, 88-atom cluster, consists of a surface layer of 37 atoms, a second layer of 30 atoms and a third layer of 21 atoms. Embedding theory is used to reduce the Ni_{88} cluster to a 41 atom model depicted as shaded atoms. Atoms surrounding the seven local region atoms in the surface layer and those surrounding the four central atoms in the second layer are described by effective potentials for $(1s)^2 \cdots (3p)^6(3d)^9(4s)^{1/2}$ and $(1s)^2 \cdots (3p)^6(3e)^9(4s)^{3/10}$ configurations, respectively. Effective potentials for the shaded atoms in the third layer describe the $(1s)^2 \cdots (3p)^6(3d)^9(4s)^{3/4}$ configuration. Unshaded atoms have neutral atom (1s–3p core)$(3d)^9(4s)^1$ potentials. All atoms have Phillips–Kleinman projectors $\Sigma|Q_m\rangle\langle Q_m|(-\epsilon_m)$ for the fixed electronic distribution. The nearest neighbor Ni–Ni distance is 2.48 Å.

atoms, a second layer of 30 atoms and a third layer of 21 atoms. Embedding theory is used to reduce the Ni_{88} cluster to the 41-atom model depicted as shaded atoms: the surface layer of 19 atoms, a second layer of 14 atoms, and a third layer of 8 atoms. For the seven-nickel-atom local surface region, a [1s–3p] core potential is used; 3d, 4s and 4p orbitals are explicitly included in the valence basis. Other Ni atoms are described by an effective core potential for [1s–3d] electrons, and a single 4s orbital. For all boundary atoms, and those in the third layer, the core potential is further modified to account for bonding to the bulk region, as described in refs. [14,15]. The basis orbitals of Ni, C, and H are the same as used in previous dissociative chemisorption studies of CH_4 on Ni(111) [17]. A double-zeta s and p basis for Na is taken from Veillard [18] and augmented with a set of p polarization functions (exponent of 0.5).

The Na, H and C interstitials are positioned below a hollow 3-fold site and midway between the first and second layers, as shown in fig. 2.

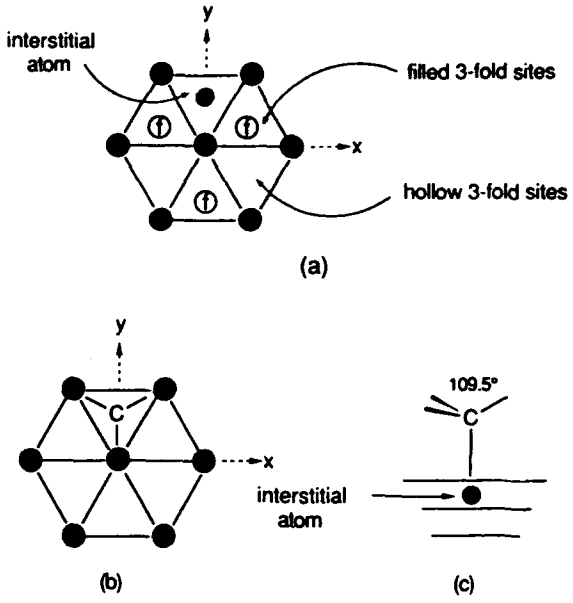

Fig. 2. CH_3 geometry and the local region of Ni(111) showing subsurface Na, H and C atoms. The interstitial species are below a hollow 3-fold site, midway between the first and second layers. The vertical distance of the interstitial to the first and second layers is 1.01 Å.

3. Results

Fig. 2 shows the geometry of pyramidal CH_3 adsorbed at a hollow 3-fold site, where there is no second layer Ni atom underneath. The interstitial Na, H or C atom is below the hollow 3-fold site, in the interstitial position midway between the first and second layers. In the initial carbon–surface distance optimization, the C–H bond lengths are fixed at 1.08 Å and the HCH angles at 109.5°. Calculated adsorption energies, distances from CH_3 to the surface, and vibrational frequencies are reported in table 1. For CH_3 on clean Ni(111), the computed adsorption energy is 38 kcal/mol with a surface–CH_3 distance of 1.90 Å. These values along with the calculated vibrational frequencies are consistent with our previous calculations of CH_3 on Ni(111), where the lattice was modeled as a 28-atom, three layer cluster [19,20].

For CH_3 adsorption at the 3-fold site above the interstitial atom, the chemisorption energy increases to 50 and 47 kcal/mol for Na and H subsurface atoms, respectively. However, the energy decreases to 17 kcal/mol in the case of a C subsurface atom. The distances of $CH_3$to the surface change only slightly from 1.85 to 1.93 Å.

Thus CH_3 adsorption energies are comparable for Na and H interstitials; while the subsurface C significantly weakens the CH_3–surface bond to a

Table 1
Adsorption energies (E_b), CH_3 distances from C to the surface (R_e), and vibrational frequencies for CH_3 adsorbed at a hollow 3-fold site on Ni(111) with subsurface Na, H and C interstitials.

	E_b (kcal/mol)	R_e (Å)	Ni–CH_3 stretch (cm^{-1})	C–H stretch (cm^{-1})
Ni(111)	38	1.90	374	3140
Na interstitial	50	1.85	361	3140
H interstitial	47	1.87	340	3130
C interstitial	17	1.93	476	3170

Results are from configuration interaction calculations and are corrected for basis superposition effects of approximately 3 to 4 kcal/mol.

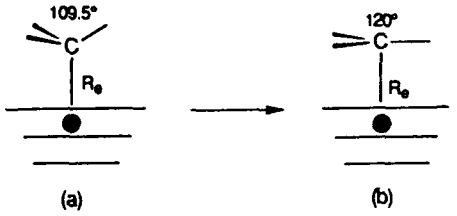

	Ni(111)	Na Interstitial	H Interstitial	C Interstitial
ΔE (Kcal/mol)	+22	+30	+24	+12

Fig. 3. Tetrahedral and planar CH_3 geometries on Ni(111) with subsurface Na, H and C interstitials (shaded circles). The interstitials are below a hollow 3-fold site, midway between the first and second layers. ΔE is the energy required to distort the tetrahedral geometry of (a) into a planar structure of (b). The CH_3–surface distances (R_e) are listed in table 1.

value less than one-half that for Ni(111) with no interstitial species. Na is an electron donor and the 3s electron is distributed over the neighboring Ni atoms in the first and second layers. It is therefore easier for CH_3 to receive electronic charge from the surface and form a strong bond. The interstitial H behaves somewhat like the Na interstitial, but its net charge is only $+0.09|e|$. On the other hand, Mulliken populations from the SCF calculations show that the C interstitial receives almost 2 electrons [21]. The surface adsorption region becomes electron deficient, and the CH_3–surface bond strength is diminished since it is more difficult for CH_3 to pull electrons from the substrate.

Fig. 3 shows the energy required to distort the tetrahedral CH_3 into a planar structure on Ni(111) with and without the interstitial species. The purpose of these calculations is to determine whether the implants stabilize or destabilize the CH_3 tetrahedral geometry. The figure shows that the energy required to distort tetrahedral CH_3 to a planar sp^2 geometry is 22 kcal/mol on Ni(111), at the surface–CH_3 equilibrium distance of 1.90 Å. For Ni(111) with an interstitial Na atom, this energy increases to 30 kcal/mol, for interstitial H, the value is 24 kcal/mol, and with the C interstitial atom, only 12 kcal/mol is required. The latter value is about one-half that required for distortion of CH_3 on Ni(111) with no implant.

As indicated above, the interstitial atoms are positioned below a hollow 3-fold site and midway between the first and second layers, i.e., at the center of an octahedral hole in the lattice. The smaller, tetrahedral hole (below the filled 3-fold site) was not investigated. The octrahedral hole is not quite large enough to accommodate Na^+ and is much too small for negatively charged carbon. Therefore, we would expect that interstitial species such as Na and C, and to a lesser extent hydrogen, will expand the lattice locally. This in turn will affect some of the properties we have calculated, but the extent is unclear. Further, the implant species are mobile and in the case of H and C may ultimately react with the adsorbed CH_3. Thus, although the large effects found in the present study are intriguing, much more work is needed before a quantitative understanding of accompanying effects will be possible.

4. Conclusions

The conclusions of the present study of CH_3 at a hollow 3-fold site on Ni(111) with subsurface Na, H and C interstitials can be summarized as follows.

(1) Tetrahedral CH_3 binds strongly to the Ni(111) when an interstitial Na or H atom implant is present; the adsorption energy is 50 or 47 kcal/mol, respectively, compared to 38 kcal/mol for Ni(111) with no implant. The adsorption energy is only 17 kcal/mol in the presence of a subsurface C implant. The corresponding CH_3–surface distances are 1.85, 1.87, and 1.93 Å for Na, H, and C cases, respectively. With no implant the value is 1.90 Å.

(2) Energies required to distort tetrahedral sp^3 CH_3 into a planar sp^2 structure are 22 kcal/mol on Ni(111), and 30, 24, and 12 kcal/mol for Na, H, and C implants, respectively.

(3) Calculated C–H stretching frequencies are all around 3150 cm^{-1} with or without the implants. The surface–CH_3 perpendicular stretch vibrational frequencies are 374 cm^{-1} on Ni(111), and 361, 340, and 476 cm^{-1} with the Na, H, and C implants, respectively.

(4) The present studies indicate that C below the Ni surface may make it easier for a carbon overlayer to revert to a planar graphite structure, while interstitial Na atoms may stabilize a tetrahedral C sp^3 structure on Ni(111).

Note added: A recent published experimental study by Ceyer and coworkers [22] has demonstrated that interstitial H is the active species in the hydrogenation of CH_3 on Ni(111). The reaction of surface hydrogen with methyl is inhibited by a substantial energy barrier [17]. The experimental evidence is consistent with H in an octahedral interstitial site reacting with CH_3 adsorbed at the 3-fold surface site above H (see fig. 2c). Our theoretical results suggest that the presence of interstitial H enhances the adsorption energy of CH_3 at this site.

Acknowledgments

This work was supported by the Office of Naval Research, the Strategic Defense Initiative Organization–Innovative Science and Technology office. Studies of the clean surface and interstitial H was supported by the US Department of Energy.

References

[1] R. Messier, J.T. Glass, J.E. Butler and R. Roy, Eds., New Diamond Science and Technology (MRS, Pittsburgh, 1991).
[2] R.F. Davis, Z. Sitar, B.E. Williams, H.S. Kong, H.J. Kim, J.W. Palmour, J.A. Edmond, J. Ryu, J.T. Glass and C.H. Carter, Jr., Mater. Sci. Eng. B 1 (1988) 77.
[3] R.A. Rudder, J.B. Posthill and R.J. Markunas, Electron. Lett. 25 (1989) 1220.
[4] K.E. Spear, J. Am. Ceram. Soc. 72 (1989) 171.
[5] H. Kawarada, J.S. Ma, T. Yonehara and A. Hiraki, Mater. Res. Soc. Symp. Proc. 162 (1990) 195.
[6] H. Itoh, T. Nakamura, H. Iwahara and H. Sakamoto, in: New Diamond Science and Technology, Eds. R. Messier, J.T. Glass, J.E. Butler and R. Roy (MRS, Pittsburgh, 1991) p. 929.
[7] W.A. Yarbrough, J. Vac. Sci. Technol. A 9 (1991) 1145.
[8] J.F. Prins and H.L. Gaigher, in: New Diamond Science and Technology, Eds. R. Messier, J.T. Glass, J.E. Butler and R. Roy (MRS, Pittsburgh, 1991) p. 56.
[9] J. Narayan, V.P. Godbole and C.W. White, Science 252 (1991) 416.
[10] Y. Sato, I. Yashima, H. Fujita, T. Ando and M. Kamo, in: New Diamond Science and Technology, Eds. R. Messier, J.T. Glass, J.E. Butler and R. Roy (MRS, Pittsburgh, 1991) p. 371.
[11] J.L. Whitten and T.A. Pakkanen, Phys. Rev. B 21 (1980) 4357.
[12] J.L. Whitten, Phys. Rev. B 24 (1981) 1810.
[13] P. Cremaschi and J.L. Whitten, Surf. Sci. 149 (1985) 273.
[14] J.L. Whitten, in: Cluster Models for Surface and Bulk Phenomena, Eds. G. Pacchioni and P.S. Bagus (Plenum, New York, 1992) p. 375.
[15] P. Cremaschi and J.L. Whitten, Theor. Chim. Acta 72 (1987) 485.
[16] P. Madhavan and J.L. Whitten, J. Chem. Phys. 77 (1982) 2673.
[17] H. Yang and J.L. Whitten, J. Chem. Phys. 96 (1992) 5529.
[18] A. Veillard, in: Handbook of Gaussian Basis Sets, Eds. R. Poirier, R. Kari and I.G. Csizmadia (Elsevier, New York, 1985) table 11.9.2.
[19] H. Yang and J.L. Whitten, J. Am. Chem. Soc. 113 (1991) 6442.
[20] H. Yang and J.L. Whitten, Surf. Sci. 255 (1991) 193.
[21] The electron charge ascribed to the C atom (and to H or Na) should not be interpreted strictly as an atomic charge but as a measure of the electron distribution in the vicinity of the interstitial atom.
[22] A.D. Johnson, S.P. Daley, A.L. Utz and S.T. Ceyer, Science 257 1992) 223.

Cathodoluminescence from diamond films grown by plasma-enhanced chemical vapor deposition in dilute CO/H_2, CF_4/H_2, and CH_4/H_2 mixtures

R. J. Graham
Center for Solid State Science, Arizona State University, Tempe, Arizona 85287-1704

J. B. Posthill, R. A. Rudder, and R. J. Markunas
Research Triangle Institute, Research Triangle Park, North Carolina 27709-2194

(Received 19 June 1991; accepted for publication 30 August 1991)

Diamond films grown by rf plasma-enhanced chemical vapor deposition in dilute CO, CF_4, and CH_4 (diluent H_2) mixtures have been examined by cathodoluminescence (CL) in a transmission electron microscope to assess the incorporation of optically active impurities and defects. The details of the CL spectra are found to be dependent on the different gas mixtures and are correlated with the different film microstructures. Dislocation-related band *A* CL due to closely spaced donor-acceptor (*D-A*) pairs was observed from both the CO and CH_4-grown films, but was absent in the CF_4-grown material. Band *A* CL due to widely separated (*D-A*) pairs was seen in all samples but was especially dominant in the CF_4-grown film. Emission due to a di-Si interstitial impurity was observed in CO- and CF_4-grown films but was absent in the CH_4-grown material.

The chemical vapor deposition (CVD) of diamond films is currently receiving much attention.[1] At present, attempts at heteroepitaxial growth, usually on Si substrates, have resulted in heterogeneous polycrystalline films containing many defects and impurities. One of the goals of such growth methods must be the control of the formation of these inhomogeneities, especially if potential optical and electronic applications are to be realized. The aim of this study was to investigate how the use of dilute CO and CF_4, rather than the usual CH_4, in the CVD process might affect the incorporation of impurities or defects and the electronic states associated with them. The analytical technique used was spectrally resolved cathodoluminescence (CL) performed in a transmission electron microscope (TEM) which allows a simultaneous correlation of CL emission with specimen microstructure.

Three polycrystalline diamond films, 1–2 μm thick, were grown on Si(100) substrates by rf plasma-enhanced CVD (PECVD) using the following gas compositions and growth conditions: (1) 1% CH_4, 99% H_2, pressure = 5.0 Torr, temperature ~650 °C; (2) 2% CO, 98% H_2, pressure = 3.0 Torr, temperature ~630 °C; (3) 8% CF_4, 92% H_2, pressure = 5.0 Torr, temperature ~820 °C. Details of the growth of this last film are described in another publication.[2] An additional film was grown using 2% CO/98% H_2 at a temperature of ~725 °C on *R*-plane ($10\bar{1}2$) sapphire to examine the effect of the substrate on the presence of impurities and defects. The substrates for the CO- and CH_4-grown films were scratched with diamond paste prior to deposition whereas the CF_4-grown film was grown on an unscratched and untreated Si substrate. Specimens were prepared for TEM by dimple polishing and milling with Ar^+ ions. Detection of CL was performed in TEM,[3] which also allowed the microstructure to be observed, using a 120 keV electron beam and liquid-nitrogen-cooled specimen stage.

Figure 1 shows CL spectra in the 300–900 nm range acquired from 15μm-diam regions from all four films. The CH_4-grown film gave a spectrum which consists of a broad peak at 428±1 nm (2.90±0.01 eV) superimposed on an even broader band with a maximum around 470±1 nm (2.637±0.005 eV). The CF_4-grown film gave a broad band centered at 540±1 nm (2.295±0.004 eV), and a small peak at 737.8±0.5 nm (1.680±0.001 eV). Spectra from both CO-grown films exhibit a number of similar spectral features as summarized in Table I.

The CH_4-grown material consists of a perforated film containing 1–2 μm-sized grains, many with well-developed growth habits and microtwins. The grains often contain a high density of other small defects, possibly stacking faults or inclusions of nondiamond carbon, and associated static

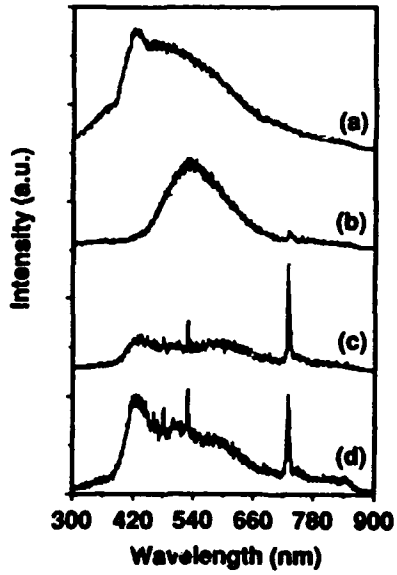

FIG. 1. CL spectra from polycrystalline diamond films: (a) 1% CH_4, 99% H_2, pressure = 5.0 Torr, temperature ~650 °C on Si(100); (b) 8% CF_4, 92% H_2, pressure = 5.0 Torr, temperature ~820 °C on Si(100); (c) 2% CO, 98% H_2, pressure = 3.0 Torr, temperature ~630 °C on Si(100); (d) 2% CO, 98% H_2, pressure = 3.0 Torr, temperature ~725 °C on *R*-plane ($10\bar{1}2$) sapphire.

 0003-6951/91/442463-03$02.00

TABLE I. CL spectral features observed in dilute CO CVD-grown diamond on sapphire and Si substrates.

2% CO/98% H_2 sapphire substrate	2% CO/98% H_2 Si substrate
431 ± 1 nm (2.88 ± 0.01 eV) band	436 ± nm (2.84 ± 0.01 eV) band
464 ± 1 nm (2.671 ± 0.006 eV) peak	not obs.
484 ± 1 nm (2.561 ± 0.005 eV) peak	484 ± 1 nm (2.561 ± 0.005 eV) peak
503 ± 1 nm (2.464 ± 0.005 eV) peak	not obs.
534 ± 1 nm (2.321 ± 0.004 eV) peak	534 ± 1 nm (2.321 ± 0.004 eV) peak
586 ± 1 nm (2.115 ± 0.004 eV) shoulder	607 ± 1 nm (2.042 ± 0.003 eV) band
737.8 ± 0.5 nm (1.680 ± 0.001 eV) peak	737.8 ± 0.5 nm (1.680 ± 0.001 eV) peak

disorder, as also evidenced by significant diffuse scatter in convergent beam electron diffraction (CBED) patterns observed from individual crystals. The CF_4-grown film is continuous with a smaller grain size (0.1–0.3 μm). Although many grains are heavily microtwinned, inclusions are generally absent. Some grains are defect-free and CBED indicates a low degree of static disorder. The microstructure of the CO-grown films is very substrate dependent. On Si the film is continuous consisting of very defective 0.1–0.5 μm-sized grains whereas on sapphire highly defective connected nodules (1 μm diameter) form a perforated film. The weak CL intensity and small grain size in some of these films precluded a detailed correlation of microstructure with CL as has been demonstrated previously in CVD-grown diamond.[4] However, a general correlation with overall film structure is described below.

The emissions listed in Table I are identified as follows. The bands at 431 and 436 nm are known as band *A* and are due to closely spaced donor-acceptor (*D-A*) pairs. This emission is normally associated with natural, rather than synthetic, diamonds[5] but has often been observed from CVD-grown material[6–11] and has been correlated with dislocations.[4] The bands at 586 and 607 are probably also band *A* but are due to widely separated *D-A* pairs and are more typical of synthetic diamond, although the peak of the band at 607 nm is at the low-energy limit for band *A*. The intense peak at 737.8 nm is the same, within experimental error, as that observed previously in CVD-grown diamond and is due to di-Si interstitial impurities.[4,11–13] The origins of the emissions at 464, 484, and 503 nm are unknown although they have been observed previously in dilute CH_4 CVD-grown diamond.[8] The 534 nm peak has also been observed in CH_4-grown material and may be due to a nitrogen-vacancy-related complex.[8,9,12] For the CH_4-grown film, the 428 nm band is again due to closely spaced *D-A* pairs. The very broad band on which this is superimposed is probably also due to *D-A* pairs although it has an uncommonly large full width at half maximum (FWHM) of over 1100 meV and peaks at a higher energy than is usually encountered in *D-A* emission. For the CF_4-grown material, the band at 540 nm is typical of band *A* emission from widely separated *D-A* pairs in synthetic diamond. The small FWHM (7 meV) of the small peak at 737.8 nm confirms that this is again due to Si interstitials.

The *D-A* pair bands are due to nitrogen and boron impurities which presumably exist as contaminants of the source gases, vacuum system, and reactor components. Secondary-ion mass spectrometry (SIMS) of the films confirms the presence of these impurities. The interstitial Si impurity is believed to originate from the etching of either the Si substrate or silica reactor walls by the plasma. No new CL emissions from the CO- or CF_4-grown films were observed, suggesting that neither O or F are present as optically active impurities, although certainly F is incorporated in the CF_4-grown film during growth, as revealed by SIMS. In natural diamond, O has been found to exist at the 30–90 ppm level,[14] as elemental or mineralogical inclusions or possibly as a substitutional or interstitial impurity.[15] No optical activity has been documented which is consistent with our observations. No information about the presence of F in diamond was found in the literature.

The details of the CL emissions and film microstructure are, however, dependent on the growth gases and we now attempt to correlate the two. Dealing first with band *A* luminescence, all specimens, except the CF_4-grown films, show emission at around 430 nm due to closely spaced *D-A* pairs. Previous studies, which show that this emission is correlated with dislocations in CVD-grown diamond,[4] suggest that dislocations are present in these films. Potentially other defects, e.g., stacking faults, nondiamond inclusions may also allow *D-A* pairs to exist in the closer proximity normally associated with defect-free natural diamond. This may account for the extremely broad band *A* observed in the CH_4-grown material where such defects in single crystals abound and to a lesser extent the CO-grown film on sapphire. However, if the density of other defects becomes too high resulting in poor crystallinity, increased nonradiative recombination reduces the overall CL intensity, as seen in the CO-grown films. Significantly, the CF_4-grown material was the least defective at a microscopic level, i.e., excluding microtwins, and showed no such band due to closely spaced *D-A* pairs. All films showed some degree of band *A* due to widely separated *D-A* pairs normally seen in synthetic diamond. In the CF_4-grown films this was the only peak of any significant intensity and the slightly higher peak energy, 2.3 eV compared with about 2.1 eV for the CO-grown films, suggests a smaller mean *D-A* pair separation. Faster growth rates have been observed when O is added to dilute CH_4,[14] which might result in *D-A* pairs being incorporated in even more random lattice sites resulting in larger mean *D-A* pair separation and a band *A* peak at lower energy.

The CO- and CF_4-grown films all showed some degree of interstitial di-Si impurity which is believed to originate from etching of Si-containing materials by the plasma in the growth zone. Although absent in the CH_4-grown film

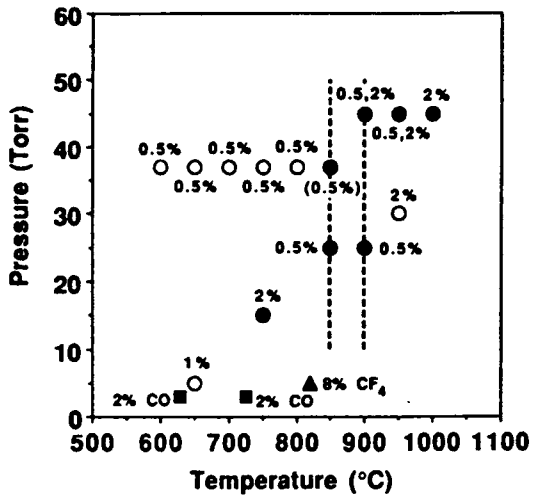

FIG. 2. Incidence of the di-Si interstitial defect, as observed by CL (1.681 eV peak), CVD-grown diamond on Si substrate as a function of growth temperature and pressure with the concentration of CH_4 used indicated; ● = peak observed, ○ = peak not observed, data from Refs. 4, 8–11, 13, and this work. For comparison, films grown using dilute CF_4 and CO (on Si and sapphire) which show the 1.681 eV peak are also represented (▲ = dilute CF_4, ■ = dilute CO). Broken vertical lines indicate range of pressures used for films shown as grown at 25 Torr, since exact pressures were not given. For the data point in parentheses, the peak in the CL spectrum was identified as GR1 due to neutral vacancy defect rather than di-Si (Ref. 9). Similarly, the peak in Ref. 10 was identified as GR1 but subsequently attributed to di-Si by the same workers (Ref. 13).

here, this has been observed in similar material by other workers.[4,11–13] The reason for this probably lies in the details of the growth conditions; previous observations by CL of the di-Si interstitial defect shown graphically in Fig. 2 suggest that it only occurs at higher growth temperatures and pressures and/or CH_4 concentration, although the limited number of data points, the different growth methods and other reactor-dependent variables make such a generalization only tentative. Intense peaks in the CO-grown films, grown under similar conditions to the CH_4-grown material, indicate that CO enhances the etching potency of the plasma resulting in higher levels of di-Si impurity. Conversely, the small size of this peak in the CF_4-grown film shows that little of this impurity has been incorporated as the optically active di-Si interstitial form during growth. This is surprising since CF_4-based plasmas are known to be very reactive; even visible etching of a glass viewport in the reactor occurred during previous runs. In addition, SIMS shows the Si content to be higher in this film than in the CO-grown films. This suggests that Si is also being incorporated as an optically inactive form and so implies that the nature of incorporation of Si depends on the gaseous species used and formed during the CVD growth process.

The source of the Si impurity has also been the subject of recent investigation. The spectra from the CO-grown material on the Si and sapphire substrates show the same basic emissions inspite of large differences in film microstructure. However, relative to band *A* and other emissions, the peak due to the di-Si interstitial defect was much more intense when the substrate was Si, indicating that much of this impurity originates from the substrate. The persistence of this peak when a sapphire substrate is used indicates that at least some of the Si originates from the reactor which contrasts with recent studies by Ruan *et al.*[13] who found that this peak only when a Si substrate was used during growth with dilute CH_4. This could be explained by the apparently enhanced etching properties of the CO-containing plasma as previously discussed. The potential for reactor "memory" due to deposits on the reactor wall from earlier depositions on Si substrates also exists.

In conclusion, use of dilute CO and CF_4 does not introduce any optically active impurity or defect states not previously observed in dilute CH_4-grown CVD diamond. The different gases do, however, result in different film microstructures and concomitant CL spectra. Dislocation-related band *A* CL is observed from CO- and CH_4-grown films but only widely separated *D-A* pairs exist in the CF_4-grown material. The di-Si interstitial impurity was most readily incorporated in CO-grown films, with both the Si substrate and reactor walls believed to be the source. In comparison, the CF_4-grown film contained a higher concentration of Si, but only a small amount as the optically active di-Si form.

We are pleased to thank G. C. Hudson and D. P. Malta for their technical input and helpful discussions. This work was supported by the Facility for High Resolution Electron Microscopy at Arizona State University, supported by NSF Grant No. DMR-89-13384. JBP, RAR, and RJM gratefully acknowledge support of this work by the Strategic Defense Initiative Organization/Innovative Science and Technology through the Office of Naval Research (Contract No. N000014-86-C-0460).

[1] See, for example, "Diamond and Diamond-like Materials," special section of J. Mater. Res. **5**, 2273 (1990).
[2] R. A. Rudder, G. C. Hudson, J. B. Posthill, R. E. Thomas, and R. J. Markunas, Appl. Phys. Lett. **59**, 791 (1991).
[3] S. H. Roberts, Inst. Phys. Conf. Ser. **61**, 51 (1981).
[4] R. J. Graham, T. D. Moustakas, and M. M. Disko, J. Appl. Phys. **69**, 3212 (1991).
[5] P. J. Dean, Phys. Rev. **139**, A588 (1965).
[6] H. Kawarada, K. Nishimura, T. Ito, J-i. Suzuki, K-S. Mar, Y. Yokota, and A. Hiraki, Jpn. J. Appl. Phys. **27**, L683 (1988).
[7] A. T. Collins, M. Kamo, and Y. Sato, J. Phys. **1**, 4029 (1989).
[8] A. T. Collins, M. Kamo, and Y. Sato, J. Phys. **22**, 1402 (1989).
[9] L. H. Robins, L. P. Cook, E. N. Farabaugh, and A. Feldman, Phys. Rev. B **39**, 13367 (1989).
[10] W. D. Partlow, J. Ruan, R. E. Witkowski, W. J. Choyke, and D. S. Knight, J. Appl. Phys. **67**, 7019 (1990).
[11] A. T. Collins, M. Kamo, and Y. Sato, J. Mater. Res. **5**, 2507 (1990).
[12] V. S. Vavilov, A. A. Gippius, A. M. Zaitsev, B. V. Deryagin, B. V. Spitsyn, and A. E. Alenksenko, Sov. Phys. Semicond. **14**, 1078 (1980).
[13] J. Ruan, W. J. Choyke, and W. D. Partlow, Appl. Phys. Lett. **58**, 295 (1991).
[14] H. W. Fesq, D. M. Biddy, C. S. Erasmus, E. J. D. Kable, and J. P. F. Sellschop, in *Physics and Chemistry of the Earth*, edited by L. H. Ahrens, J. B. Dawson, A. R. Duncan, and A. J. Erlank (Pergamon, Oxford, 1975), Vol. 9, p. 817.
[15] J. Walker, Rep. Prog. Phys. **42**, 1605 (1979), and references therein.

Thermal desorption from hydrogenated and oxygenated diamond (100) surfaces

R. E. Thomas, R. A. Rudder, and R. J. Markunas
Research Triangle Institute, Research Triangle Park, North Carolina 27709

(Received 17 December 1991; accepted 3 February 1992)

Low energy electron diffraction (LEED) has been used to study the effects of atomic and molecular species of hydrogen and oxygen on the reconstructed C(100)-(2×1) surface. Thermal desorption spectroscopy was also used to study desorption products and kinetics from hydrogenated and oxygenated surfaces. Atomic hydrogen appears relatively inefficient at breaking C–C dimer bonds on the (100)-(2×1) surface. Atomic oxygen, in contrast, readily converts the surface from the 2×1 state to the 1×1 state. This process is reversible for a limited number of cycles before degradation of the surface obscures the 2×1 LEED pattern. Oxygen is thought to adsorb in one of two configurations, bridging carbon atoms on the surface, or double bonded to a single carbon atom on the surface. Thermal desorption of molecular hydrogen from hydrogenated C(100)-(2×1):H surfaces occurs at approximately 900 °C for a heating rate of 20 °C/s. Molecular hydrogen is the major desorption product and the desorption temperature appears to be coverage independent. Thus the desorption kinetics are most likely first order. Thermal desorption of carbon monoxide from oxygenated C(100)-(1×1):O surfaces occurs at approximately 600 °C for a heating rate of 20 °C/s. Carbon monoxide is the major product seen, with small quantities of carbon dioxide also observed. For increasing oxygen coverages, the desorption peak is observed to shift to lower temperatures. A peak shift to lower temperatures can be interpreted as either first order kinetics with a coverage dependent activation energy or second order kinetics. The reaction order is not known in this case, but from analysis of the peak shapes and from the fact that CO can desorb without prepairing, the data suggest that the reaction is first order.

I. INTRODUCTION

Hydrogen plays an integral role in many of the chemical vapor deposition (CVD) diamond growth processes developed to date.[1] Hydrogen is thought to function in the growth process in a number of ways, including maintenance of sp^3 hybridization of carbon atoms at the growth surface. Oxygen has been used in concentrations of approximately 1%–2% in H_2/CH_4 plasmas to extend the diamond growth regime with respect to gas composition and substrate temperature.[2,3] The role oxygen plays is perhaps more complicated. It has been suggested that oxygen increases the atomic hydrogen concentration through gas phase reactions and also etchs nondiamond carbon.[2] Recently, however, oxygen has been introduced to the growth process in much larger concentrations in the form of water and alcohols.[4] Bachmann *et al.* have assembled data from a variety of growth techniques to produce an empirical H–C–O diamond growth phase diagram.[5] The diagram indicates that diamond can be successfully grown with carbon and oxygen alone. In spite of numerous growth studies, the details of the roles of hydrogen and oxygen in the CVD growth environment are still unclear, as are fundamental questions concerning interactions of these two gasses with the diamond surface. In order to greatly simplify the systems under consideration, we have used a combination of low pressure gas dosing, temperature programmed desorption, and low energy electron diffraction (LEED) to study interactions of relatively simple gasses such as atomic hydrogen and atomic oxygen with a clean diamond surface.

Although similar in structure to the silicon (100) surface, the diamond (100) surface has not been studied nearly as intensively, with only a handful of experimental studies published to date.[6–10] Important questions remain concerning the details of the reconstruction and the effect of adsorbates on surface structure. As with silicon (100) the diamond (100) surface reconstructs to a rotated 2×1 dimer configuration upon heating.[6,8,10] Due to the higher bond strengths in the carbon system the reconstruction does not occur until the diamond is annealed to approximately 1000 °C, as opposed to 450 °C for silicon. There is also evidence that the reconstruction is not necessarily coupled with the thermal desorption of hydrogen from the surface as in the case of silicon. Hamza *et al.* report that both thermal desorption signals and "fast" protons generated by electron stimulated desorption are eliminated below 925 °C.[6] However, they report that the LEED half-order spot intensity does not begin to appear until the sample is annealed at 965 °C.[6]

Adsorption of atomic hydrogen has been reported to convert the surface back to the 1×1 configuration.[6] However, subsequent annealing to 1200 °C did not convert the surface back to the 2×1 configuration.[6] Theoretical calculations indicate a substantial barrier for the insertion of hydrogen into the C–C dimer bond.[11–13] From these calculations it appears difficult to form the dihydride from the

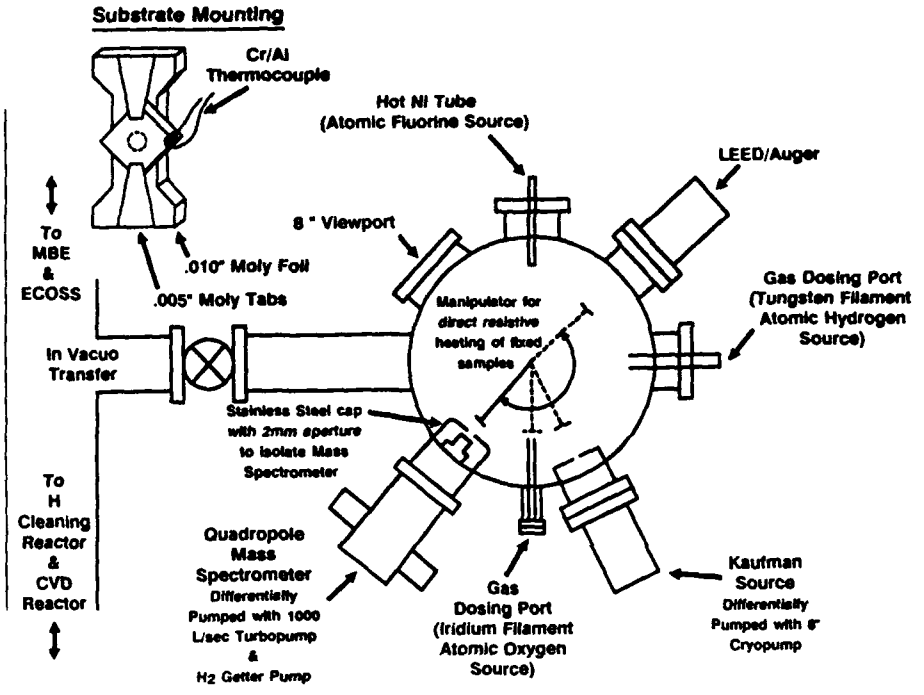

FIG. 1. Schematic view of system. Inset is a drawing showing details of the sample mounting and heater geometry.

monohydride by the exposure of the 2×1 surface to atomic hydrogen at 25 °C.

Oxygen interactions with the (100) surface are less well studied than those of hydrogen. Lurie and Wilson report no observable effect on LEED patterns upon exposure of the (100) surface to molecular oxygen.[10] Matsumoto exposed diamond powder to molecular oxygen at atmospheric pressure and room temperature and at 1 Pa at 500 °C.[14] In the case of the powder desorption, CO desorption peaks were seen at approximately 600 °C. Smaller desorption peaks were seen for CO_2 at approximately 500 °C.

In the present article we have used LEED to study the effects of atomic and molecular species of hydrogen and oxygen on the reconstructed 2×1 surface. Thermal desorption spectroscopy was also used to study desorption products and kinetics from hydrogenated and oxygenated surfaces.

II. EXPERIMENTAL PROCEDURES

Thermal desorption spectroscopy and LEED observations were performed in a stainless steel UHV system shown in Fig. 1. Turbomolecular pumps were used both on the main chamber and to differentially pump the chamber housing the quadrupole mass spectrometer. Additional hydrogen pumping capacity for the quadrupole chamber was provided by a bulk getter pump. Base pressure was 5×10^{-10} Torr for the sample chamber and 1×10^{-10} Torr for the quadrupole chamber. The sample chamber was separated from the quadrupole chamber by a 2 mm diam stainless steel aperture.

Sample heating was accomplished by clipping the crystals to a 0.25 mm thick molybdenum resistive strip heater. (inset Fig. 1) All parts associated with the heater stage, including the clamps and current leads were manufactured from molybdenum. The sample temperature was measured by a 0.125 mm diam chromel/alumel thermocouple threaded through a laser drilled hole in the diamond and held in tension against the crystal. (inset Fig. 1) Sample heating was controlled by feedback from the thermocouple to a silicon controlled rectifier power supply. After an initial warm-up phase, temperature ramps are linear from approximately 150 °C to over 1100 °C.

A series of control experiments were performed to ensure that thermal desorption signals observed actually originated from the sample surface. For both atomic hydrogen and atomic oxygen, samples were dosed in the standard manner and thermal desorptions run with the sample either adjacent to, but not in front of, the aperture, or with the aperture centered on a portion of the sample mounting assembly. No thermal desorption peaks were observed in any of the control experiments.

Two type IIa (100), $5\times5\times0.25$ mm, diamond crystals were used in the course of the present study. Other than thermal cleaning, no technique is available *in situ* for removing surface contamination from the diamond crystals. Particular attention was therefore paid to preparing the diamond surface before mounting in the vacuum system. The samples are initially hand polished for 5 min with 0.25 μm diamond grit and deionized (DI) water on a nylon polishing pad. The samples are then ultrasonically degreased in a series of solvents, trichloroethylene, acetone, methanol, and deionized water. Following the deionized water rinse, the samples are swabbed under DI water to remove particles. The samples are rinsed again in the solvent series and then placed in CrO_3/H_2SO_4 (125 °C) solution for 20 min to remove nondiamond carbon. The sam

ples are rinsed in DI water and then boiled in a 3:1 solution of HCl/HNO_3 for 20 min to remove any metals contamination. Finally the samples are rinsed in DI water and blow-dried with compressed nitrogen. Samples subjected to this cleaning process typically show a good quality 1×1 LEED pattern at beam voltages as low as 50 V with no annealing. For the initial thermal cleaning the samples were ramped up in temperature at approximately 10 °C/s until the pressure in the main chamber rose to 5×10^{-8} Torr at which point the power was shut off and the samples cooled. This cleaning cycle continued until a maximum temperature of 1150 °C was reached.

In all cases atomic hydrogen was generated via a tungsten filament operating at a temperature of approximately 1500 °C. Filament temperatures were measured with a hand held optical pyrometer. The sample was positioned approximately 2 cm from the filament during dosing. The sample was not actively cooled and at the lowest dosing pressures remained at room temperature. Atomic oxygen was generated via an iridium filament at 1100 °C. Very large scale integrated (VLSI) grade hydrogen and oxygen gasses were used with no further purification. No attempt was made to quantify the percentage of atomic species generated by the filaments. From earlier experiments on silicon (100) substrates, under conditions identical to those used in the present study, we can estimate the degree of molecular hydrogen dissociation. It was found that for unterminated silicon 2×1 surfaces an exposure for 300 s at a chamber pressure of 1×10^{-6} Torr was sufficient to convert the surface to the 1×1 configuration. Therefore, the surface has been exposed to at least one monolayer of atomic hydrogen. The effective pressure at the surface from the doser is probably higher than 1×10^{-6} Torr so the maximum degree of dissociation is approximately 1%. We have not performed similar experiments for oxygen dissociation but given the higher bond strength for the oxygen molecule, 119 kcal/mol, and the lower filament temperature used, we expect the degree of dissociation to be much less than that of molecular hydrogen. All doses quoted in the text are given for the total H_2 and O_2 exposure from uncorrected ion gauge tube readings. X-ray photoelectron spectroscopy was done *ex situ* after extensive dosing with both the tungsten and the iridium filaments and no evidence of metals contamination was seen.

III. EXPERIMENTAL RESULTS

A. Hydrogen dosing studies

Upon annealing more than 90% of the freshly polished surfaces used in the present study exhibited a transformation from the 1×1 configuration to the 2×1 configuration. During the initial annealing sequence the samples would typically show indications of the 2×1 structure at approximately 800 °C, with the transformation completed by 1050 °C on successive anneals. No correlations were observed between sample preparation conditions and failure of the surface to reconstruct.

Initial studies were concerned with exposure of the reconstructed diamond surface to atomic hydrogen. We find that even after extensive dosing with atomic hydrogen the surface remains in a 2×1 configuration. The maximum dose the samples received was approximately 40 000 $L(H/H_2)$. In contrast, a dose of 600 L under identical conditions is sufficient to convert the silicon (100) surface from the 2×1 state back to the 1×1 state. Given that we were unable to convert the surface back to the 1×1 configuration with atomic hydrogen, the subsequent adsorption and desorption experiments were all performed on the 2×1 surface.

In the next series of experiments clean 2×1 surfaces were dosed with varying quantities of atomic hydrogen and thermal desorption spectra were recorded. The primary desorption product observed was molecular hydrogen at approximately 900 °C. Figure 2 shows a series of desorption spectra taken after increasing atomic hydrogen exposures. There is no evidence of a shift in desorption peak temperature as a function of coverage, indicating the desorption process is first order. Exposure of the clean surface to equivalent doses of molecular hydrogen with no heated filament gave no thermal desorption features. Figure 3 shows a plot of integrated H_2 desorption peak area versus hydrogen dose. We can see that uptake for the surface is not linear with dose and that the surface appears to approach saturation while still in the 2×1 configuration. In addition to monitoring hydrogen, masses 12–18, 26–32, and 44 were scanned in the course of the experiments. Small quantities of masses 15, and 26 were observed to desorb from the surface but contamination from the source gas cannot be ruled out at this time.

B. Oxygen dosing results

Exposure of a reconstructed 2×1 surface to a mixture of atomic and molecular oxygen at 1×10^{-6} Torr for 300 s results in conversion of the surface to the 1×1 state. Exposure of an identical surface to a molecular oxygen dose an order of magnitude larger has no apparent affect on the surface structure; the LEED remains in a 2×1 pattern. Annealing of the 1×1:O surfaces to 1000 °C results in the restoration of the 2×1 surface. The cycle can be repeated approximately 10–15 times before the LEED pattern is left with weak first order spots only and a very high background. It should be emphasized that the surface is etched during each CO desorption cycle which may lead to roughening of the surface and deterioration of the LEED pattern.

Figure 4 shows a series of thermal desorption spectra for mass 28 (CO) from a diamond surface. The desorption traces show very broad peaks with a maximum in the desorption rate at approximately 600 °C. We also see a shift to lower desorption temperatures as coverage increases. Figure 5 shows the integrated area under the desorption peaks plotted as a function of total oxygen exposure. The sample shows a steep initial uptake followed by a much slower uptake at the higher exposures. The sample does not completely saturate after a dose of 4500 L although the uptake does decrease markedly.

In addition to mass 28, masses 2,16,17,18,32, and 44 were monitored. Small amounts of mass 44 were observed

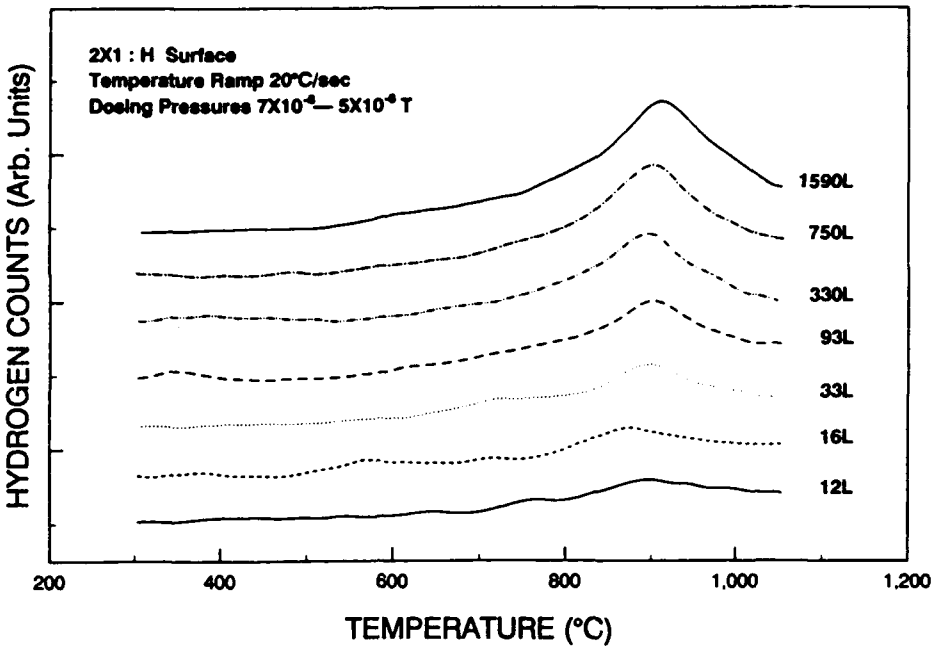

FIG. 2. Thermal desorption spectra from hydrogenated diamond-(2×1) surfaces. Molecular hydrogen was the major desorption product observed from all surfaces dosed with atomic hydrogen. All dosing was performed at 25 °C. Samples were exposed to a mixture of H and H_2 produced by the tungsten filament.

and were presumed to arise from CO_2. Figure 6 shows a comparison of the mass 44 thermal desorption and the mass 28 from the same desorption experiment. Note that the vertical scale for mass 44 has been expanded by a factor of 4. The maximum desorption rate occurs at approximately 550 °C for both masses but the CO_2 peak is much more asymmetric than the CO peak.

IV. DISCUSSION

Reconstruction of the diamond (100) surface to the 2×1 state is a well documented phenomena.[6–8,10] However, most researchers report that a percentage of the freshly polished surfaces studied do not reconstruct to the 2×1 structure upon annealing. Hamza *et al.* have reported an association between residual oxygen on the surface detected by electron stimulated desorption and the ability of the surface to reconstruct.[6] Samples with the most oxyge detected were less likely to reconstruct. Given the surfac preparation techniques available (both *in situ* and *ex situ*) for diamond, it seems reasonable to assume that surfac contamination may explain the failure of some samples t reconstruct. The effect of impurities on surface reconstruction has been noted in a number of other systems including silicon and platinum.[15]

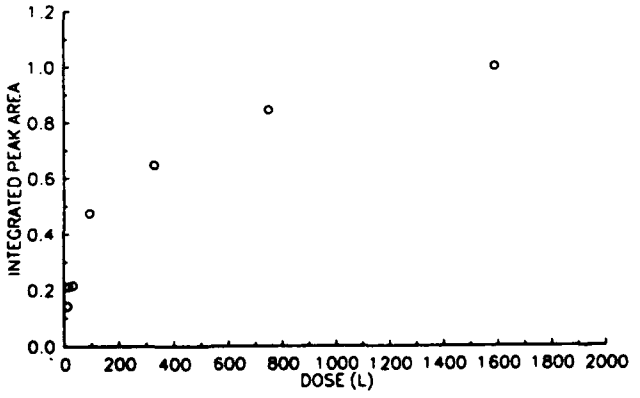

FIG. 3. Plot of H_2 integrated peak area vs total dose H/H_2. The peak areas were normalized to the largest H_2 area measured.

Conversion of the surface back to the 1×1 state by exposure to atomic hydrogen has been studied in detail by only one other group.[6] Results reported by Hamza *et al* indicated that the surface converted to the 1×1 configu ration upon dosing with atomic hydrogen at 180 K coupled with annealing at 700 K.[6] LEED patterns disappeared fol lowing the dosing and the 1×1 pattern was then seen afte annealing.[6] We see no evidence of either obscuration of the LEED pattern following dosing or of a reversion to th 1×1 surface structure. The LEED patterns gradually de teriorated with repeated dosing and desorption cycles until only weak first order spots remained coupled with a very high background. One expects the dimer bond on th C(100)-(2×1) surface to be stronger than what is seen on the Si(100)-(2×1) surface given the greater C–C bond strength, 83 kcal/mol versus 46 kcal/mol for Si–Si, and th ability of carbon to form double bonds. Calculations o hydrogen addition to the 2×1 surface by several groups indicates that there is an energy barrier to the breaking o the dimer bond by the addition of atomic hydrogen.[11–13] Verwoerd[10] calculates an energy barrier of approximately 39 kcal/mol, an energy barrier of 34.1 kcal/mol was esti mated by Zheng, and Smith,[12] and 48.7 kcal/mol by Tho

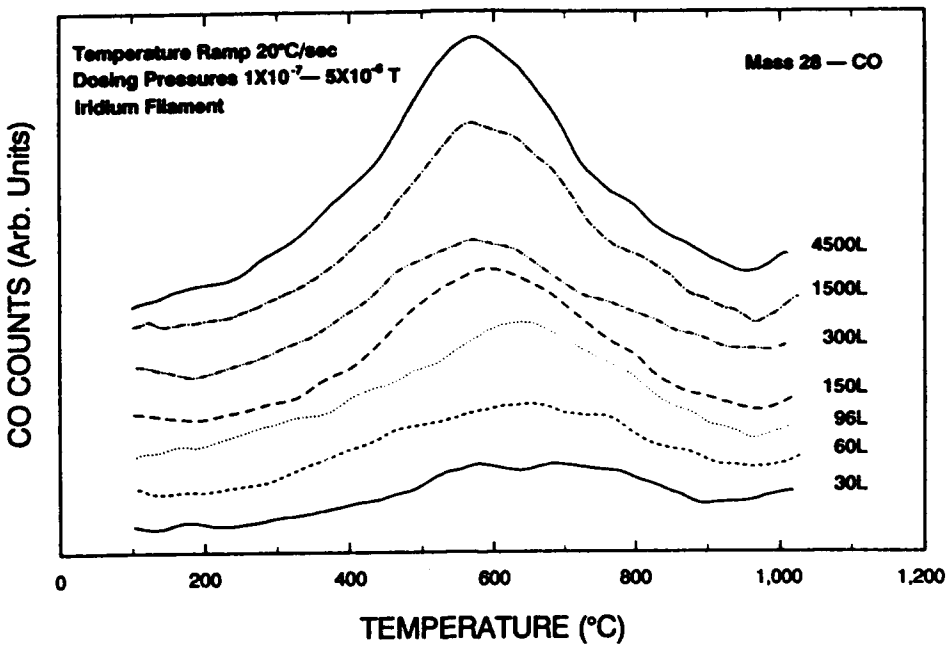

FIG. 4. Thermal desorption spectra showing CO desorption from oxygen dosed diamond surfaces. Samples were exposed to a mixture of O and O_2 after molecular oxygen was passed over an iridium filament.

mas *et al.*[13] Yang and D'Evelyn have argued that steric constraints severely limit the ability of the surface to saturate in the dihydride phase, and at most the surface assumes a disordered dihydride with random dihydride units scattered among monohydride pairs.[16] Based on these results it appears unlikely that adsorption of atomic hydrogen at room temperature will result in a conversion to the dihydride state.

As noted above, since we were unable to obtain a 1×1 structure by hydrogen adsorption, all desorption results discussed here are from a 2×1 surface. Saturation coverage for the 2×1 surface corresponds to one hydrogen atom per carbon atom. We see no evidence of a peak shift with respect to surface coverage to within the resolution of the measurement, (10 °C). The lack of a peak shift argues for first order desorption kinetics. Application of the rate equation with an assumed frequency factor of 10^{13}/s gives 72.7 kcal/mol for the activation energy of desorption. Although we have only observed a single desorption peak, Hamza *et al.* have measured hydrogen evolution by electron stimulated desorption from diamond (100) surfaces at temperatures above the thermal desorption peak.[6] We have no means of directly measuring hydrogen on the diamond surface and it may be that there are higher energy bonding sites available to the hydrogen. The maximum desorption temperature used in the present study was 1150 °C. No evidence of additional desorption features were observed up to the maximum temperature. If in fact there are additional sites available, then with the temperatures used in the present study we are probing only a portion of the bonding sites. In control experiments several samples were dosed with atomic hydrogen and then had thermal desorption spectra collected. After cooling, the samples were ramped in temperature again with no intentional dosing. No thermal desorption features were observed for these samples. If there are multiple sites it is apparently not easy for hydrogen to diffuse between the sites.

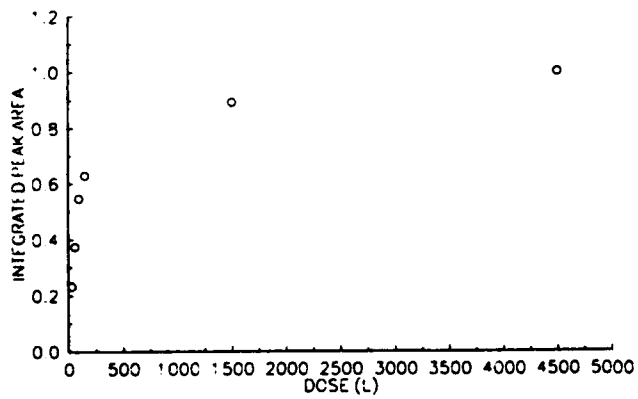

FIG. 5. Plot of CO integrated peak area vs total dose of O/O_2. As in Fig. 3, the peak areas were normalized to the largest CO peak area measured.

Oxygen behaves in a very different fashion than hydrogen on the diamond surface. The most dramatic difference is the apparent ability of atomic oxygen to break the C–C dimer bonds on the surface. We have no effective method of monitoring products formed during dosing as a result of atomic oxygen interactions with the diamond surface. As such, the oxygen may be etching the C–C dimers from the surface and then attaching oxygen atoms to the bulk crystal structure. The other case of course is for oxygen to attack the dimers directly and break the dimer bond.

Once the oxygen has attached to the surface there are several possible bonding configurations. The oxygen could bridge two adjacent carbon atoms with a single bond to

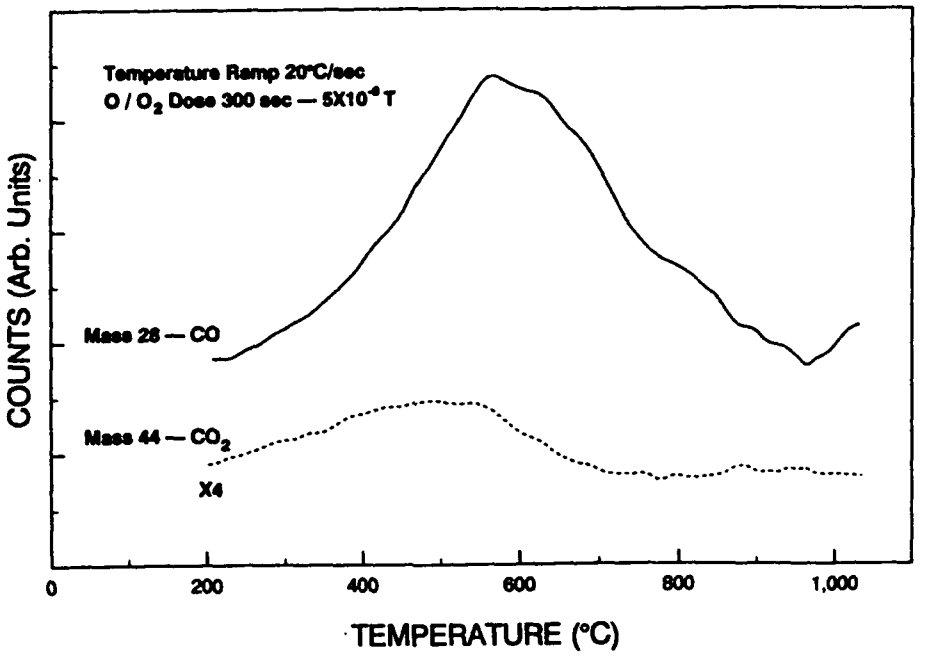

FIG. 6. This desorption spectrum shows both mass 28 (CO) and mass 44 (CO_2) as taken simultaneously from an O/O_2 dosed sample. The mass 44 vertical scale has been expanded by a factor of 4 for clarity.

each, as shown in Figure 7. Table I shows the bond angle oxygen would have to assume in the bridging configuration. At 125°, the angle is well within the range of bond angles that oxygen assumes in various molecules. In order to calculate the bond angle the C–O bond length was taken as 1.43 Å and the separation distance between the two carbon atoms that the oxygen bridges was taken as 2.52 Å.

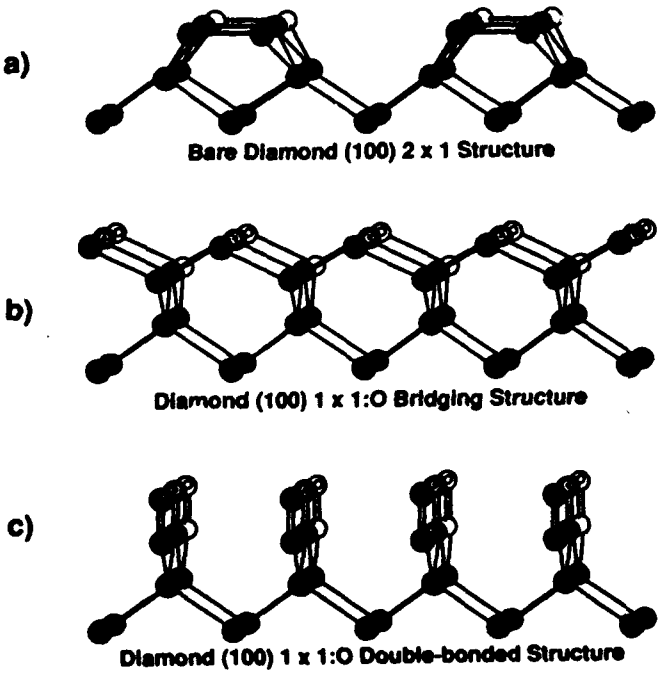

FIG. 7. (a) shows a clean diamond (100) surface in the 2×1 configuration. (b) and (c) show 2 possible oxygen bonding configurations which would give a 1×1 LEED pattern.

Another possibility is for each oxygen to double bond to a single carbon as shown in Fig. 7. One would expect 1×1 LEED patterns from both of these bonding configurations so it may be difficult to distinguish between the two cases on the basis of qualitative electron diffraction. Based on the models described above, oxygen should exhibit very different behavior on the diamond (111) surface. On the unreconstructed diamond (111) surface there is only one dangling bond available. In order to satisfy both oxygen bonds the adsorbed oxygen will either have to break a C–C bond or try and bridge two dangling bonds.

Results from thermal desorption experiments indicated that as the coverage increased the temperature for the maximum CO desorption rate decreased. This can be interpreted as either a first order desorption with a coverage dependent activation energy or a second order desorption process. One might expect desorption of CO from the surface to be first order rather than second order as there is no requirement for pairing of atoms prior to desorption. For a first order process we would expect to see an asymmetric peak with the high temperature side of the peak more steeply sloped. In fact the asymmetry appears to be in the opposite direction with the high temperature side of the

TABLE I. Bonding angles of oxygen.

Molecule	Bond angle (deg)		Bond length (Å)
Water	104	O–H	0.96
α-quartz	144	O–Si	1.6
Methyl ether	110	O–C	1.43
Diamond	125	O–C	1.43(assumed)

peak less steeply sloped than the low temperature side. One explanation for the asymmetry may be additional peaks on the high temperature side of the main peak. A slower heating rate, perhaps 1 °C/s may resolve any additional peaks which may be present. Figure 7 shows two possible bonding configurations for oxygen on the diamond surface. Although it does not appear that LEED can distinguish the two cases the desorption process may be radically different for the two. For the bridging structure, two C–C bonds and two C–O bonds need to be broken to desorb a CO pair, while for the double-bonded structure only two C–C bonds need be broken. It is not clear if both structures coexist on the surface after atomic oxygen dosing but if that is the case one may expect desorption from the bridging structure to be a higher energy process and thus occur at a higher temperature than from the double-bonded structure. Supporting evidence for additional CO peaks above 600 °C comes from powder desorption work done by Matsumoto.[14] Matsumoto has measured oxygen desorption from diamond powders exposed to molecular oxygen at temperatures between 420 and 554 °C.[14] Adsorption was done at a pressure of 1 Pa. CO peaks are seen at 600 and 800 °C for heating rates of 20 °C/min. A smaller CO_2 peak is seen at approximately 500 °C. The heating rate used by Matsumoto *et al.* is a factor of 60 slower than the rate used in the study reported here. One might expect the peak to shift down in temperature as a result of the slower heating rate.

The peaks seen for CO desorption are very broad, with a full width at half-maximum (FWHM) of approximately 350 °C for the highest coverages. Hydrogen desorption peaks in contrast had a FWHM of about 100 °C. Part of the peak width may be explained if in fact there are additional peaks in the CO desorption curves. Relatively broad CO desorption peaks, FWHM approximately 300 °C, are also observed from from oxygen dosed single crystal graphite surfaces.[17] It is interesting that two peaks, 800 and 1000 °C, were recorded from these surfaces.

V. CONCLUSIONS

Thermal mass desorption and LEED have been used to study and contrast atomic hydrogen and atomic oxygen interactions with the diamond (100)-(2×1) surface. Atomic hydrogen appears relatively inefficient at breaking C–C dimer bonds on the (100)-(2×1) surface. Atomic oxygen, in contrast, readily converts the surface from the 2×1 state to the 1×1 state. This process is reversible for a limited number of cycles before degradation of the surface obscures the 2×1 LEED pattern. Oxygen is thought to adsorb in one of two configurations, bridging carbon atoms on the surface, or double bonded to each carbon atom on the surface.

Thermal desorption from hydrogenated C(100)-(2×1):H surfaces occurs at approximately 900 °C for a heating rate of 20 °C/s. Molecular hydrogen is the major desorption product and the desorption temperature appears to be coverage independent. Thus the desorption kinetics are most likely first order. Thermal desorption from oxygenated C(100)-(1×1):O surfaces occurs at approximately 600 °C for a heating rate of 20 °C/s. Carbon monoxide is the major desorption product seen, but small quantities of carbon dioxide were also observed. For increasing oxygen coverages, the desorption peak is observed to shift to lower temperatures. The reaction order is not known in this case, but from analysis of the peak shapes and from the fact that CO can desorb without prepairing, the data suggest that the reaction is first order. Clear differences exist between the behavior of hydrogen and oxygen on the diamond (100) surface. Oxygen is able to convert the 2×1 surface back to the 1×1 configuration whereas hydrogen appears relatively inefficient at this process. Although the dosing studies were performed at room temperature the results may help to explain the role of oxygen in H_2/CH_4 growth environments. If surface dimers form during the growth process it appears that atomic hydrogen is relatively inefficient at breaking the dimer bonds. Atomic oxygen appears to restore the surface much more efficiently than atomic hydrogen.

ACKNOWLEDGMENTS

The authors wish to thank R. Alley, R. Hendry, C. Jones, and D. Brooks for technical support on this research. The financial support of the Strategic Defense Initiative Organization/Innovative Science and Technology Office through the Office of Naval Research (N-00014-86-C-0460) is gratefully acknowledged.

[1] See references in *Proceedings of the Second International Conference on New Diamond Science and Technology*, edited by R. Messier, J. T. Glass, J. E. Butler, and R. Roy (Materials Research Society, Pittsburgh, PA, 1991).
[2] J. A. Mucha, D. L. Flamm, and D. E. Ibbotson, J. Appl. Phys. **65**, 3448 (1989).
[3] S. J. Harris, and A. M. Weiner, Appl. Phys. Letts. **55**, 2179 (1989)
[4] R. A. Rudder, G. C. Hudson, J. B. Posthill, R. E. Thomas, R. C. Hendry, D. P. Malta, R. J. Markunas, T. P. Humphreys, and R. J. Nemanich, Appl. Phys. Lett. **60**, 329 (1992).
[5] P. K. Bachmann, D. Leers, and H. Lydin, Diamond Rel. Mater. **1**, 1 (1991).
[6] A. V. Hamza, G. D. Kubiak, and R. H. Stulen, Surf. Sci. **237**, 35 (1990).
[7] B. B. Pate, Surf. Sci. **165**, 83 (1986).
[8] R. E. Thomas, R. A. Rudder, and R. J. Markunas, *Proceedings of the Second International Symposium on Diamond Materials*, edited by A. J. Purdes, J. C. Angus, B. M. Meyerson, K. E. Spear, R. F. Davis, and M. Yoder (The Electrochemical Society, Pennington, NJ, 1991), p. 186.
[9] J. P. F. Sellschop, C. C. P. Madiba, and H. J. Annegarn, Nucl. Instrum. Methods **168**, 529 (1980).
[10] P. G. Lurie, and J. M. Wilson, Surf. Sci. **65**, 453 (1977).
[11] W. S. Verwoerd, Surf. Sci. **108**, 153 (1981).
[12] X. M. Zheng, and P. V. Smith, Surf. Sci. **256**, 1 (1991).
[13] R. E. Thomas, R. A. Rudder, R. J. Markunas, D. Huang, and M. Frenklach, J. Chem. Vapor Deposition **1**, 1 (1992).
[14] S. Matsumoto, and N. Setaka, Carbon **17**, 485, (1979); S. Matsumoto, Y. Sato, and N. Setaka, *ibid.* **19**, 232, (1981).
[15] A. Zangwill, *Physics at Surfaces* (Cambridge University, Cambridge, England, 1988), pp. 96, 258.
[16] Y. L. Yang, and M. P. D'Evelyn, J. Am. Chem. Soc. (in press).
[17] B. Marchon, J. Carrazza, H. Heinemann, and G. A. Somorjai, Carbon **26**, 507 (1988).

INVITED TALK

Meeting: **1992 TMS Fall Meeting, Chicago, IL**
Symposium: **Beam Processing of Advanced Materials**

NUCLEATION OF DIAMOND FILMS ON NON-NATIVE SUBSTRATES

J.B. Posthill, R.A. Rudder, D.P. Malta, R.E. Thomas, G.C. Hudson, and R.J. Markunas, *Research Triangle Institute, Research Triangle Park, NC 27709.*

Different materials have been examined for their intrinsic propensity for nucleation of diamond from the vapor phase. Certain standard and unconventional sources have been employed to grow diamond in an rf-driven plasma-enhanced CVD system. These include: (1) CH_4/H_2, (2) CO/H_2, (3) CF_4/H_2, and (4) alcohol/H_2O-based mixtures. It has been found that diamond heteronucleation can be radically affected by the specific growth chemistry as well as the identity of the substrate material. For example, CF_4/H_2 mixtures have been found to nucleate diamond on Si(100) without the need for any substrate pretreatment. An amorphous interlayer has been observed between the diamond film and single crystal Si. Using a more conventional mixture of CH_4/H_2, we have achieved nucleation and growth of diamond with complete coverage and well-faceted topography on sintered cubic BN compacts without any surface pretreatment. These and other results will be discussed in the context of the interplay between different gas phase chemistries and different substrates used for diamond heteronucleation.

Chemical vapor deposition of diamond films from water vapor rf-plasma discharges

R. A. Rudder, G. C. Hudson, J. B. Posthill, R. E. Thomas, R. C. Hendry, D. P. Malta, and R. J. Markunas
Research Triangle Institute, Research Triangle Park, North Carolina 27709-2194

T. P. Humphreys and R. J. Nemanich
North Carolina State University, Raleigh, North Carolina 27695-8202

(Received 3 September 1991; accepted for publication 29 October 1991)

Polycrystalline diamond films have been deposited from water vapor rf-plasma discharges at 1.0 Torr containing various alcohol vapors. No other gases such as H_2, F_2, or Cl_2 were admitted to the growth chamber. Scanning electron microscopy and Raman spectroscopy have been used to characterize the diamond films. In addition, a water-ethanol mixture has been used for homoepitaxial deposition with a full-width-half-maximum narrower than the bulk substrate (2.60 and 2.75 cm^{-1}, respectively). This technique represents a remarkable new approach to the growth of diamond which does not depend on delivery of hydrogen, fluorine, hydrocarbon, or halocarbon gases that have been typically used by other workers. The nucleation density and topography of the polycrystalline diamond films deposited from the water alcohol mixtures are quite sensitive to the choice of alcohol. Water vapor discharges, by producing H atoms and OH radicals, become the functional equivalent to molecular H_2 discharges producing H atoms characteristic of many other diamond chemical vapor deposition techniques.

A variety of techniques have been developed for the deposition of diamond from the gas phase using plasma and thermal activation.[1-10] Early theories of diamond deposition hypothesized that the deposition of diamond was a codeposition process in which both diamond and graphite were being deposited simultaneously.[1,2] Atomic hydrogen produced by dissociation of molecular hydrogen in plasma discharges, arc discharges, or hot filaments dissolves the nondiamond phases from the depositing layer and, thus, promotes the diamond phase. Recently, oxyacetylene torches have been used to grow diamond films.[9,10] The oxyacetylene flame, in addition to forming H_2O, CO, and CO_2 by-products, provides atomic hydrogen to the growth surface. Many gaseous carbon sources have been used for the deposition of diamond. Hydrocarbons, halocarbons, fluorocarbons, and alcohols have all been used in the deposition of diamond films. In a plasma or a thermally activated process, those carbonaceous gases are driven toward their high-temperature, equilibrium product distributions. Not surprisingly, the quality of the diamond films does not depend as critically on the carbon source as it depends on the C/H ratio, or perhaps more appropriately, the C/H/O ratio in the gas phase.[11] If one examines the list of radicals and gases which gasify graphite, H atoms, F atoms, and F_2 molecules are included on the list.[12] Also present on the list are O atoms, OH radicals, and O_2 molecules. Oxygen has certainly been added to diamond producing environments, either by using carbon carriers containing oxygen or through intentional addition of oxygen to the gas stream in microwave discharges. Indeed, Buck *et al.*[13] have deposited diamond in a relatively limited set of conditions using only methanol or methanol/A_r mixtures. Initial microwave plasma results showed an improvement in diamond growth with a small percentage of O_2 addition, but they also showed a degradation in crystalline quality for films deposited with more than 2% O_2 addition.[14] However, more recently, the work of Bachmann, Leers, and Lydtin,[11] and Chen, Hon, and Lin[15] has demonstrated that higher oxygen concentrations can certainly yield diamond deposition with correspondingly higher carbon concentrations.

We report here on a novel, low temperature growth technique for the chemical vapor deposition (CVD) of diamond films from low-pressure, rf-plasma discharges containing principally water vapor. Carbon for diamond deposition was supplied to the plasma gas by admitting alcohol vapor with the water vapor. No other gases were admitted to the growth chamber. Hence, this work is quite different from the work of Saito *et al.*[16,17] wherein 0%–6% concentrations of water in H_2-CH_4 microwave plasmas were investigated for diamond growth. In this letter, predominantly water-based discharges produce OH and H radicals. The water discharge becomes functionally equivalent to hydrogen discharges in other diamond CVD techniques. Emission from a pure water discharge and the water-alcohol discharges described in this letter show strong H_α emission and OH emission. The atomic hydrogen emission from a pure water rf-plasma discharge at 1.0 Torr is so dominant that the plasma has a characteristic red color from the 656 nm emission. The ratio of water to alcohol admitted to the growth chamber was fixed by the partial pressures of water and alcohol above the mixed solutions of 20% alcohol in water. In addition to polycrystalline growth, homoepitaxial diamond growth has been accomplished.

Study of polycrystalline diamond growth in the water vapor system was undertaken using Si(100) substrates. Prior to introduction into the growth chamber, the samples were subjected to polishing with graphite fibers[18] and/or

 0003-6951/92/030329-03$03.00

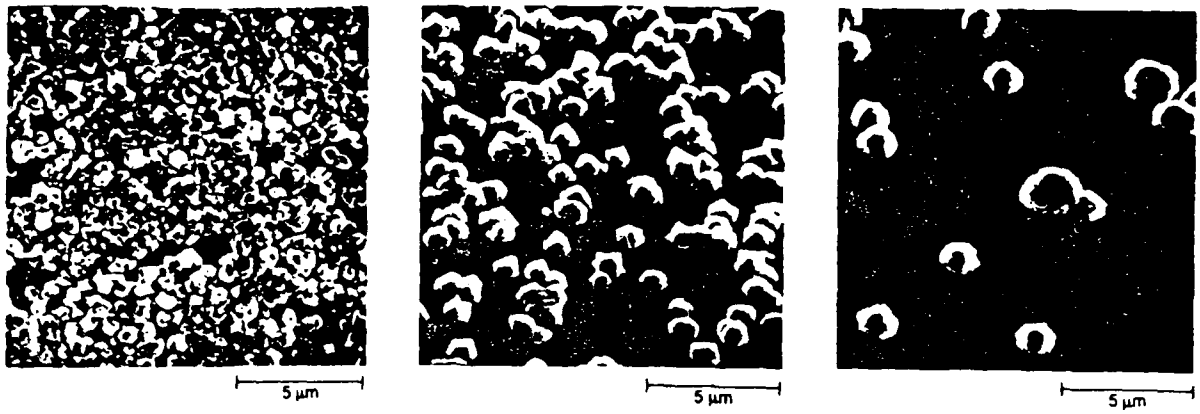

FIG. 1. SEM micrographs of the polycrystalline deposits on Si(100) obtained using water/methanol, water/ethanol, and water/isopropanol.

diamond paste to promote nucleation. Descriptions of the growth system have been reported elsewhere.[19] The samples are located on a graphite susceptor just beneath a three-turn rf induction coil. The rf induction coil maintains the water vapor discharge and heats the graphite susceptor upon which the sample is located. The liquid mixture is stored in a metal flask connected to the vacuum chamber. The water vapor/alcohol gas mixture is metered into the chamber at a rate of ~ 20 sccm. The vapor mixture was admitted into the metal vacuum cross at the base of the plasma tube. The ratio of water to alcohol admitted is determined by the product of the mole fractions of water and alcohol and the respective vapor pressures of the water and the selected alcohol. A process pressure control valve is used to vary the effective pumping speed in order to maintain a pressure in the growth chamber of 1 Torr. To initiate deposition, a 1000 W, 13.56 MHz signal is applied to the rf coil. The power level results in a sample temperature of 625 °C during deposition. Following 2 h of deposition, the samples were removed from the reactor and examined with a scanning electron microscope (SEM) prior to Raman analysis. Figure 1 shows electron micrographs of the samples deposited for 2 h using water vapor mixtures containing either methanol, ethanol, or isopropanol. The micrographs show that the nucleation is highly dependent on the choice of alcohol. The alcohols with the higher vapor pressures nucleate at a higher density. If one uses the average crystallite size as a measure of the growth rate, the growth rate does not vary considerably with the choice of alcohol. However, the morphology of the diamond crystallites does change as the alcohol molecular group becomes larger. Using methanol or ethanol, the crystallites growing from the nucleation sites are composed of individual diamond crystals, some of which appear to be twinned. Using isopropanol, the crystallites growing from the nucleation sites are composed of many diamond crystals clustered about the nucleation site. Raman spectroscopy from all the samples (see Fig. 1) shows a distinct 1332 cm^{-1} diamond longitudinal optical peak on a broad background which is centered around 1500 cm^{-1}. Figure 2 shows the Ramanspectra for the water/methanol, water/ethanol, water/isopropanol growths.

In addition to polycrystalline growth on Si(100) substrates, homoepitaxial growth on a natural Type IA diamond (100) substrate was accomplished using a water/ethanol mixture equivalent to the one used for the polycrystalline growth. The Raman spectrum from the homoepitaxial deposition did not exhibit any scattering from the 1500 cm^{-1} nondiamond material. The full-width-half-maximum (FWHM) of the homoepitaxial layer, as determined using micro-Raman focused on the epitaxial layer, is 2.60 cm^{-1}. Examination of the bulk substrate by performing micro-Raman on the opposite substrate face from the

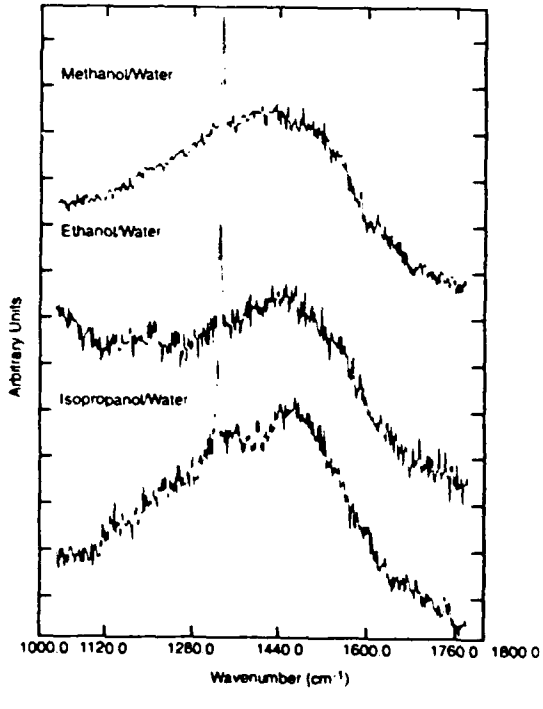

FIG. 2. Raman spectra from the polycrystalline deposits on Si(100) obtained using water/methanol, water/ethanol, and water/isopropanol.

epitaxial layer found the FWHM of the bulk material to be 2.75 cm^{-1}. Hence, the growth using water/ethanol produced a diamond epitaxial layer of apparently higher structural perfection than the starting natural diamond crystal.

This work clearly demonstrates that water vapor discharges can promote diamond growth. Attempts to grow diamond with only methanol vapor admitted to the reactor resulted in poor nucleation and growth. Faceting was not observed on any of the diamond particles grown using only methanol. These results contrast the results of Buck *et al.*,[13] where microwave discharges of pure methanol deposited well-faceted diamond. Conversely, attempts to deposit diamond with only water vapor admitted to the reactor (in the attempt to grow by chemical vapor transport from carbon on the graphite susceptor) resulted in no deposition. The water vapor discharges contribute both OH and H radicals to the growth environment. Obviously, the activation or production of atomic hydrogen from water vapor and from molecular H_2 will be different. We have no way to *in situ* measure the relative production of atomic hydrogen in these processes; however, we can measure the relative dissolution rates of solid graphite for the two processes by measuring dimensional changes on the graphite susceptor. The water process at 1000 W and 1 Torr etches graphite at approximately 25 μm/h as compared to 5 μm/h for the H_2 process at 2000 W and 5 Torr. Hence, it is observed that the water process at lower pressure and lower power produces a much higher graphite etch rate. Despite this higher gasification rate, no chemical vapor transport growth is observed. Alcohol must be added to the water for diamond growth to occur.

The authors cannot dismiss the possibility that the water vapor discharge is merely a hydrogen source and that the role of OH in diamond deposition is minor. However, growth of diamond in the same reactor using H_2-CH_4 rf discharges produces high-quality diamond, but only at much higher pressures and higher power levels. Typically, 5.0 Torr and 2500 W of rf power input are necessary for well-faceted crystallites when 1% CH_4 in H_2 discharges are used. Furthermore, in the H_2-CH_4 rf discharges, the ratio of carbon to hydrogen in the gas phase is small, typically less than 2% for high-quality diamond growth. Using the vapor pressures of water and methanol, the ratio of carbon to hydrogen to oxygen in this process is calculated to be 1:6:2. Emission spectra from water-alcohol discharges are dominated by emissions from the atomic hydrogen Balmer series. In addition, OH emission is observed. Emission from atomic O was not observed.

In conclusion, we have demonstrated the growth of polycrystalline diamond films from rf-plasma discharges fed solely by water and alcohol vapors. Characterization of the films by SEM shows the films to be well faceted with the choice of alcohol effecting the nucleation density and the crystal habit. Characterization of the films by Raman spectroscopy shows the polycrystalline films to be diamond with some nondiamond bonding. Raman spectroscopy shows the single-crystalline homoepitaxial films to have a FWHM of 2.60 cm^{-1} which is narrower than the starting natural crystal whose FWHM was 2.75 cm^{-1}. This technique represents a remarkable method for the manufacture of diamond films through the use of noncorrosive, nonexplosive, and relatively inexpensive sources. Design and implementation of growth systems using water-based processes should be straightforward and should avoid the complexities, the safety hazards, and the expense of H_2 or halogen gas processing.

The authors wish to acknowledge the financial support of the Strategic Defense Initiative/Innovative Science and Technology Office through the Office of Naval Research, Contract No. N-00014-86-C-0460. The authors also wish to thank M. J. Mantini, A. D. Brooks, S. A. Ammons, and R. V. Durkee for technical support of this work.

[1] B. Derjaguin and V. Fedoseev, Russ. Chem. Rev. 39, 783 (1970).
[2] B. V. Spitsyn, L. L. Bouilov, and B. V. Derjaguin, J. Cryst. Growth 52, 219 (1981).
[3] S. Matsumoto, Y. Sato, M. Kamo, and N. Setaka, Jpn. J. Appl. Phys. 21, 183 (1982).
[4] Y. Hirose and Y. Teresawa, Jpn. J. Appl. Phys. 25, L51 (1986).
[5] M. Nakazawa, T. Nakashima, and S. Seikai, Appl. Phys. Lett. 45, 823 (1984).
[6] M. Kamo, Y. Sato, S. Matsumoto, and N. Setaka, J. Cryst. Growth 62, 642 (1983).
[7] S. Matsumoto, M. Hiro, and T. Kobayashi, Appl. Phys. Lett. 51, 737 (1987).
[8] K. Kurihara, K. Sasaki, M. Kawarada, and N. Koshiro, Appl. Phys. Lett. 52, 437 (1988).
[9] L. M. Hanssen, W. A. Carrington, J. E. Butler, and K. A. Snail, Mater. Lett. 7, 289 (1988).
[10] G. Janssen, W. J. P. Van Enckevort, J. J. D. Schaminee, W. Vollenberg, L. J. Giling, and M. Seal, J. Cryst. Growth 104, 752 (1990).
[11] Peter K. Bachmann, Dieter Leers, and Hans Lydtin, Diamond Rel. Mater. 1, 1 (1991).
[12] D. E. Rosner and J. P. Strakey, J. Phys. Chem. 77, 690 (1973).
[13] M. Buck, T. J. Chuang, J. H. Kaufman, and H. Seki, Mater. Res. Soc. Symp. Proc. 162, 97 (1990).
[14] J. A. Mucha, D. L. Flamm, and D. E. Ibbotson, J. Appl. Phys. 65, 3448 (1989).
[15] C. F. Chen, T. M. Hon, and C. L. Lin, presented at 18th Int. Conf. on Metallurgical Coatings and Thin Films (ICMCTF), San Diego, CA, April 23, 1991.
[16] Yukio Saito, Kouji Sato, Hideaki Tanaka, Kazunori Fujita, Shinpei Matuda, J. Mater. Sci. 23, 842 (1988).
[17] Yukio Saito, Kouji Sato, Kenichi Gomi, Hiroshi Miyadera, J. Mater. Sci. 25, 1246 (1990).
[18] R. A. Rudder, G. C. Hudson, R. C. Hendry, R. E. Thomas, J. B. Posthill, and R. J. Markunas, Materials Science Monograph 73, 395 (1991).
[19] R. A. Rudder, G. C. Hudson, D. P. Malta, J. B. Posthill, R. E. Thomas, and R. J. Markunas, Materials Science Monograph 73, 583 (1991).

HOMOEPITAXIAL DIAMOND LAYERS GROWN WITH DIFFERENT GAS MIXTURES IN A RF PLASMA REACTOR

J.B. Posthill, D.P. Malta, R.A. Rudder, G.C. Hudson,
R.E. Thomas, and R.J. Markunas
Research Triangle Institute
Research Triangle Park, North Carolina 27709-2194

T.P. Humphreys and R.J. Nemanich
Department of Physics, North Carolina State University
Raleigh, North Carolina 27695-8202

The thermal and electrical properties of diamond make it an excellent candidate for electronic applications in extreme environments, but significant device development in this materials system cannot take place unless larger area single crystals are available. While significant progress has been made towards increasing the areal size of diamond crystals by different means[e.g.1,2], it is also recognized that a reliable and inexpensive method of growing high-quality epitaxial diamond will be necessary to grow device structures and to increase the thickness of diamond crystals and films. To this end, we have examined the effect of gas phase chemistry on the homoepitaxial growth of diamond on natural diamond single crystals. A brief outline of some of these results obtained in an rf-driven plasma-enhanced chemical vapor deposition (PECVD) reactor follows.

The substrates used in this study were nominally (100) and (110) oriented [$\pm$ 3°] natural type Ia diamonds. It has been established previously by both X-ray topography and ion channeling studies that type Ia substrates are crystallographically superior[3], and it is believed that this would result in improved diamond homoepitaxial films. Transmission electron microscopy (TEM) of a type Ia diamond showed the expected presence of nitrogen-containing platelets lying on {100}-type planes (Fig. 1). However, no dislocations could be seen in the field of view, hence, the dislocation density is $< 10^5$ cm^{-2}. This contrasts with substantially larger dislocation densities observed in type IIb substrates[4]. Prior to loading into the reactor, substrate preparation involved swabbing in deionized water and blow drying with clean nitrogen. Swabbing has been shown to remove particles from the diamond surface, thereby minimizing the sporadic regions of polycrystallinity that are thought to be caused by this contamination[3].

The system used for the growth of homoepitaxial diamond consists of a 13.56 MHz inductively-coupled plasma-enhanced chemical vapor deposition (PECVD) system. The sample is positioned near the rf coil on a graphite susceptor, and the growth temperature was achieved by a combination of rf inductive coupling to the susceptor and additional heating from an independently driven radiative source beneath the susceptor. A variety of different gas mixtures have been used for diamond growth. In addition to conventional CH_4/H_2 mixtures, we have also explored oxygen-containing mixtures which utilized combinations of CO, CH_4, and H_2. Recently, polycrystalline diamond has been grown using water:alcohol and water:alcohol:organic acid mixtures[5,6]. This new method of CVD diamond growth using inexpensive liquids has been extended to homoepitaxial diamond growth.

Fig. 2 shows an SEM micrograph taken from an epitaxial film grown on a (100) substrate with a 1%CH_4/99%H_2 mixture at a pressure of 5 Torr and temperature of $\sim$ 900°C. An extensively 'shingled' morphology is evident. Interestingly, micro-Raman spectroscopy taken from the near-surface region of this sample was not found to be severely degraded; the full-width at half-maximum (FWHM) of the diamond LO phonon line at 1332 cm^{-1} was measured to be 2.8 cm^{-1}. Fig. 3 shows a much improved surface topography from an epitaxial film grown on a (110) substrate with a 0.62%CO/0.23%CH_4/99.15%H_2 mixture at P = 5 Torr and T $\simeq$ 900°C. There are some regions on this sample that exhibit polycrystallinity, which is believed to be due to incomplete particle removal. The micro-Raman shows a FWHM of 2.7 cm^{-1} (Fig. 4). Given that smooth (100) diamond epilayers have been observed previously when grown with comparable CO/CH_4/H_2 mixtures[3], it is believed that the presence of the CO is the dominant factor responsible for the superior morphology. However, previous research has shown good (110) diamond epitaxial surface morphologies using only CH_4/H_2 mixtures[7].

Fig. 5 shows the surface of a (100) homoepitaxial film grown by introducing the vapor pressure of a 33.3%CH_3OH/66.7%H_2O liquid mixture at P = 1 Torr and T $\simeq$ 400°C. The diamond epilayer shows little roughness. Perhaps the most remarkable aspect of this water:methanol diamond film is the measured concentrations for some of the common (and potentially detrimental) elemental impurities. Secondary ion mass spectrometry (SIMS) showed that Si, B, and N were at measured instrumental background, while H and O were measured to be 2×10^{18} cm^{-3} and 3×10^{18} cm^{-3}, respectively. *All* these values are the lowest that we have observed in any of our high-temperature-grown homoepitaxial diamond films. No special distillation/purification was performed to the liquid reagents to achieve this result. It appears that water:alcohol mixtures can be used where a low temperature diamond epitaxial process is desired or required.

Acknowledgements: The authors gratefully acknowledge the support of this work by the SDIO/IST through ONR (Contract No. N00014-92-C-0081).

References

1. M.W. Geis, H.I. Smith, A. Argoitia, J. Angus, G.-H.M. Ma, J.T. Glass, J. Butler, C.J. Robinson, and R. Pryor, Appl Phys. Lett., 58, 2485 (1991).
2. B.R. Stoner and J.T. Glass, Appl. Phys. Lett., 60, 698 (1992).
3. J.B. Posthill, R.A. Rudder, G.C. Hudson, D.P. Malta, G.G. Fountain, R.E. Thomas, R.J. Markunas, T.P. Humphreys, R.J. Nemanich, and D.R. Black, Proc. of the 2nd Intl. Symp. on Diamond Materials, 91-8, [The Electrochemical Society], 274 (1991).
4. D.P. Malta, J.B. Posthill, E.A. Fitzgerald, R.A. Rudder, G.C. Hudson, and R.J. Markunas, [this proceedings].
5. R.A. Rudder, G.C. Hudson, J.B. Posthill, R.E. Thomas, R.C. Hendry, D.P. Malta, R.J. Markunas, T.P. Humphreys, and R.J. Nemanich, Appl. Phys. Lett., 60, 329 (1992).
6. R.A. Rudder, J.B. Posthill, G.C. Hudson, D.P. Malta, R.E. Thomas, R.J. Markunas, T.P. Humphreys and R.J. Nemanich, Mater. Res. Soc. Symp. Proc., 242, 23 (1992).
7. W.J.P. van Enckevort, G. Janssen, W. Vollenberg, M. Chermin, L.J. Giling, and M. Seal, Surf. and Coating Tech., 47, 39 (1991).

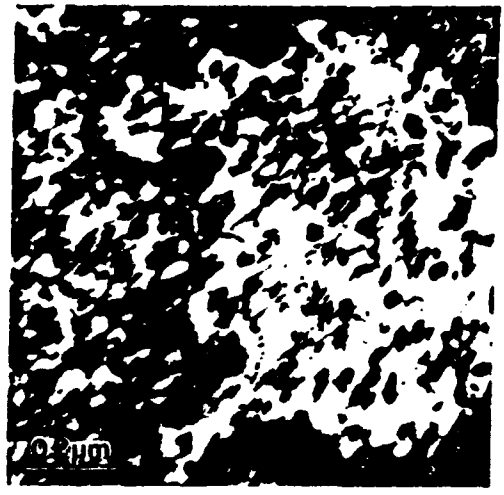

Fig. 1 -- TEM of natural type Ia diamond substrate showing 50nm diameter nitrogen platelets on {100}-type planes. No dislocations were observed.

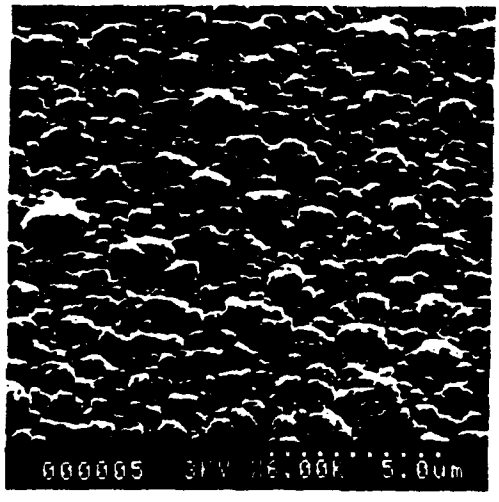

Fig. 2 -- SEM of 1%CH_4/99%H_2 homoepitaxial (100) diamond.

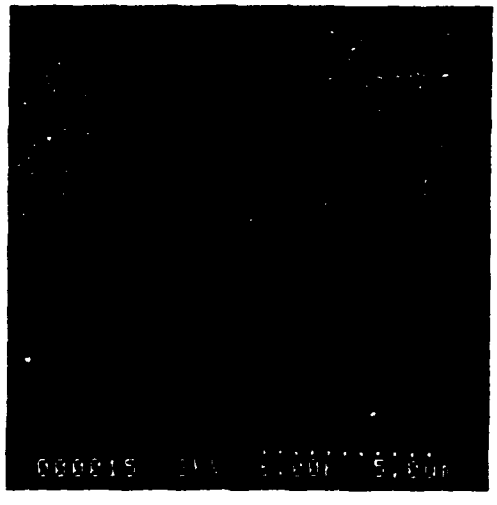

Fig. 3 -- SEM of 0.62%CO/0.23%CH_4/99.15%H_2 (110) homoepitaxial diamond.

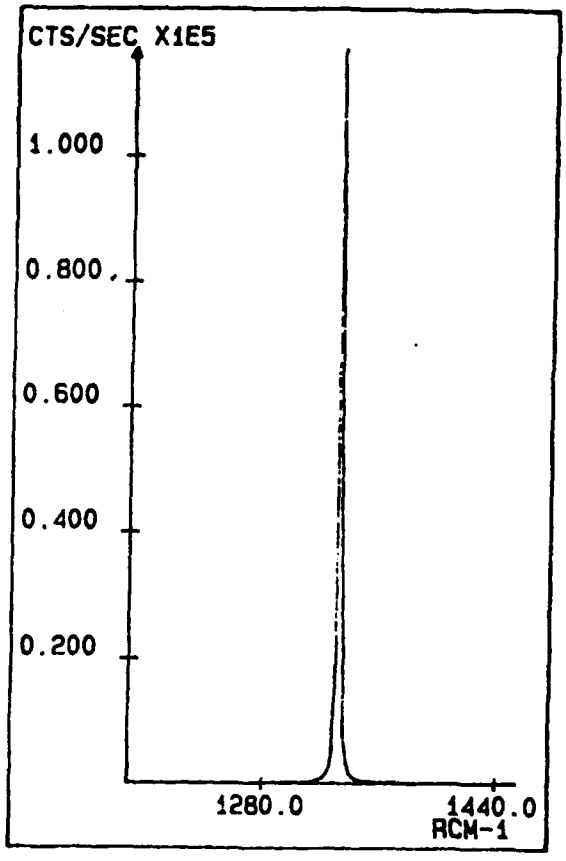

Fig. 4 -- Micro-Raman spectrum from the near-surface of 0.62%CO/0.23%CH_4/99.15%H_2 (110) homoepitaxial diamond.

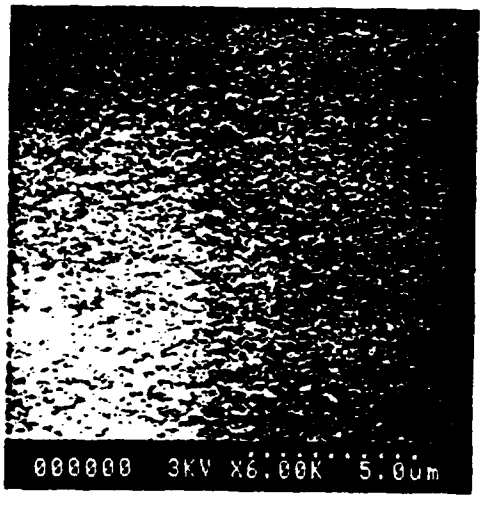

Fig. 5 -- SEM of 33.3%CH_3OH/66.7%H_2O (100) homoepitaxial diamond.

Materials Research Society Symposium Proceedings, Volume 202 (1990).

GROWTH AND CHARACTERIZATION OF HETEROEPITAXIAL NICKEL FILMS ON DIAMOND SUBSTRATES

T.P. HUMPHREYS *, HYEONGTAG JEON *, R.J. NEMANICH*, J.B. POSTHILL**, R.A. RUDDER**, D.P. MALTA**, G.C. HUDSON**, R.J. MARKUNAS**, J.D. HUNN*** and N.R. PARIKH***

* Department of Physics, North Carolina State University, Raleigh, North Carolina 27695-8202.

** Research Triangle Institute, Research Triangle Park, North Carolina 27709-2194.

*** Department of Physics and Astronomy, University of North Carolina, Chapel Hill, North Carolina 27599-3255.

ABSTRACT

In the present study epitaxial Ni(001) films have been grown on natural C(001) substrates (type Ia and IIa) and homoepitaxial C(001) films. Two deposition techniques including electron-beam evaporation of Ni in a molecular beam epitaxy (MBE) system and evaporation of Ni from a resistively heated tungsten filament have been employed. As evidenced by scanning electron microscopy (SEM), the Ni films deposited by electron-beam evaporation were found to replicate the very fine, unidirectional scratches present on the as polished C(001) substrates. Indeed, the coverage and uniformity of the deposited films would imply a two-dimensional (2-D) growth mode. In comparison, the thermal evaporation of Ni on C(001) substrates results in a highly textured and faceted surface morphology indicative of three-dimensional (3-D) nucleation and growth. Moreover, Rutherford backscattering/channeling measurements have demonstrated that the Ni(001) films deposited by electron-beam evaporation are of superior crystalline quality. Differences in the observed microstructure and apparent growth modes of the epitaxial Ni(001) films have been attributed to the presence of oxygen incorporation in those layers deposited by thermal evaporation.

INTRODUCTION

There is at present a significant scientific and technological interest in the growth and use of diamond thin films for high temperature-resistant and radiation-hard electronic device applications [1]. Indeed, it is evident that the fabrication of metal contacts to diamond will play an important role in the development of diamond-based device technologies. Moreover, it is envisaged that an epitaxial metal contact to diamond could find utility in specific device structures and applications. For instance, an epitaxial metal layer could potentially be used in the fabrication of a metal base and/or permeable base bipolar transistor. At present Ni is considered as a suitable choice since both diamond and Ni are face-centered cubic and Ni has a near-lattice match to diamond(a_o(dia) = 3.5668 Å, a_o(Ni) = 3.5238 Å, lattice mismatch ~ -1.2%). For this reason Ni has also been investigated as a potential substrate for the nucleation of heteroepitaxial diamond growth by chemical vapor deposition (CVD) processes [2]. However, this approach has to date proved unsuccessful, although epitaxial (0001) graphite has been grown on Ni(111) [3]. The difficulty experienced to date in nucleating diamond on nickel may find utility by patterning an epitaxial Ni overlayer on diamond single crystal for subsequent selective-area diamond deposition and possible epitaxial lateral overgrowth (ELO) [4].

In this paper we present a comparative study pertaining to the growth of epitaxial Ni(001) films on C(001) substrates using electron-beam and thermal evaporation growth techniques.

EXPERIMENTAL PROCEDURE

Several commercially supplied (D. Drukker & ZN.N.V.) type Ia and type IIa, natural C(001) substrates were chemically cleaned using various concentrated acids and standard RCA cleaning procedures [5]. Homoepitaxial C(001) films of typically ~750 nm thickness were grown

on the chemically clean type IIa C(001) substrates using low pressure rf-plasma-enhanced chemical vapor deposition (PECVD). Prior to Ni deposition, the substrates were annealed by heating to 1200°C for 10 minutes in UHV (<8 x 10^{-9} Torr) to thermally desorb possible physi-adsorbed gas contaminates. For those Ni films deposited by tungsten filament evaporation, *in-situ* low energy electron diffraction (LEED) and Auger electron spectroscopy (AES) techniques were used to examine the corresponding surface structure and interface chemistry of the Ni layers after each evaporation step. Ni films were deposited on type IIa, natural C(001) substrates and homoepitaxial C(001) films at a temperature of 500°C with an evaporation rate of ~0.2 - 0.4 nm/min as determined by a quartz crystal monitor. The pressure during deposition was typically better than 1 x 10^{-8} Torr. The final thickness of the Ni films were ~14 - 24 nm as determined by profilometer measurements. In comparison, the Ni films deposited by electron-beam evaporation in a molecular beam epitaxy (MBE) system were grown at 500°C with an enhanced deposited rate of ~18 nm/min. The pressure in the MBE chamber was typically <10^{-9} Torr during growth. The thickness of the corresponding Ni films were typically ~50 nm.

The grown layers were examined by scanning electron microscopy (SEM), Rutherford backscattering (RBS)/channeling of 1.6 and 2.0 MeV He^+ ions.

RESULTS AND DISCUSSION

Shown in Fig. 1 is an unreconstructed (1x1) LEED pattern obtained from the chemically clean type IIa, natural C(001) substrates. A similar surface structure was observed on subsequent annealing of the substrates to 1200°C in UHV and cooling to room temperature for LEED analysis. In contrast, a (2x1) surface reconstructed pattern was observed from the homoepitaxial C(001) films following high temperature annealing. As reported in the literature, the occurrence of a (2x1) surface reconstruction may be related to the microstructural quality and surface topography of the C(001) surfaces [6]. In particular, SEM inspection of the polished C(001) substrates has revealed the presence of scratches which were visibly absence from the surface of the homoepitaxial C(001) films. Therefore, it is reasonable to conclude that the presence of these microscopic surface imperfections on the natural C(001) substrates may inhibit the surface reconstruction process.

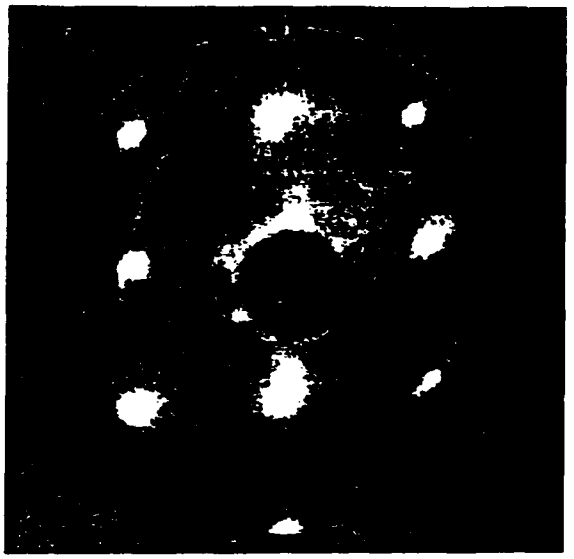

Fig. 1 Unreconstructed (1x1) LEED pattern obtained from the chemically clean C(001) surface, E_p = 135 eV.

The crystalline quality of the C(001) homoepitaxial films grown on type IIa, natural C(001) substrates have been examined using Micro-Raman spectroscopy. In particular, the measured full-width-half-maximum (FWHM) of the 1332 cm^{-1} diamond line for the homoepitaxial films is 2.2 cm^{-1} compared to 2.3 cm^{-1} obtained from the natural C(001) substrates. Corresponding LEED patterns of the Ni films deposited by evaporation from a tungsten filament on the homoepitaxial and natural C(001) substrates are shown in Fig. 2(a) and (b), respectively. The superposition of a p(2x1) and p(1x2) nickel structure is clearly evident for those films deposited on both (1x1) unreconstructed and (2x1) reconstructed homoepitaxial C(001) surfaces. Also observed were extra beams in the diffraction pattern which moved between the integral-order beams in both the <100> and <110> directions as the primary beam energy was changed. These features can be clearly seen in the bottom left hand corner of Fig. 2(a). In contrast, the formation of a p(2x2) nickel structure has been observed on type IIa, natural C(001) substrates which exhibit a clean (1x1) unreconstructed surface structure prior to deposition. Extra features in the LEED pattern which change with beam energy have also been observed in these layers. The presence of the extra diffraction beams have been attributed to the formation of a faceted surface morphology characteristic of the early nucleation of epitaxial Ni(001) islands of preferred orientation on the

C(001) surface. Indeed, AES measurements of the deposited Ni films have established the presence of Ni islands for films of <7 nm thickness. However, with increased Ni coverage there is an apparent coalescence of the individual islands to form a continuous layer.

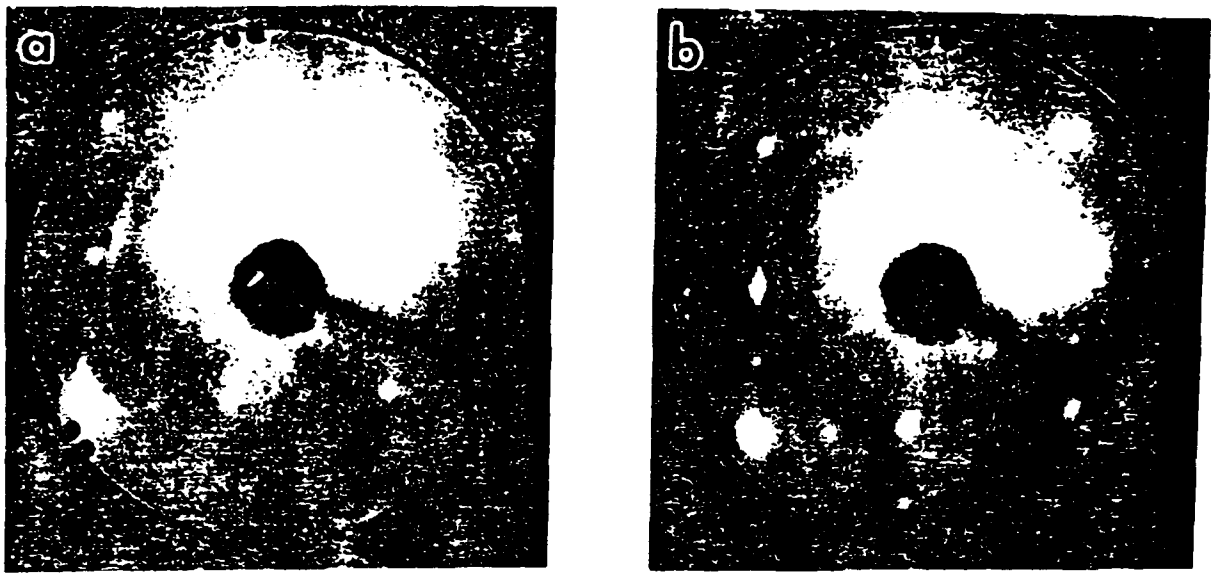

Fig. 2 LEED patterns showing (a) superposition of a p(2x1) and p(1x2) nickel structure and (b) p(2x2) nickel structure for Ni films deposited on homoepitaxial and type IIa, natural C(001) substrates, respectively, E_p = 135 eV.

The SEM micrographs pertaining to the surface morphology of the epitaxial Ni films deposited by tungsten filament evaporation on homoepitaxial C(001) and type IIa, natural C(001) substrates are shown in Fig. 3(a) and (b), respectively. The thickness of the Ni films were typically ~24 nm and ~14 nm, respectively. Clearly, both films exhibit a textured and faceted surface morphology indicative of initial island nucleation and partial coalescence during growth.

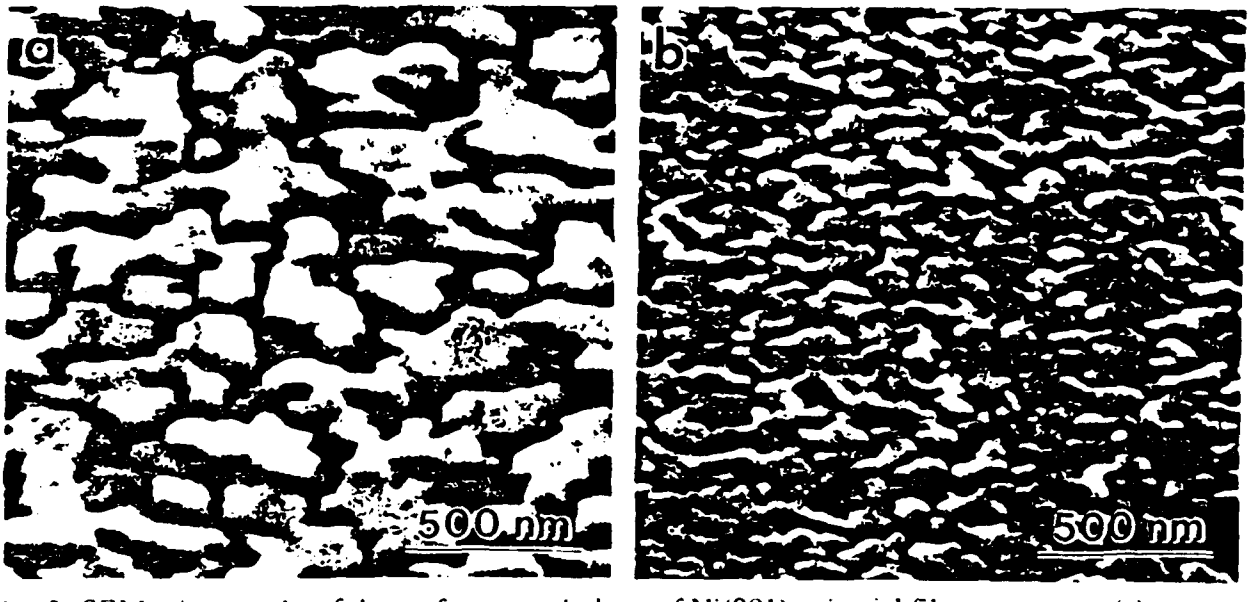

Fig. 3 SEM micrographs of the surface morphology of Ni(001) epitaxial films grown on (a) homoepitaxial C(001) films and (b) type IIa, natural C(001).

The epitaxial quality of the deposited Ni films has been analyzed by RBS/channeling using 1.6 MeV He^+ ions (Fig. 4). The presence of a <001> axial channeling direction clearly indicates that Ni(001) epitaxy has been achieved on C(001). Moreover, the degree of surface roughness and non-uniformity of the Ni films is clearly evidenced by the presence of steps in the backscattering yields of the aligned <001> spectrum for both samples. For instance, the presence of a step at 525 keV in the aligned spectrum of Fig. 4(a) is a consequence of non-uniform Ni coverage indicative of three-dimensional (3-D) film growth. A quantitative measure of the crystalline quality of the Ni

epitaxial layers is given by χ_{Ni}, which is the ratio of the aligned and nonaligned integrated, backscattering ion yields for the Ni layers. The determined values of χ_{Ni} are 33% and 26% for the corresponding epitaxial Ni films deposited on type IIa, natural and homoepitaxial C(001) substrates, respectively. However, it is apparent from RBS analysis that the microstructural quality of the Ni(001) films is degraded by the present of oxygen impurities. Indeed, the presence of oxygen at 730 keV in the Ni films is clearly evident in both RBS spectra. The incorporation of oxygen in the Ni films is a consequence of the relatively slow growth rate and the subsequent degradation of the chamber vacuum as a result of tungsten filament outgasing and/or desorption of oxygen from the chamber walls during Ni deposition. Furthermore, it is believed that the observed 3-D nucleation of the Ni (001) epitaxial films on C(001) is determined by these impurity considerations.

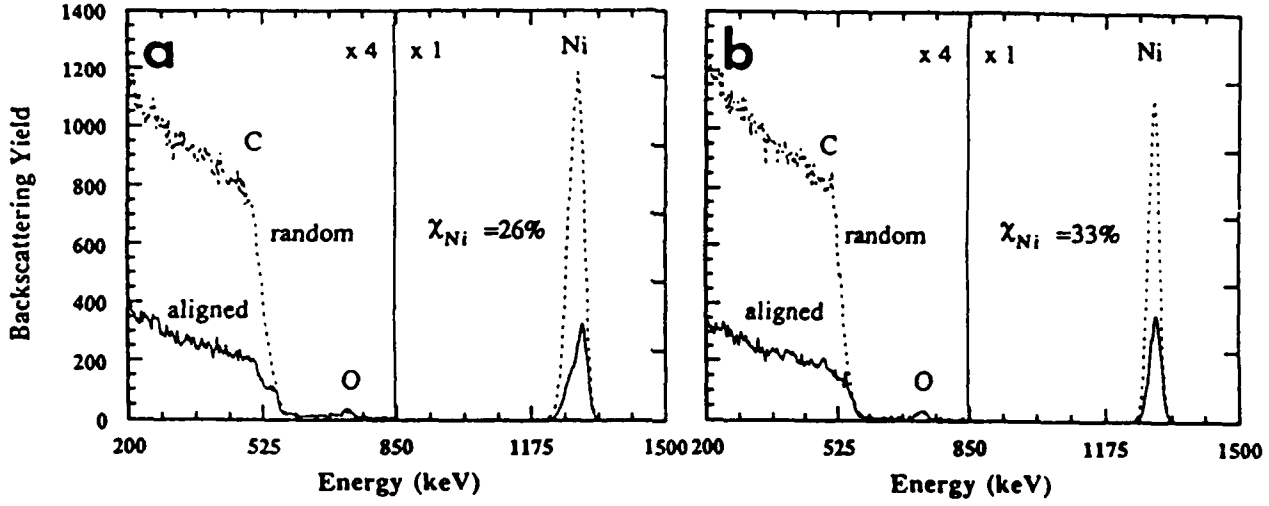

Fig. 4 RBS random (dashed line) and aligned (solid line) spectra for Ni (001) films deposited by tungsten filament evaporation on (a) homoepitaxial C(001) films and (b) type IIa, natural C(001) substrates.

In a comparative study of Ni films deposited by electron-beam evaporation on type Ia, natural C(001) substrates, SEM examination has shown that the Ni films replicate the very fine, unidirectional scratches which are present on the as-polished C(001) substrates (Fig. 5).

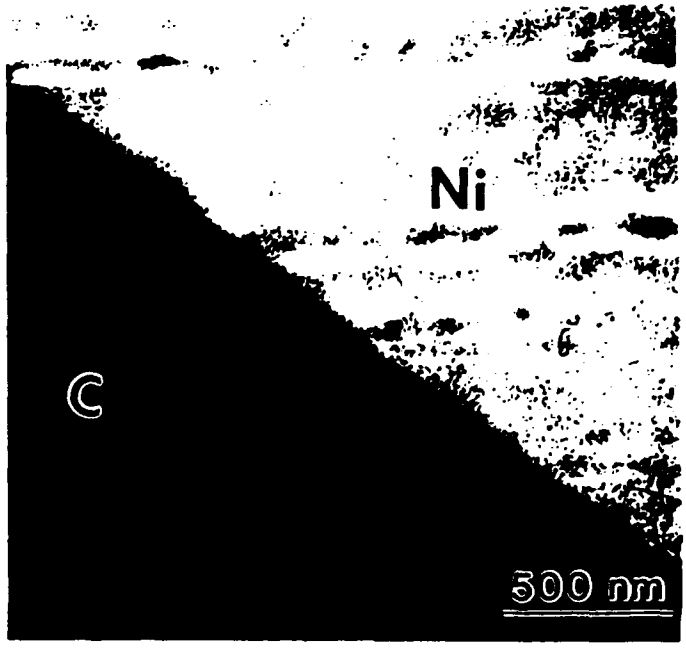

Fig. 5 SEM micrograph of the surface morphology of electron-beam deposited Ni(001) films on type Ia, C(001) substrates.

Corresponding patterned regions pertaining to the Ni epilayer (bright) and the exposed diamond substrate (dark) are clearly shown. Since the Ni layers have been patterned for subsequent selective-area epitaxial studies of diamond, corresponding regions pertaining to the Ni epilayer and the exposed diamond substrate are clearly visible. Evidently, the scratches on the surface of the single crystal diamond are the result of damage incurred by mechanical polishing of the C(001) substrates [7,8]. Moreover, under the deposition conditions employed, the coverage and uniformity of the deposited Ni films would imply a two-dimensional (2-D) growth mode for the nucleation of Ni on C(001). Fig. 6 shows RBS/channeling results obtained using 2.0 MeV He^+ ions which indicate that epitaxial Ni(001) films have been achieved. The determined value of χ_{Ni}~18% is indicative of the superior microstructural quality of the epitaxial Ni(001) layers. Moreover, it is apparent that RBS analysis did not reveal the presence of oxygen incorporation in the Ni films deposited by electron-beam evaporation.

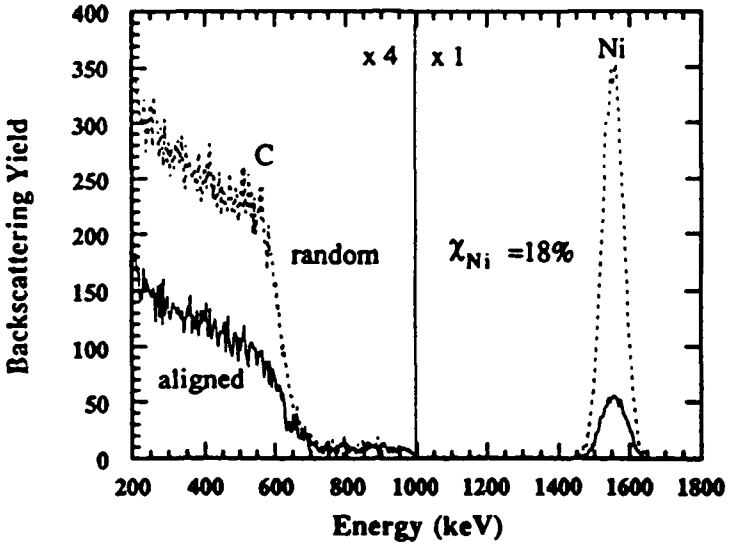

Fig. 6 RBS/channeling spectra for Ni(001) film growth on type Ia, natural C(001) by electron-beam evaporation.

It is also interesting to note that the crystalline quality of the commercially-supplied natural diamond substrates is not consistent as indicated by variations in RBS/channeling backscattered yields [9]. It would therefore appear that utilizing diamond epitaxial films grown by plasma-enhanced chemical vapor deposition (PECVD), which are smoother and may be less defective, represents another potential means to obtain topographically smooth and microstructural upgraded epitaxial metal films on diamond.

CONCLUSIONS

In summary, epitaxial Ni(001) films have been grown on C(001) substrates using thermal and electron-beam evaporation techniques. It has been demonstrated that the thermal evaporation of Ni from a tungsten wire filament on C(001) substrates results in a highly textured and faceted surface morphology indicative of three-dimensional nucleation and growth. In contrast, the Ni epitaxial films deposited by electron-beam evaporation on C(001) substrates has a surface morphology that mimics the topography of the initial, as-polished single crystal C(001) substrate. Differences in the observed microstructure and apparent growth modes of the epitaxial Ni(001) films have been attributed to the presence of oxygen incorporation in those layers deposited by thermal evaporation. Suggestions for future studies to optimize the epitaxial growth of metal films on diamond have been proposed.

ACKNOWLEDGEMENTS

TPH, HJ and RJN gratefully acknowledge partial support from the National Science Foundation (Contract No. DMR-8717816) and also the Office of Naval Research (Contract No.

N00014-90-J-1707). JBP, RAR, DPM, GCH and RJM gratefully acknowledge support from the Strategic Defence Initiative Organization / Innovative Science and Technology through the Office of Naval Research (Contract No. N00014-86-C-0460). JDH and NRP acknowledge the Office of Naval Research (Contract No. N00014-89-K-0243) for support. We also thank Dr. R.E. Thomas (RTI) for many helpful discussions.

REFERENCES

1. M.W. Geis, N.N. Efreman and G.D. Pathman, J. Vac. Sci. Tecnnol. A 6, 1953 (1988).

2. D.N. Belton and S.J. Schmieg, J. Appl. Phys. 66, 4223 (1989).

3. R.A. Rudder, J.B. Posthill,G.C. Hudson, M.J. Mantini and R.J. Markunas, SPIE, 969, 72 (1988).

4. R.A. Rudder, J.B. Posthill, G.C. Hudson, D. Malta, R.E. Thomas, R.J. Markunas, T.P. Humphreys and R.J. Nemanich. presented at the 2nd New Diamond Science and Technology Conference ICNDST-2, Washington, DC (1990).

5. Chemical cleaning of diamond using concentrated acids includes the following processing steps: (1) boiling CrO_3:H_2SO_4 for 15 mins, (2) boiling HCl:HNO_3 for 15 mins, (3) HF:$10H_2O$ for 15 mins, (5) DI rinse and N_2 dry.

6. P.G. Lurie and J. M. Wilson, Surface Science 65, 453 (1977).

7. M.J. Paisley and R.F. Davis, 1990, private communication of unpublished results, North Carolina State University, Raleigh.

8. R.A. Rudder, G.C. Hudson, D.P. Malta, J.B. Posthill and R.J. Markunas, (1989), unpublished results.

9. G.S. Sandu, N.R. Parikh and M.L. Swanson, 1989, private communication of unpublished results, University of North Carolina, Chapel Hill.